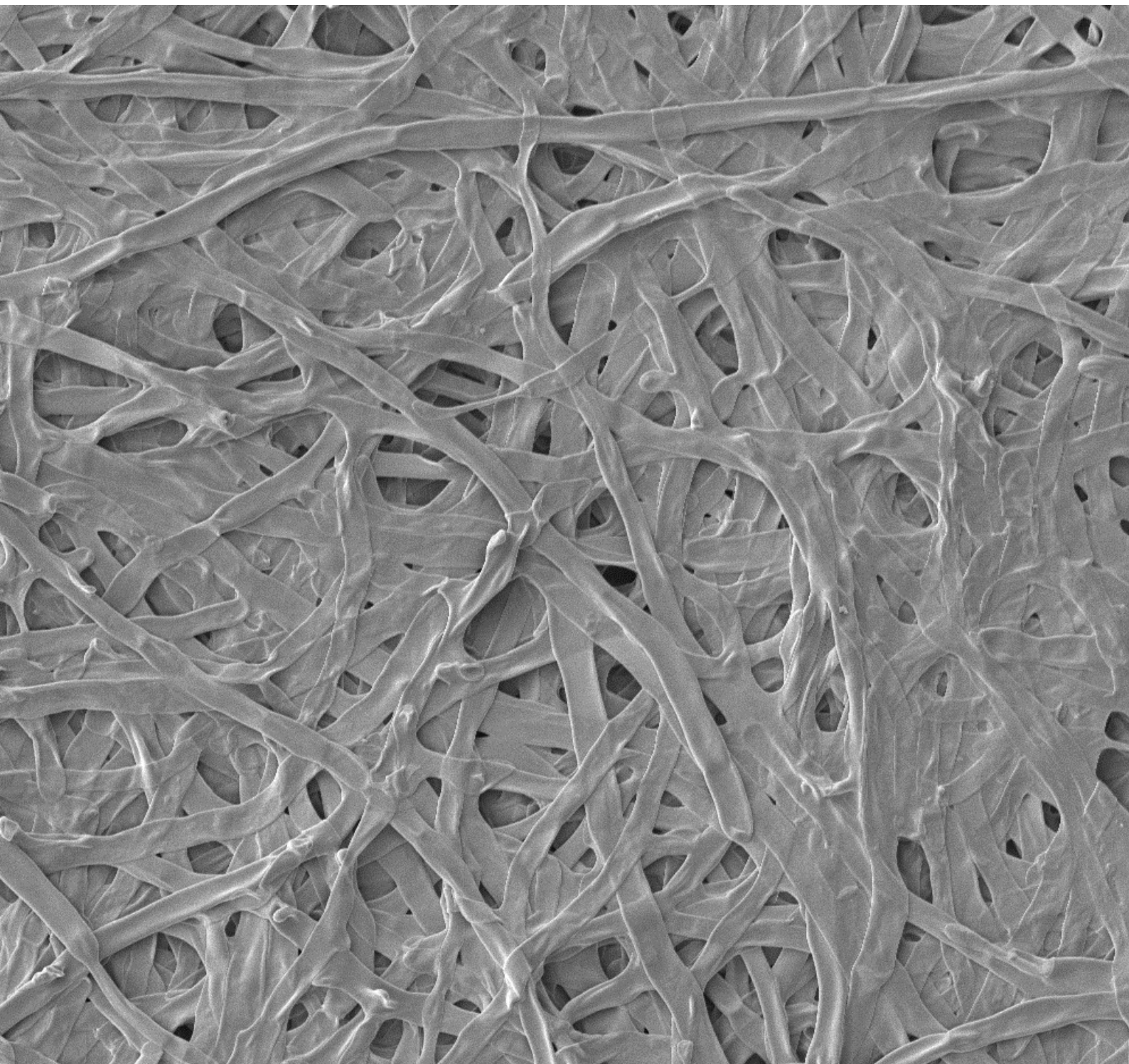MARK ABLONCZY

EXPLORING THE POTENTIAL OF FILAMENTOUS FUNGI AS COATINGS FOR AEROSPACE ALUMINUM ALLOYS

MSc Thesis

Exploring the potential of filamentous fungi as coatings for aerospace aluminum alloys

Master thesis report

by

Mark Ablonczy

in partial fulfilment of the requirements for the degree of

Master of Science
in Aerospace Engineering

at the Delft University of Technology,
to be defended publicly on Thursday, December 16th, 2021, at 11:00 AM.

Supervisor:	Dr. S.J Garcia Espallargas	TU Delft
Thesis committee:	Prof. dr. H.A.B Wösten	Utrecht University
	Dr. J.J.E. Teuwen	TU Delft
	Dr. M. Nijemeisland	TU Delft

This thesis is confidential and cannot be made public until December 31st, 2022.

An electronic version of this thesis is available at https://repository.tudelft.nl/

TUDelft

Delft University of Technology
Faculty of Aerospace Engineering
Department of Aerospace Structures and Materials

Graduation Committee

Date: 16th December 2021

Committee chair:

Dr. S.J Garcia Espallargas

Committee members:

Prof. dr. H.A.B Wösten

Dr. J.J.E. Teuwen

Dr. M. Nijemeisland

"I shall be telling this with a sigh

Somewhere ages and ages hence:

Two roads diverged in a wood, and I—

I took the one less traveled by,

And that has made all the difference."

-Robert Frost

ABSTRACT

Filamentous fungi grow large networks of biomass with minimal energy input. This biomass consists of polysaccharide-based filamentous networks and adherent extracellular polymeric substances (EPS). Recent reports show that this biomass can be formed into plastic-like thin film materials. Further, non-filamentous fungi have been applied as living coatings on wood. Even so, filamentous fungi remain unexplored for coating applications. This work fills that gap by studying how a selected filamentous fungus (*Schizophyllum commune*) and its lab-produced biomass interact with aerospace aluminum alloys, and to explore their potential as a sustainable resource to create coatings.

Two complementary routes were explored in this work. In the first one, *S. commune* was allowed to grow—under controlled conditions—on the surface of bare aluminum alloys of different compositions and surface treatments. The growth extent, filament density, and structure were investigated as a function of the underlying metal composition, surface treatment, and nutrient availability. In the second route, thin-film coatings were produced from processed biomass extracted from liquid cultures of *S. commune*. The quality of the consolidated films and their scratch resistance and adhesion as a function of a range of processing parameters and aluminum surface treatments was investigated.

S. commune grew further and more densely on AA6082 than on AA2024 and AA7075. Differences decreased after grinding, which suggests that the alloy-dependent near-surface deformed layer and alloy composition heavily influence fungal growth. The in-situ-grown fungi led to intense local surface corrosion and weakly adhered biomass. Alternatively, films produced from processed liquid culture biomass led to semi-transparent coatings with microstructure dependent on the processing conditions and fungal extract used. Although processing steps led to improvements in scratch resistance and porosity, coating macroporosity remained high and insufficient for barrier requirements. Surface treatments led to clear improvements, but even then, film adhesion remained well below that of more broadly studied and developed biopolymer coatings (>10x better adhesion). This research showed the potential of fungi to create films on aluminum alloys with ample room for improvement toward fungi-based coatings. Future research should focus on more extensive species screening, adhesion optimization, decreasing porosity, and better understanding fungi-metal local interactions.

ACKNOWLEDGMENTS

I apologize that these acknowledgements will be very long, but there are so many people who positively affected me through this process, and I must mention them all.

First, I would like to thank my supervisor, Dr. Santiago Garcia, for giving me the opportunity to work on this most interesting and unique study. I deeply appreciated his involvement in the project through his supervision, recommendations, and trust. We encountered many challenges throughout this project, but he was always there to put us on the right path and provide motivation, inspiration, and guidance. I am exceedingly grateful to Dr. prof. Han Wösten, without whose support none of this would have been possible. I am humbled to have had the chance to work with and learn from such an expert. Thank you, Dr. Wösten, for assisting us in exploring the unexplored. I must thank both of my supervisors for making time in their schedules to meet with me and guide me through this challenging project. Their enthusiastic and insightful feedback helped me to learn and grow into a more independent researcher. I am truly grateful for the impact they have had on my development. To the other two members of my committee—Dr. Marlies Nijemeisland and Dr. Julie Teuwen—I am thankful and honored that you are spending time out of your busy schedules to evaluate my work.

I cannot go any further without mentioning Jeroen van den Brandhof. Without your help, I would have been lost. I am entirely and eternally in your debt for all of the time and energy you spent advising me. Our discussions were the most impactful of the duration of my thesis, and I truly believe that it was in those moments that we did the most interesting work. I wish you all the best with your studies, soon you will be Dr. Brandhof! To all other PhD students who helped and motivated me—Tinashe, Miisa, Jingjing, Hugo, Anton, Satya, Dimos, and any others that escape me at the moment—I feel very fortunate that we crossed paths along the way. I wish you all nothing but the best for your futures. To Durga Mainali, our faithful lab manager, I am very thankful for your help and patience while I tried these new experiments and brought fungi into your lab.

To my fellow master students at TU Delft, I am deeply saddened that our time together at TU Delft has come to an end. I do not exaggerate when I say that some of my life's greatest moments have been spent with you all. To Sera, you saved me at the darkest moments of my

thesis, I hope you know you can always count on me to return the favor. I am rooting for you all the way! To Siddharth, thanks for the laughs, you always knew how to turn my bad day into a happy one. Thanks for being there when I really needed a friend. To Krishna, my co-sufferer in the lab, you are a mean cook, and an even better friend. To Nikhil, your positive attitude in the face of insurmountable challenges is an enormous inspiration to me. Thank you for always putting a smile on my face. To Willem, you never hesitated to offer your help, and made my life much easier by default. I am in your debt big-time. I know you will be able to overcome your challenges and finish strong! To Anuj, your hard-working attitude, kind heart, and motivating spirit affected me in such a positive way that I cannot describe. I will always cherish the memory of that late-night molecular simulations project turn-in. To Caspar, you finished far before us but nonetheless I am grateful for our friendship. I felt that you were a true companion, and I love your honest and open attitude to life. Thanks for not being too upset when I interrupted your work to unload my troubles. To everyone else, I am sorry that I cannot mention you all by name, for you all deserve a page of your own. I hope that we can meet many more times and make many more wonderful memories. I am always just one text away.

To my family members who were with me every step of the way, I would surely have failed without you. To my dad, who inspired me to follow my dreams to Holland, and who spared no expense for my education, I am eternally in your debt. You have showed me what it means to be a good father, and I can only hope to model my life on yours. To my grandparents, who accepted me into their home with loving arms, I do not know what I would have done without you. To my uncle, Bence, thank you for being there when nobody else was. Your motivation and support was what helped me through the final push. I am eternally grateful that I have such a loving and supportive family.

Finally, to Chus, the love of my life, I dedicate this work to you. Because if I had never come to Holland to learn about fungal materials, I never would have met you. And meeting you is unequivocally the greatest thing that has ever happened to me. You are my rock, my inspiration, and my motivation. I love you.

-Mark Ablonczy

Delft, December 2021

TABLE OF CONTENTS

LIST OF FIGURES

LIST OF TABLES

1 INTRODUCTION

1.1   Background

The aerospace industry is undergoing a surge in interest towards environmentally friendly and sustainable development, including in the materials sector [1]. One particular area of focus is on bio-based protective coatings, which have drawn the interest of academics and industry alike in research for potential novel functionalities. These are different from other bio-based materials in that they don't aim to solve the energy crisis or reduce fossil fuel use. Rather, they aim to form new protective systems not possible with conventional methods [2]. Bio-based facilitated or induced properties could range from active corrosion protection, to fire retardancy, to anti-microbial [2]. Bio-based coatings can be made of bio-based chemical components like self-healing polyimides and polyurethanes. Also, bio-based coatings have been described as a polymer matrix with an added "bio-touch", which is either inseparable (intrinsic) or separable (extrinsic) from that matrix [2]. For example, a bio element like whey protein-derived polymers could be combined with polyvinyl alcohol to create a blend or layered coating system with barrier properties against oxygen and water [3].

One of the newest ideas in the field of bio-based coating systems is to incorporate microbes such as algae and bacteria. So far, this idea has been implemented as protection of aluminum alloys from corrosion by inhibitor-loaded diatomaceous earth—which is the hard, micron-sized exoskeleton of algae [4]. Current research on microbial coatings is focusing on how these microbes grow on aerospace alloys, how they adhere, and the kind/quantity of EPS they produce "Zalman, Nijemeisland, Brussaard, Garcia, NovAM, TUDelft, ongoing research". This is an inherent shift in ideology from the typical standpoint of looking for ways to keep microbes off the surface of aerospace structures, to prevent microbial-induced corrosion [5, 6]. Of the microbes under investigation for protecting aerospace structures, fungi have received practically no attention to this point. This is even though fungi are quickly gaining ground as a sustainable source to develop biomaterials in other fields such as construction and textiles (leather).

In the past ten years, research on fungi-based materials has exploded as new companies are developing this material as bio-degradable alternatives to traditional materials. Fungi grow in large quantities with little energy input and are circular due to their polysaccharide-based composition [7, 8]. They can be grown in a variety of substrates, particularly in low-cost agriculture by-products, that otherwise would be wasted [9]. With low-energy, non-toxic processing fungal biomass can be converted into plastic-like [10, 11] and leather-like [12] materials that resemble their animal-based counterparts [13] (Figure 1.1a). Further, fungi can

be processed into stiff and strong chitin-based thin films [14], potentially interesting for coating applications. Research has shown that fungi adhere to a variety of substrates thanks to their versatile proteins and exo-polysaccharides [15-17], and fungal mycelium is being investigated as stand-alone adhesives for wood [18]. Unfortunately, quantitative data on adhesion of fungi is difficult to find, as adhesion testing methods usually involve cell counting pre- and post-washing. Therefore, implementing more quantitative methods—like those used for measuring adhesion of polymeric coatings for aerospace—could be of great value to the literature. Further, a company called Xylotrade in the Netherlands has been developing biofilms of *A. pullulans* fungi to coat and protect wooden structures from UV, water, and microbial degradation (Figure 1.1b) [19-21].
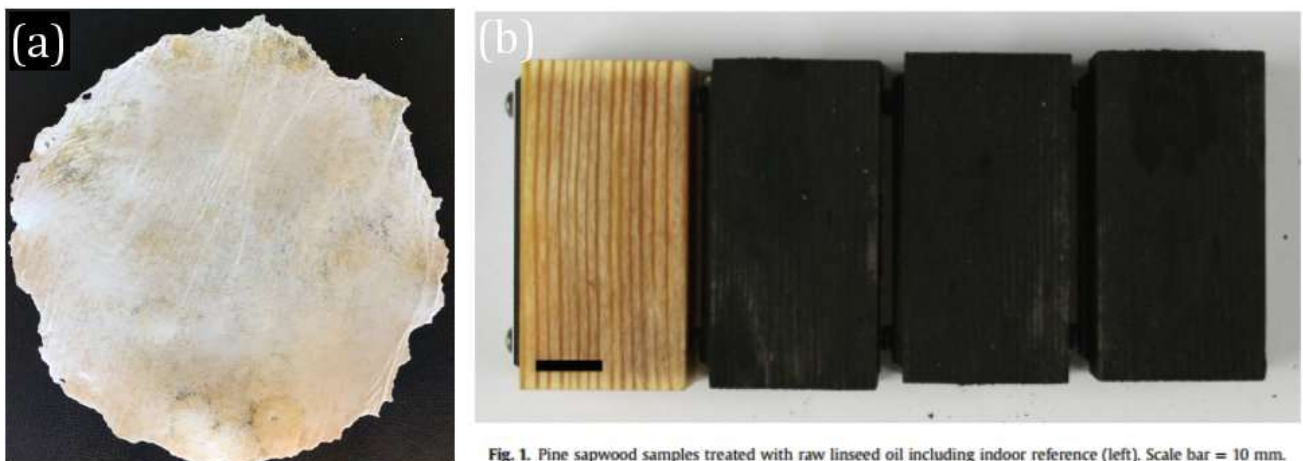
Fig. 1. Pine sapwood samples treated with raw linseed oil including indoor reference (left). Scale bar = 10 mm.

Figure 1.1 Examples of a fungi film and fungi coatings. (a) example of a mycelium film, sourced from Brandhof (2018), (b) biofilm of A. Pullulans grown on blocks of wood, sourced from Phoophajai et al 2021.

This work is meant to explore the possibility of fungi-based coating system for protection of aerospace structures, more specifically aluminum alloys. However, the lack of information describing fungi and their interaction with aerospace structural materials limited the scope of this thesis. The work can therefore be seen as the first steps towards fungal protection of aerospace structures in which we focus on two main aspects: (i) the interaction of living fungi with aerospace aluminum alloys, and (ii) the adhesive potential of mycelium to those alloys.

1.2 Fungi & mycelium

1.2.1 What are fungi?

Fungi are a diverse group of organisms that make up the third kingdom of the eukaryotes. They have complex cell structures, tissues, and organs associated with higher organisms [22]. Fungi are ancient, appearing on the fossil record some 2.4 billion years ago [23]. At some point, they may have been the dominant life-form on the planet [24]. Still today, as primary decomposers, fungi are critical to the survival of all life on earth. They are responsible for breaking down the most complex organic matter—like cellulose and lignin from plants which bacteria don't usually degrade [25]—into simple molecules and nutrients, which they absorb and use to grow. This degradation process helps create nutrient-rich soils that allow plant life to flourish. Further, fungi form symbiotic (mycorrhizal) relationships with plants in which they exchange nutrients and water for sugar produced by the plant. Somewhere between 80 and 95% of terrestrial plants depend on these so-called mycorrhizal relationships with fungi [22, 25]. Despite their importance, fungi are still relatively unknown to science. Scientists have currently described only 10% of the estimated species of fungi, which could number between 2.2 and 3.8 million [26]. Of these species, each has unique means of growth, cellular structures, and reproductive methods. This great diversity opens the possibility of selecting species for the desired material property.

1.2.2 Filamentous fungi & mycelium

The most recognizable part of a fungus is the mushroom, however, that is only a small part of the mass of a fungus. Mushrooms are the reproductive organs of fungi, which otherwise form large networks or biofilms of cells that form the largest part of their mass. One of the most important distinctions between types of fungi is the way that they grow. There are two kinds of fungal growth: filamentous and yeast-like [8]. Yeast-like fungi grow as self-replicating single cells and have been vital to humans for the production of bread, wine, and beer for millennia [8]. They also are the kinds that form biofilms, like those *A. pullulans* biofilms being used to coat and protect wood by Xhylo Biofinish [19]. The other form of fungi, filamentous fungi, are the kinds that have attracted so much attention as biomaterials due to the large amounts of mass they can produce. The way they grow is summarized in Figure 1.2, from a recent review on fungal biotechnology [8]. The process starts with spores germinating and extending at one end—what

we call apical growth—into elongated, tubular cells called hyphae. These hyphae are usually a few microns in diameter but can grow to be centimeters in length [8, 22]. They also branch off into new hyphae and fuse with other hyphae in a process called anastomosis [22]. In this way, a fungus can form a massive, interwoven, and cross-linked network that is referred to as mycelium (singular) or mycelia (plural).
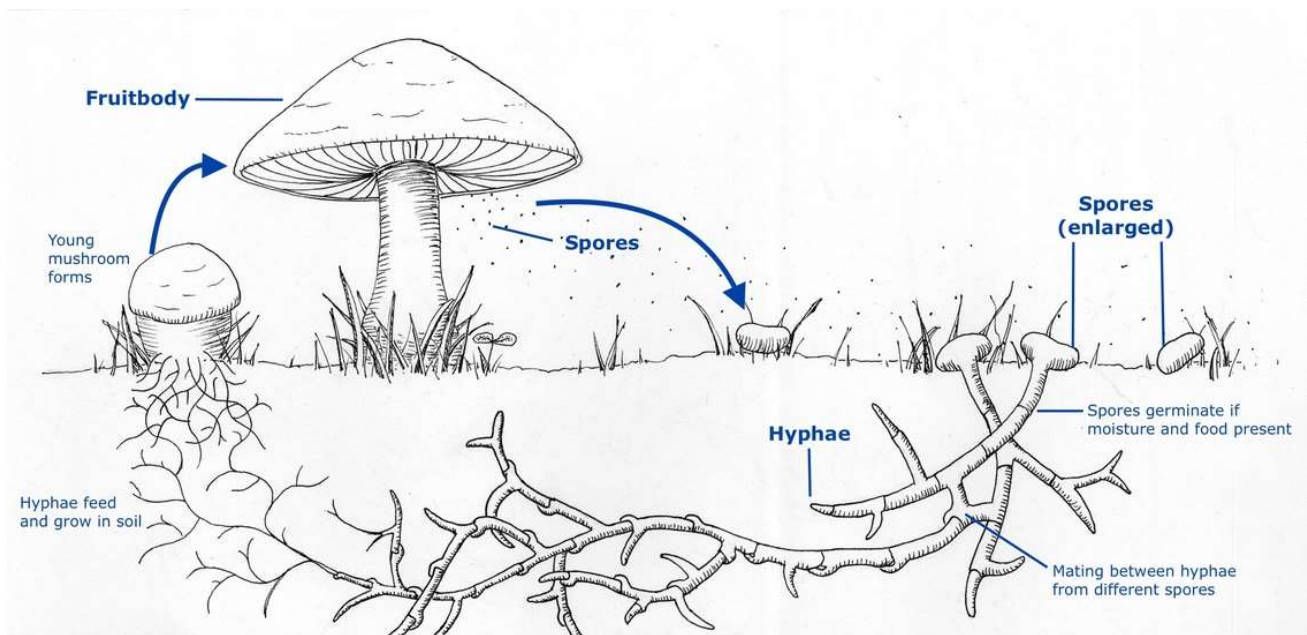
Figure 1.2 Mushroom life cycle. Original source: "Science Learning Hub – Pokapū Akoranga Pūtaiao, University of Waikato, www.sciencelearn.org.nz"

Mycelia can survive in various environments thanks to their growth plasticity. This means they can change they ways they grow to adapt to their environments. The primary goal of mycelia is to find food sources they can exploit to further their growth. In pursuit of the goal, a colony can grow adaptively, depending on the situation it finds itself in. In areas of low nutrition, it may limit the branching rate and focus on extending forwards, though not much is known on the exact mechanics for each species. When one hypha reaches a nutrient-rich area, the colony increases the branching rate and slows down extension to capture the nutrient source [22, 25]. The mycelia capture nutrients by secreting a wide variety of extracellular enzymes and organic acids that break down the substrates they colonize into simple chemical building blocks. The fungi then

convert these into more cell wall material to build an even bigger network [27]. These mycelial networks can become enormous, as evidenced by one honey fungus that has colonized about 1000 hectares of forest, making it the most massive organism on earth [28]. What's more, the fibrous structure of mycelium grants it an exceedingly high surface-to-volume ratio [27]. For example, in one square meter of soil, we can expect to find 20,000 km of fungal hyphae [22].

1.2.3   What fungi need to survive

At the most basic level fungi require oxygen, water, and food to survive. They are oxygen-breathing, and carbon dioxide-emitting, like animals and humans. Most fungi are obligate aerobes, meaning their speed of growth is highly stunted in low partial pressure oxygen conditions [22]. Like oxygen, water availability is critical to fungal growth. All fungi need water to aid with nutrient uptake, enzyme function, and metabolic function [25]. The inside of fungal hyphae—similarly to humans—is mostly water. Thus, fungi need water nearby to maintain turgor pressure—which keeps the thin-walled tubular hyphae inflated and allows them to penetrate substrates and perform cellular functions [22]. Very few fungi can withstand long droughts, though some species may be able to survive and re-grow after short-term desiccations [29]. In summary, the basic conditions for fungal growth are air exchange and a high humidity environment.

Requirements for growth concerning conditions such as temperature, pH, and nutrition are species-dependent, and the kingdom of fungi covers a remarkable range of these conditions. For example, the hyperthermophile *T. lanuginosus* prefers a temperature range of 30 to 62°C, while the psychrophile *S. borealis* grows between -5 to 15°C [25]. Most fungi-like those used in this work—prefer moderate temperatures between 10 to 40°C [22]. The high (~60 to 65C) and low (-12C) limits are set by the temperatures at which the cell starts thermally decomposing or is unable to perform cellular functions at a sufficient rate, respectively [25]. Similar to temperature, most fungi prefer a moderate pH range of between 5-7 pH, though there are both acid-tolerant and alkali-tolerant species [25]. Concerning nutrition, fungi can break down a wide array of substrates. The major ones range in complexity from simple molecules like long-chain hydrocarbons, methanol, and glucose to complex molecules like lipids, lignin, and chitin. Which specific food source a fungus prefers is based on their evolutionary history and what enzymes, organic acids, or synthase molecules they have available. Micronutrients required by fungi include Nitrogen, Phosphorus, and Iron, as well as—in small concentrations—cations like Zinc,

Manganese, Magnesium, Copper, and Silicon [30]. Fungi can generally tolerate one suboptimal condition, but their growth is hampered when they have to deal with multiple at once [25]. Even more so when they are competing with other micro-organisms—which is why sterility is so important to reduce competition and encourage fungal growth.

1.2.4   Hyphae & the fungal cell wall

Hyphae are the elongated, thin-walled, tubular cells that make up the majority of a mycelium. Figure 1.3 shows an illustration of what a cross-section of what a typical hypha may look like. They range from 1-5µm in diameter, though that is species-dependent [31, 32]. Most of their volume is either empty space or filled with cytoplasm and organelles. The cell wall is typically a couple of hundred nanometers thick, or about $1/10^{th}$ of the diameter of inflated hyphae. It is important to note that there is enormous diversity in the size distribution and shapes of hyphae. For example, a colony can differentiate its hyphae production for distinct functions, so that some are large-diameter and thin-walled (transport hyphae), and others small-diameter and thick-walled (support hyphae). Another feature of hyphae is their ability to form cross-walls called septa, which allow cytosolic flow but prevent catastrophic cytoplasm loss if one segment of hyphae gets ruptured. As mentioned earlier, hyphae are also able to fuse together by anastomosis, which allows the creation of large hyphal aggregates called cords [22]. These are important in transporting food and water over large nutrient-depleted zones. Finally, hyphae exhibit tropisms thanks to calcium signaling at their tips, which means they re-orient their growth direction based on external stimuli like physical barriers, chemicals, or electric fields [33].

Hyphae directly transform their surroundings into new cell wall material by absorbing molecules, breaking them down, and synthesizing them into the needed components. They absorb molecules either by diffusion or with the help of transporter proteins [22]. Those molecules then flow to the tip where synthase enzymes transform them into cell wall material like glucans and chitin [25, 34]. Chemically, the cell wall is composed mainly of β-glucans, which make up ~64% of the cell wall by mass [35]. Also present are alpha-glucans, chitin, and then proteins and lipids [36]. The cell wall forms in two stages: extension at the deformable tip, and then rigidification behind the tip. The deformable tip is the leading 2µm of the hyphae and has been described as "viscoelastic", where polymers can flow in and out of the not yet fully formed cell wall [22]. Behind the tip, the cell becomes more rigid, as β-glucans are progressively

crosslinked with each other and with chitin. This process of cross-linking is driven by amino acids in the cell wall and may happen spontaneously even if the supply of cytoplasm to the tip is halted [25]. For this reason, it is hypothesized that hyphal cell walls become stiffer and less dynamic as they get older.
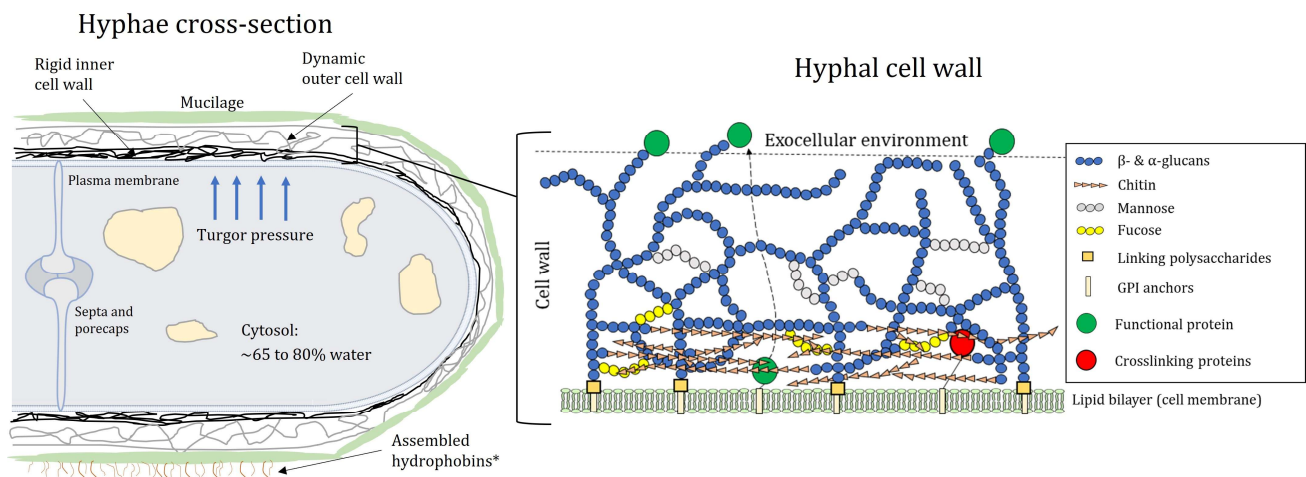
Figure 1.3 The structure of the fungal hyphae and the fungal cell wall. Illustration based on information of fungal cell wall composition of S. Commune. Note: this illustration is meant to help readers understand the general structure, the specifics are not meant to be exact and will vary considerably for different species.

Structurally, the cell wall is a composite-like 3-D network. The innermost layer of the cell wall of basidiomycetes such as *S. commune* consists of crystalline microfibrils of chitin cross-linked to and embedded in an amorphous matrix of highly branched β-(1,3)-(1,6)- glucans, α-(1,3)-glucans and polymeric fucose and mannose [36, 37]. The chemical structure of β-(1,3)-(1,6)- glucan is shown in Figure 1.4. This chitin-glucan network is insoluble in water and alkali solutions and forms the rigid, load-bearing exoskeleton of the fungi [36]. This layer resists internal hydrostatic pressure and grants structural integrity that allows the fungi to exert mechanical force on its substrates and penetrate them [37]. A flexible layer—composed of β-(1,3)-(1,6)-glucans, α-glucan, and mannan residues—exists on top of the rigid layer [36]. This layer serves to immobilize structural and functional proteins—such as hydrophobins and adhesins—as well as enzymes to the outer edge of the cell wall [38]. Proteins may be covalently

linked to the glucan network, though most are noncovalently bound and soluble—PBS washing led to the disappearance of lipid and protein signals. Research for the basidiomycete *S. commune* indicates that these proteins are not a permanent part of the cell wall, but exist inside the cell, and mobilize based on the changing environment of the fungi [36]. That behavior is what lends to the highly dynamic and responsive nature of the fungi cell wall. It is also highly species-dependent, so this behavior only applies for *S. commune*. At the very outer layer, hyphae may be embedded in a matrix of their excretion called EPS, or mucilage, composed of polysaccharides, proteins, and lipids that are loosely bound to the cell wall. Fungal EPS plays an important role in biofilm formation, which helps the fungus adhere, form complex hyphal structures, and provides a layer of protection from predators and the environment [22].
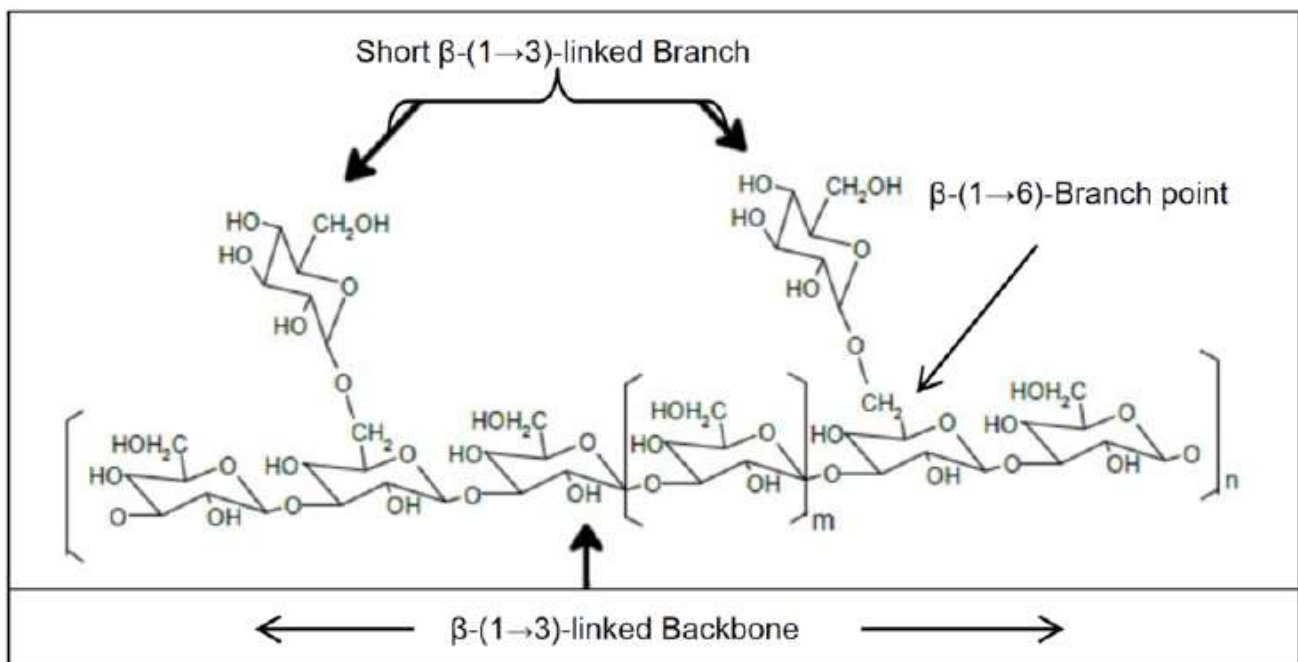
Figure 1.4 The chemical structure of β-(1,3)-(1,6)-glucan. Source: Spent Brewer's Yeast and Beta-Glucans Isolated from Them as Diet Components Modifying Blood Lipid Metabolism Disturbed by an Atherogenic Diet - Scientific Figure on ResearchGate. Available from: https://www.researchgate.net/figure/An-example-of-the-molecular-structure-of-soluble-yeast-b-glucan_fig1_235328333 [accessed 7 Dec, 2021]

1.3 Filamentous fungi as materials

Humans have been extracting useful materials from filamentous fungi for thousands of years. The earliest example is pre-historic people using polypore (tree bracket) fungi as tinder, dating as far back as 12,000 years ago [39]. The most popular example of such materials lies with the remains of "Otzi the Iceman", a 5,000-year-old traveler frozen in ice [40]. Archeologists discovered three objects of fungal origin in the Iceman's bag. Researchers believe Otzi used this fungal biomass for spiritual, medicinal, or fire-starting purposes. We now refer to materials like this as Amadou. Amadou-like materials had a strong presence in early European cultures as a leather alternative until the 1900s [13, 41]. Thanks to its fibrous structure and ease of processing fungi drew interest for mycelium-derived paper [42, 43], textiles [44], and fibrous packaging material [45] in the 1950-70s. A later patent described the process of co-incubating mycelia with synthetic fibers to produce bio-composites [46]. Still, none of these patents or ideas generated enough interest to establish mycelium as an alternative to conventional materials.

In the late 90s and early 2000s, a renovated interest for mycelium materials started. For example the company Ecovative based its business model on the commercialization of bio-based composites made out of mycelium for foam and packaging applications [47, 48]. Currently, fungal materials can be subdivided in three big groups: mycelium composites, mycelium-derived materials, and pure mycelium & hybrids. The focus of this work is on pure mycelium materials, but we will first briefly introduce the other two sub-groups. In mycelium composites, fungal growth is deactivated after colonizing and binding together an organic substrate [49-53]. New research is exploring how to use the living aspect of fungi in these composites for self-healing and joining [9]. Interested readers are referred to recent critical reviews [48, 54-57] which nicely summarize the scientific literature. Mycelium-derived materials refers to relatively high-stiffness thin films composed of chitin-glucan extracted from fungi networked polymers extracted from fungi [58]. This is a new alternative to traditional chitin-based films which come from crustacean shells [59]. In fungi, chitin is linked to β-glucans, which could provide benefits to the toughness of fungi-derived chitin-based materials [60]. Interested readers are referred to this recent critical review which has more thoroughly summarized the topic [61].

The final category that mycelium materials fall into is pure mycelium materials & hybrids. These are materials that use fungi "as-is", with hybridizations to improve properties. A recent review has termed these types of materials as "flexible fungal materials" [13] and provided a useful suggestion to further break down these types of materials based on how the fungi are

cultured. This creates three categories: solid-state fermentation (SSF), static liquid fermentation (SLC), and agitated liquid fermentation (ALC).

1.4   Mycelium lab production routes

In solid-state fermentation (SSF), fungi are grown either at the surface of or within a substrate containing sufficient nutrients to support growth. This is the same method used for producing mycelium composites, except in that situation fungal growth is halted before the substrate can be fully converted into biomass. In case the substrate is fully consumed, pure mycelium foam would be leftover. This foam can be manufactured also by forcing aerial hyphae growth off the surface and collecting that biomass [62]. This bio-foam is a low density (30 to 50kg/m^3) fibrous structure. When put through certain chemical and physical processing steps this bio-foam can be made into leather-like materials, which are currently gaining interest as bovine leather replacements [13]. Processing can include deproteination, deacetylation, cross-linking, compression, and plasticizing [12]. These steps are meant to reduce brittleness and increase mechanical strength by creating new covalent bonds in the chitin-glucan chains and opening up H-bonding sites [12]. By the end, the mycelium-based leathers resemble traditional leathers not only visually and to the touch, but also in tensile strength, tear and scratch resistance, and UV resistance [13, 63].

Another way to use SSF to grow mycelium into materials is to grow the materials directly onto their intended substrate as a coating. As far as we know, this has been done once before with filamentous fungi, in research exploring the use of mycelium as adhesive for wood veneer [18]. In this work, fungi grew within 8 days to cover the wood panels entirely. Two fungi-coated panels were then hot-pressed together in a lap-shear configuration and assessed for adhesive strength. Their results showed that mycelium-coated lap-shear samples adhered more strongly than lap-shear samples hot-pressed without mycelium coating. They also reported differences in morphology and properties of mycelium that grew at the top (mycelium-air interface) vs. at the bottom (wood-mycelium interface). Mycelium at the top grew sparse, aerial hyphae with high water contact angle due to their porous structure and hydrophobin proteins. Meanwhile, mycelium at the wood interface grew like a biofilm, with hyphae embedded in a matrix. In this thesis we explore for the first time how mycelium grown using the SSF method interacts with aluminum alloys.

1. Introduction

Mycelium grown in static liquid culture (SLC) forms materials more closely resembling paper and thin films. In SLC fungi grow in liquid medium containing sugars (usually glucose or dextrose) and micronutrients. The mycelium converts these nutrients into a sheet of interconnected biomass at the air-water interface. After this sheet is removed and dried, it forms a thin film-like material resembling the fungi bio-foam from SSF except with lower porosity and higher density (515 to 2101kg/m^3) [31, 32]. The densest reported samples resemble low-stiffness polymers like PVA in specific stiffness [64]. Films from SLC are also hygroscopic, uptaking 12 to 24% weight in water after a few days in 100% humidity condition [31]. Reported water contact angles are high (>120°)[31, 32], however, those values are likely explained by entrapped air in micropores. The differences in morphology of top and bottom surface mycelia observed for SSF are also present in SLC mycelium films [32, 64]. The air-exposed side showed a fibrous structure of sparsely networked hyphae, while the water-exposed surface showed hyphae embedded in an EPS matrix [32].

The final way to produce pure mycelium materials is to grow fungi in agitated liquid culture (ALC). This technique is the one used in bio-fermentation to maximize fungal production of enzymes, organic acids, and EPS [22]. Stirring the culture aids oxygen and nutrient diffusion and allows rapid growth of biomass. In ALC mycelium is inoculated as many small particles or spores which then grow into discrete "pellets" of mycelium. These pellets are spherical-shaped outgrowths of hyphae, which are densest at the center. After growth, while being filtered out of the culture, the pellets intertwine and entangle to form a cohesive "wet filter cake". This wet filter cake dries into a thin film [65] which is very similar to the films from SLC, with slightly lower porosity thanks to the pelleted structure of the mycelium. It seems that these films have a more homogenous microstructure compared to films from SSF or SLC [65]. Water soaking/washing, glycerol soaking, and hot-pressing were found to be effective for increasing density and thus mechanical properties of such films [11]. Other research has demonstrated the possibility of co-incubating mycelium with nanocellulose particles [66]. During growth, fungal hyphae grew on and around the nanocellulose particles, and also incorporated them into their cell walls. Films formed from the co-incubation showed 5x increased strength and ductility compared to 'mycelium-only' films. In this thesis we explore for the first time if mycelium produced through ALC can be used to create protective films on aluminum alloys.

1.5   Purpose of this study & research questions

The purpose of this study is to explore if filamentous fungi (mycelium) are a suitable candidate to develop bio-based coatings for protecting aerospace structures, specifically focused on aerospace aluminum alloys. For this purpose two routes to produce mycelium are explored (SSF and ALC) in order to study the mycelium-alloys interaction upon direct growth on the surface and the mycelium-alloys interaction of the mycelium extracted mass applied on aluminum alloys in the mode of coatings. The research is summed up by the following research questions and sub questions:

1. **Will fungi grown on aluminum surfaces show any coating potential?**
    1.1 How is the growth of mycelium on aerospace aluminum alloys dependent on nutrient availability?
    1.2 How is the growth of mycelium on aerospace aluminum alloys surface chemistry dependent?
    1.3 Is the biomass which is grown at the surface interesting for coating applications
        1.3.1 Does the biomass have a microstructure suitable for protecting aluminum alloys?
        1.3.2 Is the biomass adhesive to aluminum?

2. **Can mycelial biomass from liquid culture be extracted and formed into coatings on aluminum?**
    2.1 Do these coatings meet the pre-requisites for serving as protective coatings for aerospace aluminum alloys?
    2.2 Can simple processing—such as blending and washing the cultures beforehand—improve the physical and chemical structure of the material?
    2.3 How adhesive the is extracted mycelial biomass to aluminum alloys?
        2.3.1 How is this adhesion affected by homogenizing and/or washing the mycelium beforehand?
        2.3.2 Can common aluminum surface treatments improve this adhesion?

1.6   Structure of this thesis document

To answer these questions, the thesis is divided into two parts. The first part (Chapter 2) explores the first main research question and its sub-questions. This part of the work investigates if it is possible to grow mycelium on aluminum, and what conditions would lead to optimal biomass production on the surface. Further, we are interested in the way mycelium interacts with aluminum, regarding toxicity to the fungi and corrosive damage to the aluminum surface. Finally, we will investigate if the material which is formed on the surface has adhesive and structural characteristics suitable for coating applications. The second part (Chapter 3) explores the second research question about forming coatings out of extracted mycelial biomass from liquid culture. In this part, we investigate the possibility of consolidating liquid culture extracts onto aluminum, and the role of processing steps like blending and washing. Further, the suitability of processed mycelial biomass for coating application will be discussed, regarding microstructure and adhesiveness. Both chapters will have separate materials & methods, results, discussions, and conclusions. In Chapter 2, the results and discussion are separate. In Chapter 3, the results and discussion are combined. In the end, Chapter 4 will summarize the work, bringing the two parts together, and give recommendations for future work based on our findings.

2 GROWING FILAMENTOUS FUNGI ONTO ALUMINUM

2.1 Introduction

For the first portion of this thesis work, we were interested in exploring how mycelium grows on and interacts with aluminum. The following sections describe how we did that, and what we found. First, we designed two experimental setups that would encourage/force *S. commune* filamentous fungi to grow on aluminum. These setups and all other methods and materials are explained in Section 2.2. The first results in Section 2.3.1 detail how mycelial growth proceeded, what kind of biomass was formed on the surface, and specific characteristics of the biomass that are of great interest. The next results in Section 2.3.2 explore how *S. commune* fungi interacted with aluminum surfaces through corrosion imaging. Section 2.3.3 gives some idea about the chemical structure and thermal properties of the biomass grown on the surface, through IR spectra and TGA curve analysis. In the final results sections, we compare how *S. commune* growth was affected by nutrient scarcity (Section 2.3.4) and aluminum surface condition & alloy type (Section 2.3.5) by testing growth under several different conditions. These results include image analysis of the biomass-covered surfaces to determine surface coverage, growth extent, and growth density. In Section 0 we will shortly discuss these results and their significance towards our aims of growing in-situ coating material at the surface of aluminum alloys. Finally, Section 2.5 will conclude and answer the research questions posed in Section 1.5.

2.2 Materials & methods

The fungi, media, and equipment used to perform the experiments described in this chapter were in large part provided by Prof. Han Wösten, Microbiology, University of Utrecht, NL. The labor of sterilizing, inoculating, and growing cultures was graciously carried out by Jeroen van den Brandhof, PhD researcher, Microbiology, University of Utrecht, NL.

2.2.1 Fungal growth media

Schizophyllum commune minimal media (hereafter referred to as SCMM) is a recipe for liquid media supporting fungal growth with the minimum amount of nutrients required. This recipe was developed in the microbiology lab at the University of Utrecht and was generously shared by Prof. Han Wösten. The recipe contains D-glucose as the main food source, with smaller concentrations of trace elements and micro-nutrient sources that optimize growth. SCMM was used for both liquid- and solid-state cultures. For solid-state growth, 30g/L agar solution was

added to [2x] SCMM at 1:1 volume ratio to solidify the media [65]. Media was sterilized at 1 bar pressure and 121°C for minimum 30 minutes, using a kitchen pressure cooker.

2.2.2   Mycelium inoculum

Basidiomycete fungi *Schizophyllum commune* was the species of interest for this study. More specifically, a wild-type (*4.39*) strain—taken from storage at the microbiology lab at the University of Utrecht—was used. All the mycelium used for the experiments in this chapter originated from a "master culture" kept in long-term storage in a freezer at -80°C. A week before the start of an experiment, these master cultures were used to start fresh cultures. Fresh cultures were grown in 90mm petri dishes on SCMM solidified with 15g/L agar at 30°C for 7 days or until full colonization. They were then stored in a fridge at 4°C until needed for inoculation. A small chunk of mycelium was transferred from one of these to the petri dishes with aluminum plates in them, to initiate growth. Transfers were performed using a sterilized needle tip in a sterile environment—either under a flow hood or directly next to a flame.

2.2.3   Metal plates & surface treatments

Metal plates were sourced from the metal plate storage room in the Aerospace DEMO lab at TU Delft. Samples were cut from large plates of aluminum to workable sizes to be treated. The thickness of these plates and the batches they originated from were not constant through all experiments, and important differences are reported where applicable. Three different alloys—Al 2024, Al 7075, and Al 6082—were used for their varying concentrations of alloying elements. The aluminum plates were then cut precisely to 50x50mm squares using a large sheet metal cutter. The surfaces of the aluminum plates were treated in one of two ways: 'degreased only' and 'degreased & grinded'.

The first condition—which we refer to as 'degreased only'—involved two steps. First, the plates were wiped on both sides with acetone-soaked paper towel to remove dirt, grime, and grease from the surface. Next, the plates were ultrasonicated at a medium setting at 20°C in distilled water for 5 minutes to shake loose bits of paper towel and other entrapped artefacts. After this, the plates were left to air dry, and then stored in plastic bags until use. These plates, along with a 2.5x magnified image of the surface, are shown in Figure 2.1a,b&c.
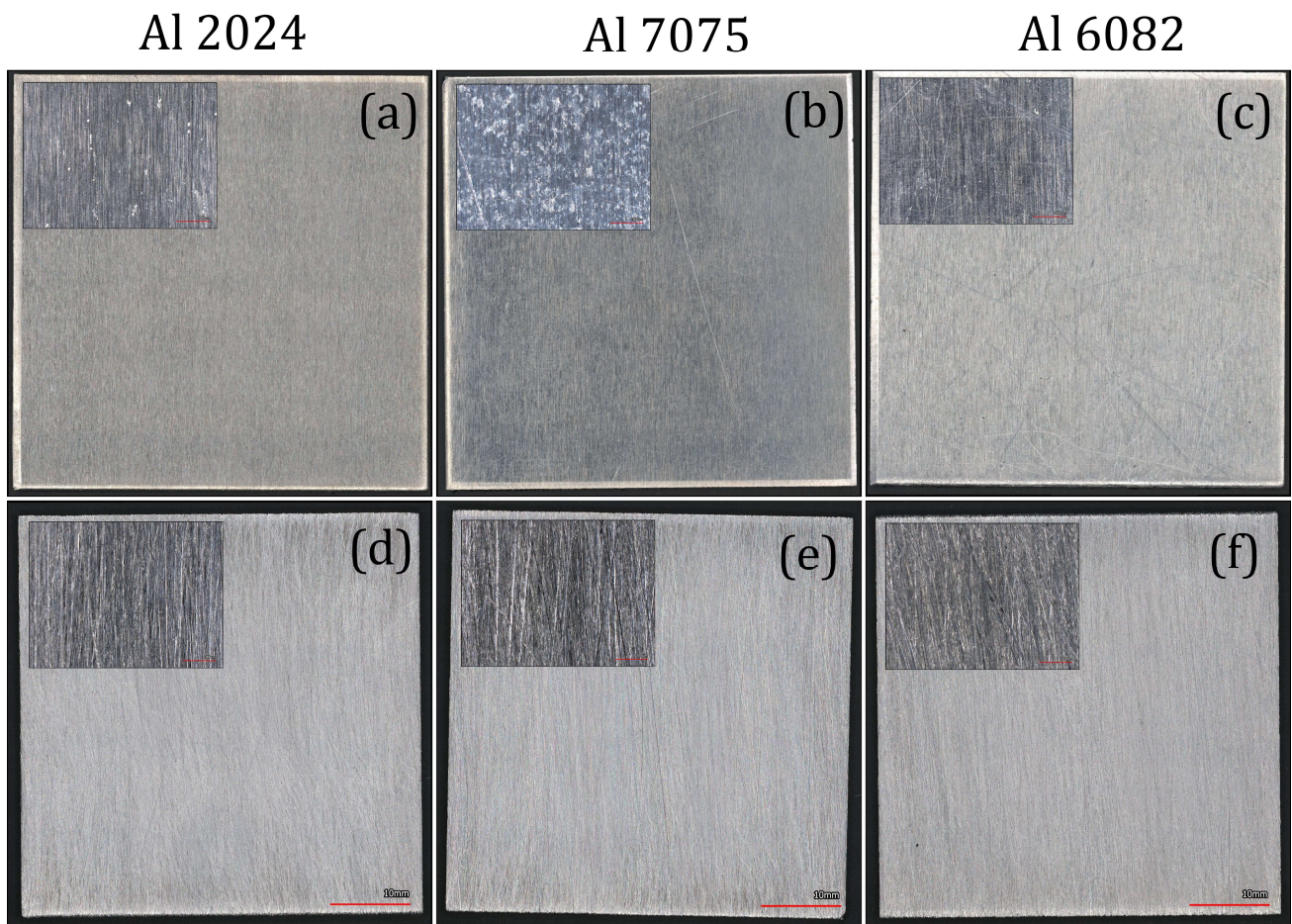
Figure 2.1 Images of aluminum plates used as substrates for growing mycelia. (a) Al 2024, (b) Al 7075, (c) Al 6082 with surface treated to the 'degreased only' condition. (d) Al 2024, (e) Al 7075, (f) Al 6082 with surface treated to the 'degreased & grinded' condition. Red lines on the zoomed-in images represent a distance of 1000μm. Red lines on the zoomed-out aluminum plates represent 10mm length.

The second condition—which we refer to as 'degreased & grinded—added a grinding step to the 'degreased only' treatment. The intention with this treatment was to remove the near-surface deformed layer that is expected to be present at the top 1-2μm of rolled aluminum alloys [67]. In this treatment, the aluminum plates were first grinded unidirectionally with 60 grit sandpaper under running water for about 60 seconds per sample, or until the surface was homogenously scratched. After this, the grinded plates were put through the same degreasing steps used for the 'degreased only' condition. Examples of the 'degreased & grinded' aluminum plates, and their surfaces at 2.5x magnification, are shown in Figure 2.1d,e&f.

2.2.4   Experimental setup

    Two setups were used to grow filamentous fungi (mycelium) on aluminum plates in this study. The major distinction between the two setups is that in one case inoculum is placed on top of an aluminum plate (Figure 2.2), and in the other case inoculum is placed to the side of an aluminum plate (Figure 2.3). There are other important distinctions that must be clarified, which we will do so in this section.

    The first setup—which for simplicity's sake will be referred to as 'inoculum on top'—was intended to force mycelia into growing on aluminum plates (Figure 2.2a). In this setup, a 50x50mm aluminum plate—which for this setup was always Al 6082 in the 'degreased & grinded' surface condition—was placed in a 10mm tall, 90mm diameter plastic petri dish directly on top of pre-sterilized, agar-based solid media. That layer of solid media—which had a volume of around 8ml—either contained SCMM or distilled water. The intention of this distinction was to determine whether mycelia can chemically sense and be motivated by the presence of food underneath the plate. The layer was cut out from a petri dish full of agar-based media to match the size of the aluminum plate placed on top. The solid media around the edges of the plate was cut out to limit the effect of chemical sensing horizontally.
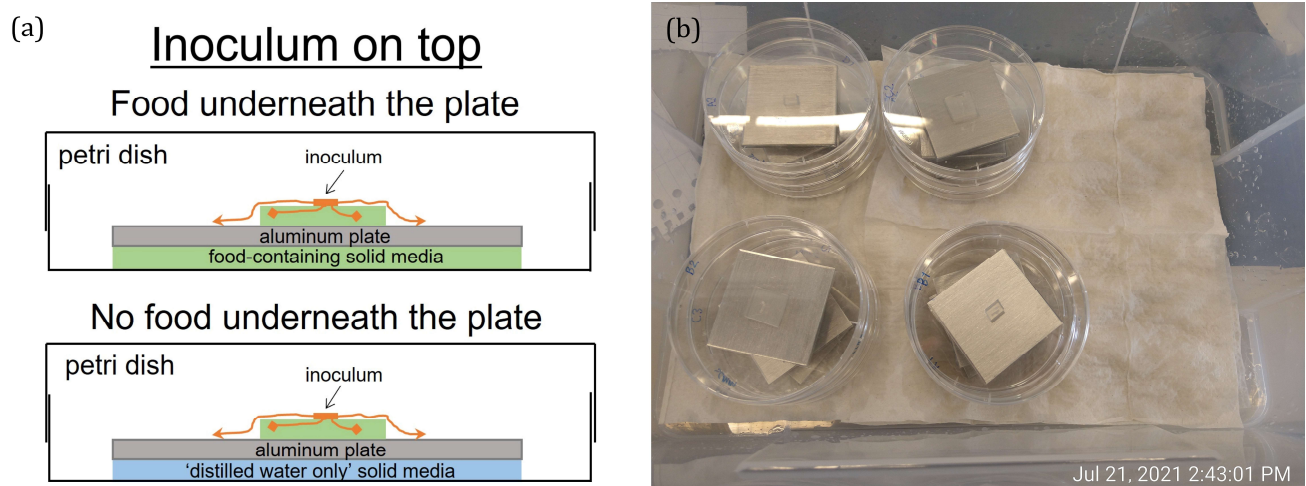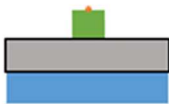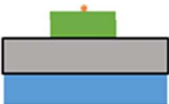
Figure 2.2 Growing mycelium on aluminum: inoculum on top. (a) cross-section of the petri dish in which mycelia were grown onto aluminum plates. The orange arrows represent possible growth directions for the inoculum of mycelium. (b) image of the inoculated petri dishes in a grow box, ready to go into the environmental growth chamber.

The aluminum plates placed on top of the solid media layer had been separately pressure-cooker sterilized at 1bar and 121C for 30 minutes. Above the aluminum plate was placed a block of agar-solidified SCMM block—that from now on will be referred to as the feeding block. This was placed so that the mycelia would have a source of food, since there was none otherwise on the bare aluminum plates. The feeding blocks were of variable size and mass, to test the effects of nutrient availability on growth. The 'large' feeding blocks were approximately 15x15mm, and the 'small' feeding blocks were approximately 7.5x7.5mm. All feeding blocks were of the same thickness. The initial masses of the feeding blocks for all samples tested are shown in Table 2.1. The feeding blocks were inoculated with previously grown solid-state *S. commune* mycelium, which was described in Section 2.2.2. Inocula were placed directly on top of the feeding blocks, centered as well as possible using the needle tip method. From here the mycelium could theoretically grow radially in all directions on the surface of the aluminum. The petri dishes were finally placed with lid unsealed into a grow box lined with wet paper towels, to initiate growth (Figure 2.2b).

Table 2.1 Initial feeding block masses for experiment "inoculum on top".

	Mass [mg]	Mass [mg]	Mass [mg]	Mass [mg]
Sample 1	132.9	899.5	113.3	779.7
Sample 2	117.5	672.4	115.7	741.8
Sample 3	120. 3	847.0	163.5	846.0
Average	123.6	806.3	130.8	789.2
STD	6.7	97.1	23.1	43.1

The second setup—which we have called 'inoculum to the side'—was intended to compare mycelial growth on various aluminum surfaces. This setup, like the previous, has two variants: one in which there is food underneath the plate, and one in which there is only food at the edges of the plate (Figure 2.3a). In the first variant, ~10ml of still-liquid, freshly-sterilized agar-based SCMM was poured around the edges of sterilized 50x50mm aluminum plates in 90mm petri

dishes. The second variant was the same expect there was already a layer of ~20ml of solidified, sterilized, agar based SCMM at the bottom of the petri dish. The purpose of these two variants is to compare how difference in nutrient availability (10ml vs. 30ml of SCMM) effects mycelial growth on aluminum plates. After-solidifying, the petri dishes were inoculated with solid-state-grown *S. commune* inoculum about 4-5mm from the edge of the aluminum plates. The petri dishes were closed and then placed in a grow box with wet paper towels to maintain humidity (Figure 2.3b). Aluminum 2024, 7075, and 6082 were tested using this setup to compare growth of mycelia on different alloys. Further, plates with 'degreased only' and 'degreased & grinded' surface treatments were tested for each alloy to investigate how the near-surface deformed layer may affect mycelial growth on aluminum.
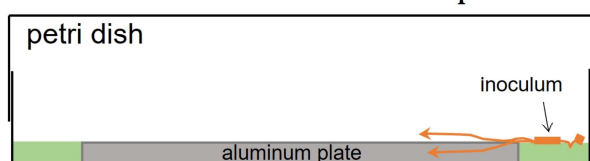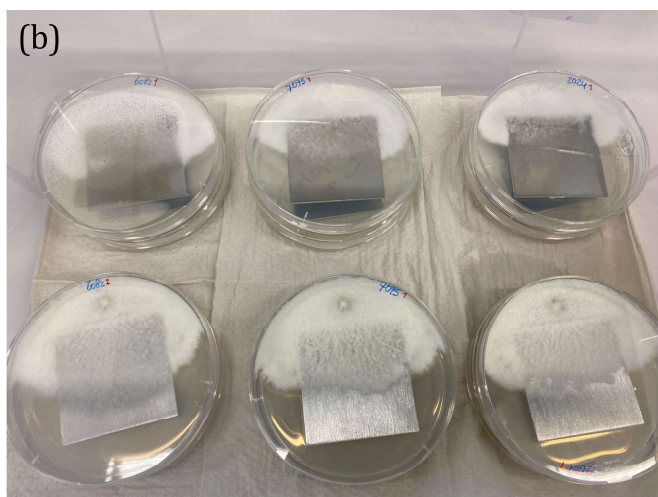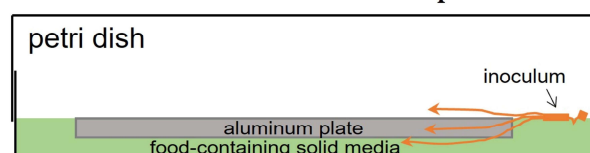
Figure 2.3 Growing mycelium on aluminum: inoculum to the side. (a) cross-section of the petri dish in which mycelia were grown onto aluminum plates. The orange arrows represent possible growth directions for the inoculum of mycelium. (b) image of the inoculated petri dishes in a grow box, ready to go into the environmental growth chamber.

2.2.5 Growth conditions

Once the petri dishes were inoculated with mycelium, they were set to grow. All dishes were put into one sealed plastic container (grow box), which was lined with wet paper towels at the bottom, to keep the humidity high. The petri dishes were left with lids on but unsealed, to allow

gas exchange. The grow box was placed in an environmental growth chamber (Sneijders incubators) with constant temperature at 30°C, and relative humidity at 55%. The petri dishes were left to grow for a set amount of time, only being removed for picture taking. The growth time for 'inoculum on top' setups was 14 days, and for 'inoculum to the side' was a maximum of 27 days. We limited the number of occasions on which samples were removed from the growth chamber for picture taking, as this required exposing them to low humidity environments. Fluctuating humidity could effect the fungi by temporarily stunting new hyphal growth, and permanently ending growth in case of severe drought [29]. Nevertheless, pictures were taken in between, so this effect must be taken into account. After the final pictures were taken, the metal plates were separated from their petri dishes and left out on the counter to dry out for a minimum of 48 hours.

2.2.6   Imaging and microscopy

Pictures of mycelial growth on aluminum were taken by our collaborator at Utrecht University, using a Nikon Z6 optical camera in a dark room with focused lighting (Figure 2.4a). Conditions were kept as much the same as possible, though in one case camera shutter speed settings had to be changed to adjust brightness for a nice image. This may act as a source of error for the analysis done later in this section. Further, samples which were grinded proved difficult to image with proper contrast. The setup shown in Figure 2.4b was found to produce images with nice contrast, and so was used for one set of grinded samples on various aluminum alloys. After that, our collaborator at Utrecht discovered that nice contrast could be achieved in the setup shown in Figure 2.4a by orienting the samples so that the grinding scratches were perpendicular to the incoming light from the illuminating lamps. All samples except for one grinded set were imaged this way. Nevertheless, this difference in imaging represents a potential source of error and thus is noted where relevant in the results and discussion.

A laser-scanning microscope was used to investigate the surface characteristics of mycelial biomass grown on aluminum. This was done at TU Delft, after the samples had been transported from Utrecht for analysis. The microscope was a Keyence VK-X3000 series 3D surface profiler, laser confocal microscope. The high-resolution images taken for analysis in this work were done in optical mode, using automated brightness and contrast settings. The magnification used is noted in the caption of each figure where it is relevant.
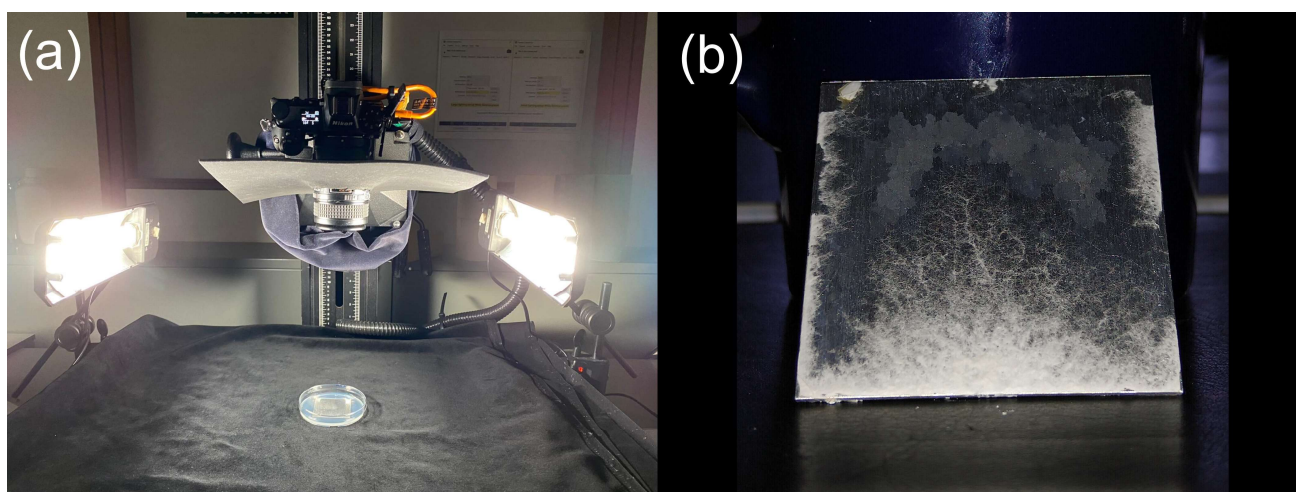
Figure 2.4 Imaging setup for capturing mycelial growth on aluminum. (a) Optical imaging setup at the University of Utrecht, were majority of imaging was done by our collaborator. This photo is the work of J. Brandhof at the University of Utrecht, Microbiology, In cases where surfaces were grinded unidirectionally, they were oriented so that the scratches were perpendicular to the incoming light. This gave the best quality image. (b) How surface coverage was imaged for specific grinded surfaces, for which it was not possible to achieve high contrast with the setup at Utrecht University. Those images were taken with a phone camera, in a dark room with flash on.

2.2.7 FTIR and TGA

One IR spectra of mycelial biomass was obtained using a PerkinElmer Spectrum 100 FTIR. First, the crystal was cleaned with acetone, and a reference spectrum was obtained using 16 scans. A small piece (~10mg) of mycelial biomass was removed from a culture grown on Al 6082 in the 'inoculum to the side' setup, with the 'food underneath' variant. This biomass was placed onto the crystal and clamped down with a force value of 50. The IR spectra was then obtained as the average of 16 scans. This sample of biomass is not necessarily representative of mycelial biomass from other aluminum surfaces, or those grown in the other setup.

One thermal degradation curve of mycelial biomass was obtained using a PerkinElmer TGA 4000 thermogravimetric analyzer. First, a ceramic sample pan was cleaned out to remove previous debris. Then, a ~3mg piece of mycelial biomass—from the same sample as for the FTIR measurement—was loaded into the TGA. The TGA was run in N_2 atmosphere, from 30 to 600°C at 5°C/min. After reaching 600°C, there was no carbon residue remaining in the sample pan.

2.3   Results

2.3.1   Mycelium growth characteristics

The first result of this work is that *S. commune* mycelium can grow on bare aluminum alloy surfaces. The way that it grew in our petri dish setup is shown in Figure 2.5. Growth starts with a needle-tip inoculum from a previously grown solid-state culture at the far side of the aluminum plate, on agar-based *S. commune* minimal media. The mycelium grows rapidly, reaching the aluminum plate in less than 3 days. After that, growth slows on the plate, while the mycelium preferentially extends around the plate on the food-rich medium. Between days 4 and 13, the mycelium continues to grow in the petri dish, though mostly avoiding the aluminum. Nevertheless, on all sides, the mycelium encroaches onto the metal at least a small distance. By day 14 mycelial growth reaches its maximum, and no further growth on the aluminum plate occurs. Something occurred between days 16 and 20 near the far side of the plate, where a large spot of discoloration occurs, right at the limits of the mycelial growth. Interestingly, this spot shows after a large amount of water accumulated on the surface at day 16. It is important to note that this growth is only representative for samples grown under similar conditions. It was not possible to collect such detailed time-lapse images for each sample and each growth condition. From our observations during the growth of the other samples, this kind of growth— surrounding the plate and encroaching from all sides—is a common occurrence in this kind of petri dish setup.
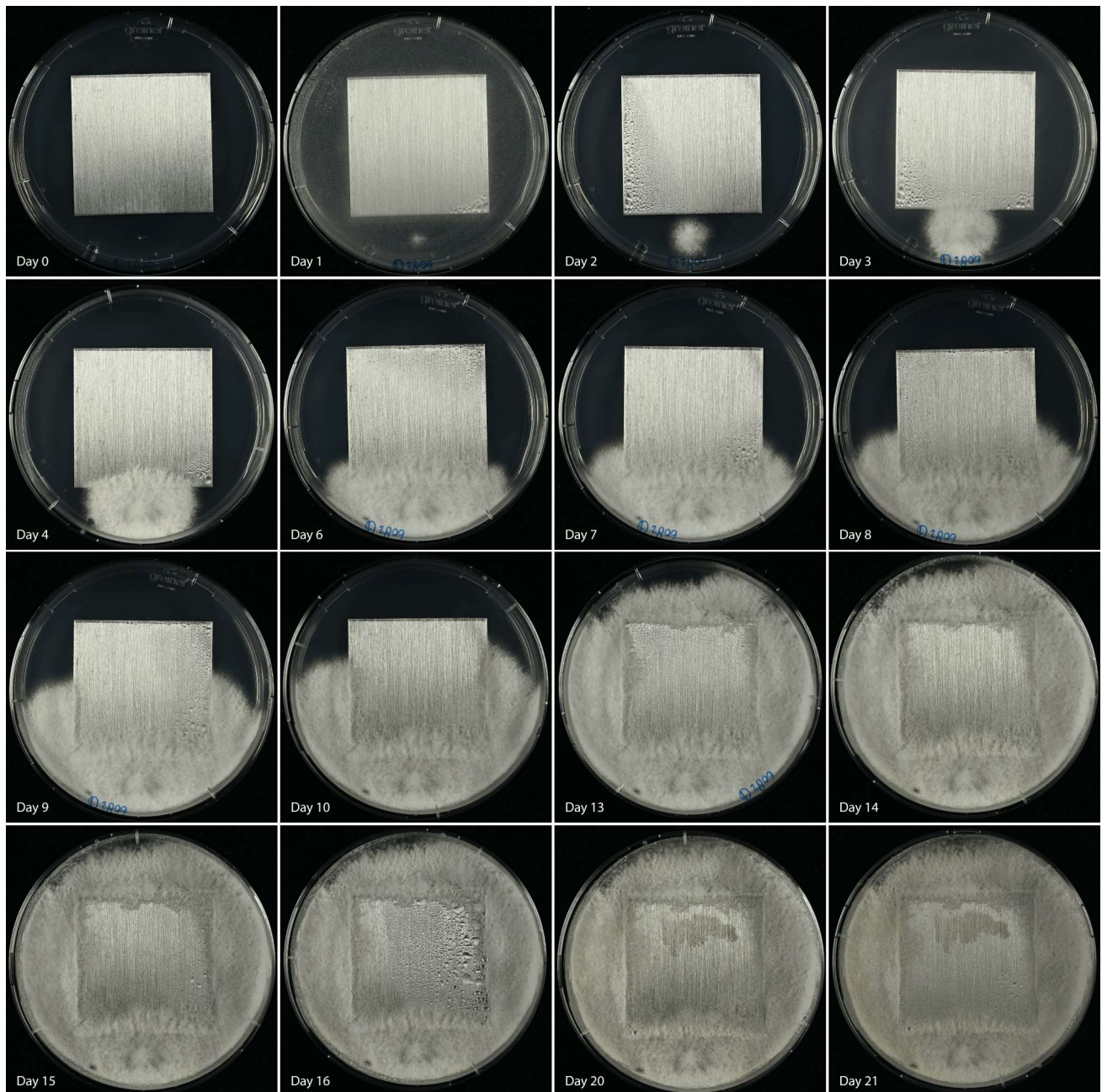
Figure 2.5 Time-lapse of mycelium growing on aluminum 6082. The series of images shown is one sample of Al 6082 that was prepared to the 'degreased & grinded' condition. The petri dish was prepared in the food-scarce condition with no agar medium underneath.

In both food-rich and food-scarce conditions, mycelium was able to grow on bare aluminum surfaces. The cropped-out surfaces of two samples—one food-rich and one food-scarce—at the end of their growth cycle are shown in Figure 2.6. In both cases, mycelium grew a random hyphal network structure and covered the aluminum heterogeneously (Figure 2.6a&d). Further, there are areas of high- and low-density growth—with higher density growth at the edges of the

aluminum plate, especially in the food-scarce condition. In both cases there are large agglomerations of hyphae, reaching up to hundreds of microns in width (Figure 2.6a&d). Mycelia in both conditions grew both on and off the surface—the particular spots shown in Figure 2.6b,c,e&f demonstrate that hyphae are growing as much as 60μm off the surface. This feature is heterogenous across the surface, so in some cases growth could be thicker or thinner. It also appears that there is a difference in the diameters of hyphae at the surface, and those far above the surface. The hyphae far above the surface are known as aerial hyphae according to other research, and those at the surface are called biofilm hyphae [18]. It appears in this case that the aerial hyphae are thinner and more intertwined. It is most important to note that in both food-scarce and food-rich conditions, mycelia grew both surface-level and aerial hyphae. In our investigations, we observed these surface-level and aerial hyphae on all mycelia grown on aluminum.
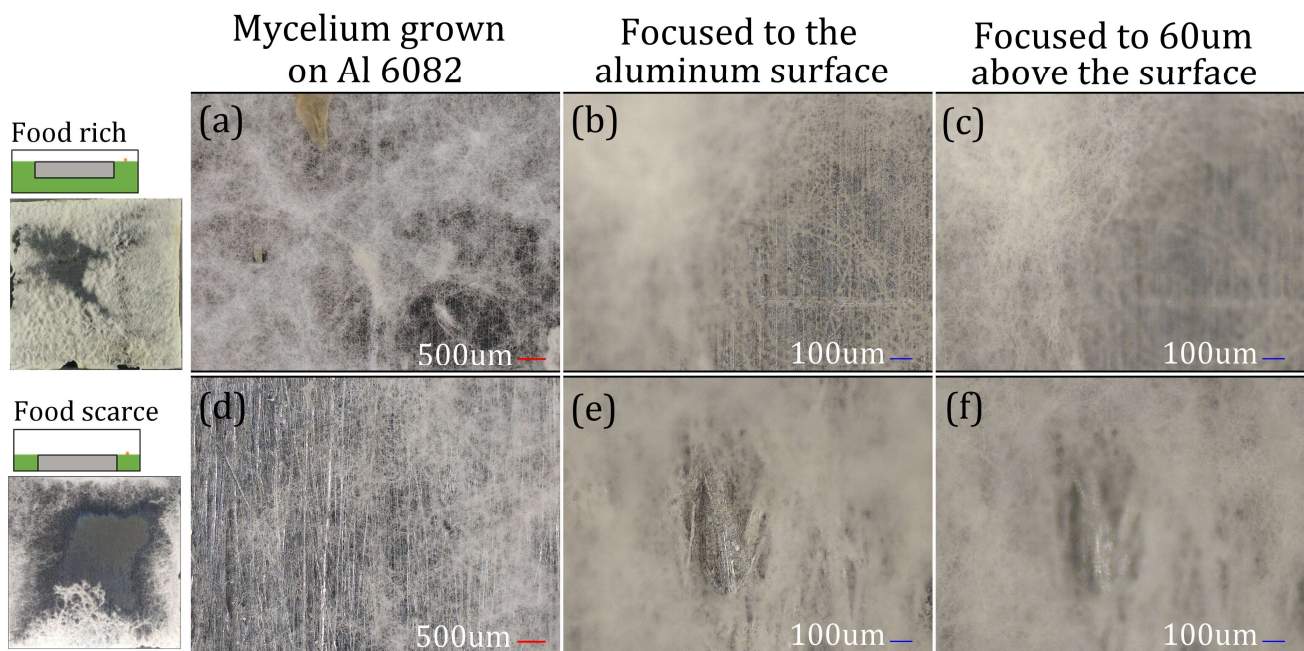
Figure 2.6 Morphology of mycelium grown on aluminum: comparison of food rich to food scarce conditions. (a,b,c) microscopic images of mycelium on aluminum 6082 (degreased only) in the setup with food underneath the aluminum plate at day 27. (d,e,f) microscopic images of mycelium on aluminum 6082 (degreased & grinded) in the setup without food underneath the aluminum plate at day 21. (a, d) 2.5x magnification of mycelium on the surface. (b,c,e,f) 10x magnification of mycelium on and above the surface.

Another important characteristic of mycelial growth on aluminum was the presence of hyphal aggregates. These structures were present on only the mycelia grown in food-rich conditions Figure 2.7. They were present independent of the surface conditions or alloy of the aluminum. These structures match the description of what fungal biologists call "cords" or "rhizomorphs" [22]. This may be the first time these hyphal cords have been recorded in such detail with *S. commune* grown in solid-state. In Figure 2.7a the presence of these cords is noticeable running down the length of an Al 6082 plate. Figure 2.7b shows the scale of these structures, which are hundreds of microns wide and more than a millimeter in length. Compared to the size of one hypha—with a diameter of 1 to 5µm—these are enormous aggregations of material. These cords are also present on the mycelium that grew on Al 7075 (Figure 2.7c). Figure 2.7d illustrates how a number of individual hyphae spread out across the surface came together to form a cord with a diameter of around 50µm. It is not clear from this image if the hyphae were growing first, and then formed the cord, or if the cord spread out into many hyphae. The important takeaway is that these structures were present all over the surface of aluminum plates in food-rich conditions.

Al 6082 food rich   Al 7075 food rich
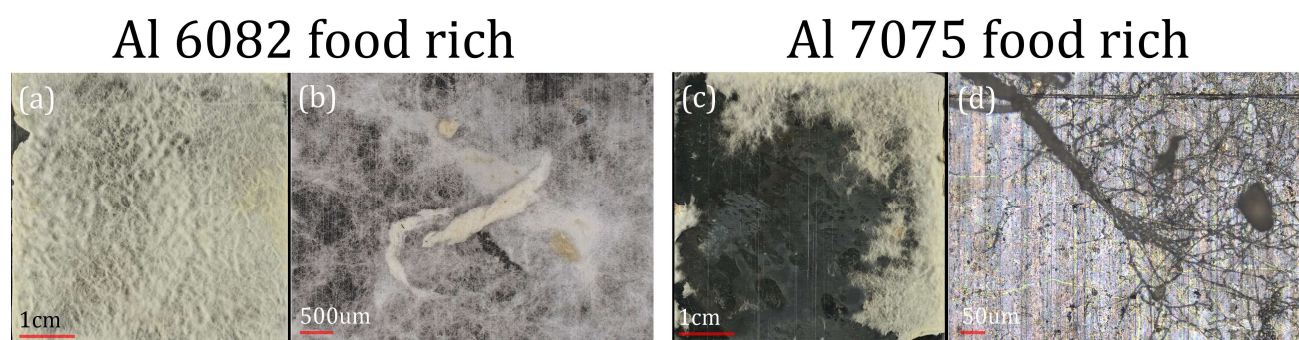
Figure 2.7 Hyphal aggregates ("cords") that grew on aluminum surfaces. (a) cropped image of mycelium grown on Al 6082 with a degreased only surface, showing the presence of hyphal cords all across the surface. (b) same sample as (a) at 2.5x magnification zoomed in on one hyphal aggregation. (c) cropped image of mycelium grown on Al 7075 with a degreased only surface, (d) same sample as (c) at 10x magnification zoomed in on a hyphal cord spreading out onto the surface.

Further investigation of mycelial growth on aluminum surfaces revealed interesting growth characteristics. Firstly, hyphae seem to grow in "highways", rather than by radially extending growth that we could expect under normal conditions [25]. The highway shown in Figure 2.8a is between 100-200µm wide and grows at a 45° angle to the parallel lines in the aluminum surface created by rolling processes during production [68]. Surprisingly, this hyphal highway takes a sharp 90° turn to grow a new branch in a perpendicular direction. Notice how the other areas of the surface in Figure 2.8a are only sparsely occupied by hyphae. We observed these sorts of highway growth patterns in all samples, regardless of surface condition or food scarcity. Next, we observed some hyphae growing perpendicular to the scratch direction of aluminum surfaces prepared to the 'degreased & grinded' condition (Figure 2.8b). This behavior was only visible in the low-density growth areas on samples in food-scarce conditions, though we can't rule out that it may have also occurred in food-rich conditions. This behavior appears to be a sort of hyphal tropism, in fact, there have been reports of fungi growing perpendicular to ridges and surface roughness [25].
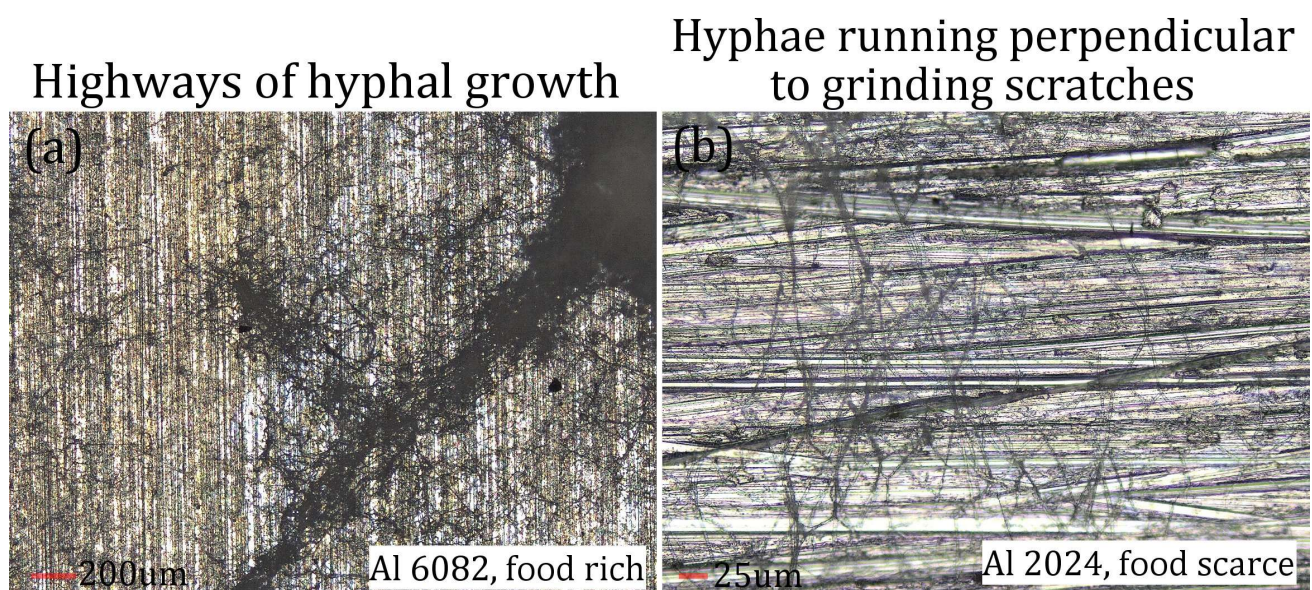
Figure 2.8 Interesting features of mycelial growth on aluminum. (a) 5x magnified image of mycelium that grew on Al 6082 degreased only surface in the food rich condition. Notice how the hyphae are growing in specific paths along the aluminum, and how the hyphae take a 90° turn. (b) 20x magnified image of mycelium grown on Al 2024 with a degreased & grinded surface in the food scarce condition, showing hyphae growing perpendicular to grinding scratches.

The final feature of mycelial growth that stood out was a distinct discoloration of the hyphae to an orange shade. Figure 2.9 demonstrates this effect on one sample of Al 7075 degreased only, in the food-rich condition. However, we observed this effect to at least some extent on all samples, regardless of aluminum surface condition, alloy, or food scarcity. Furthermore, we know this discoloration occurred during growth, and not after, since mycelium was discolored already at day 14 of growth, in the case of the sample shown in Figure 2.9. In Figure 2.9a, mostly the mycelium at the growth front is discolored, as opposed to Figure 2.9b, in which the discoloration is widespread. These images were taken at the same time, so whatever causes the discoloration is not homogenously distributed across the surface of the aluminum. Further, the heavy discoloration of hyphae at the growth front (Figure 2.9c) hints at the possibility that these hyphae are taking up something that changes their color, which then gets transported through the rest of the mycelial network. In any case, it seems that this discoloration effect is caused by the interaction of mycelium with the metal surface.

Pigmented mycelium on Al 7075
degreased only, food rich
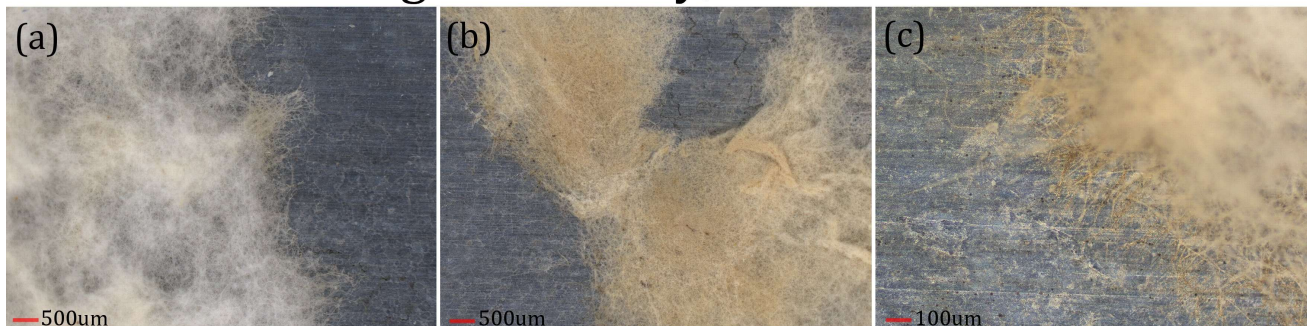
Figure 2.9 Pigmentation of mycelium that grew on aluminum. (a) 2.5x magnified image of mycelium grown on Al 7075 with a degreased only surface in the food rich condition, showing the presence of slightly discolored mycelium at the growth front. (b) same sample as (a) at 2.5x magnification showing widespread discoloration. (c) same sample as (a) at 10x magnification showing discolored hyphae at the aluminum surface.

2.3.2   Aluminum surface corrosion after mycelial growth

An unexpected result of this work was the discovery of unique forms of aluminum surface changes, that we interpret as corrosion. Corrosion did not occur on all samples on which mycelium grew. Further, it is uncertain if corrosion occurred in the area underneath the mycelial biomass, as the biomass was never removed. One cause of corrosion may have been the micro-environment inside the petri dish, as it was 100% humid inside the petri dish. Unfortunately, we did not test a reference sample of an aluminum plate in a petri dish setup without mycelium, as that would have shed light on whether the mycelium was the causing agent of the corrosion. In any case, there are notable differences in the types of corrosion between 'degreased only' and 'degreased & grinded' surfaces, which are reported here.

On the 'degreased only' aluminum surfaces, corrosion was widespread on all three alloys (Figure 2.10). In all cases, the features shown were present by day 14 of mycelial growth. Unfortunately, we do not have any pictures of the surfaces from before day 14, so we can't say with certainty when those features appeared. Nevertheless, the features were not present before the plates were placed in the Petri dishes, so we can say that the corrosion occurred during the mycelial growth experiment. The Al 2024 plate in Figure 2.10 shows three local dark regions. At higher magnification, those regions show separated grains (of the same color as the aluminum surface) surrounded by a black region between the grains. The grains have diameters ranging from 10 to 500µm. This may be some form of intergranular corrosion, but it is difficult to say with certainty. Al 6082 shows similar patterns of corrosion, though in that case, the black regions surrounding the grains appear much more widespread. On Al 7075 the intergranular corrosion is present, as well as orange spots that may represent some kind of oxidative event. In all cases, there is no correlation between where the mycelium has grown and where the corrosion has occurred. It is interesting to note that some of the hyphae in region 3 on Al 7075 are black as opposed to clear colored, suggesting that they may be picking up ions that change their color from the corroded area.

Corrosion on 'degreased only' surfaces

Al 2024
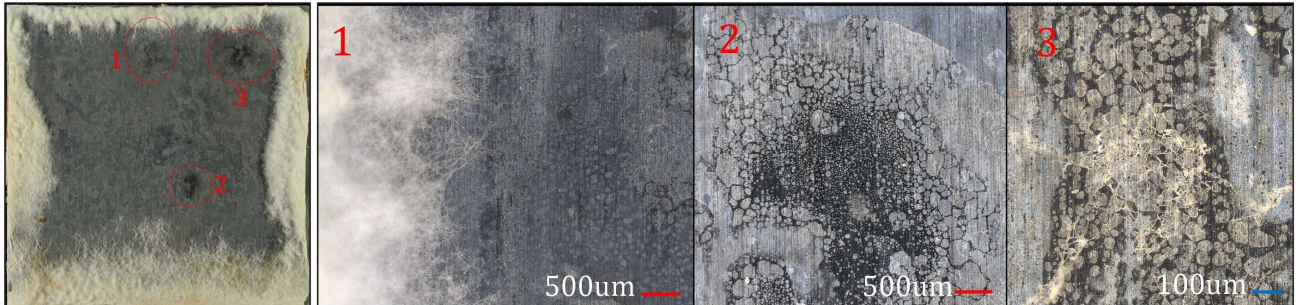
Al 7075
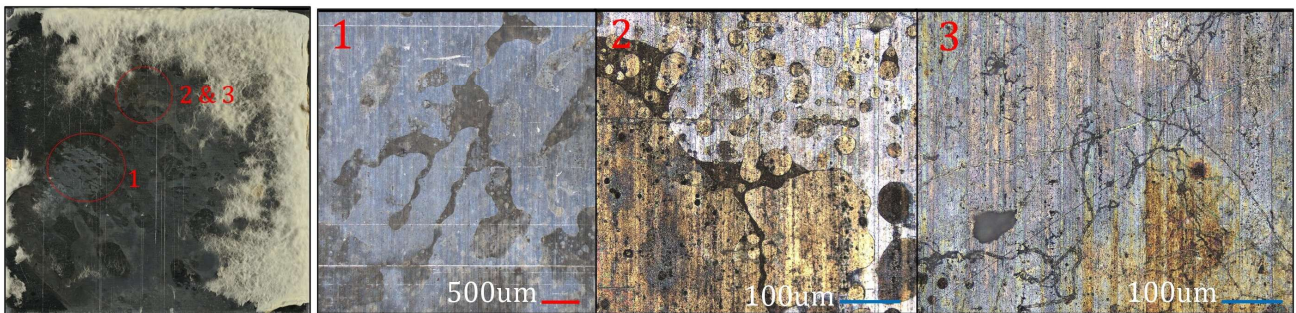
Al 6082
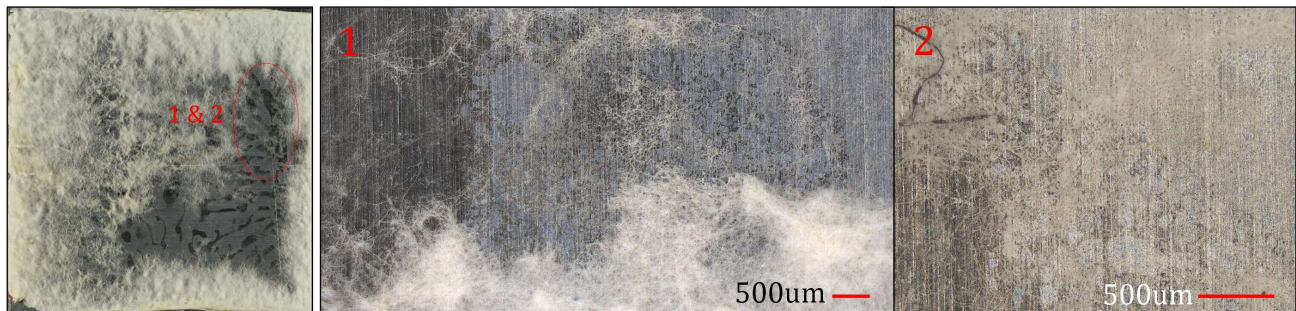
Figure 2.10 Corrosion features of 'degreased only' aluminum surfaces taken after mycelial growth. The samples shown here for each alloy are representative of the population of 'degreased only' aluminum plates in the food rich setup. These select samples are meant only to illustrate some of the types of corrosion observed, there were many more unique corrosion features that are omitted as aluminum corrosion is not the main focus of this report.

On the 'degreased & grinded' aluminum surfaces, corrosion looks quite different (Figure 2.11). Firstly, corrosion in all cases occurred suddenly between days 16 and 20, while the 'degreased only' surfaces were already corroded by day 14. We previously mentioned how a large amount of water had precipitated on the surfaces on day 16, right before the corrosion spots appeared. Further, the corrosion on the grinded surfaces was highly localized and occurred almost exclusively in regions of the surface where mycelium did not grow. Aluminum 2024 was the least corroded of the alloys, with spots (~100 to 200μm) of discoloration appearing in one region of the surface. The plate of aluminum 7075 had a much larger region of corrosion and a smaller region where corrosion was much more severe. In this region (2&3) it appears some material has been deposited on the surface. Those deposits are around 50μm or less in diameter and reached up to 40μm above the surface. Further, it seems the mycelium grew on top of these deposits and bridged them together. These deposits only appeared exclusively on the aluminum 7075 surfaces. On aluminum 6082, the corrosion is similar to the intergranular kind seen in Figure 2.10, though in this case, the grains are a darker color, rather than their surroundings. At higher magnification, those grains appear to be colored spots on the surface. No cracking or physical separation of grains is noticeable.

Corrosion on grinded surfaces

Al 2024
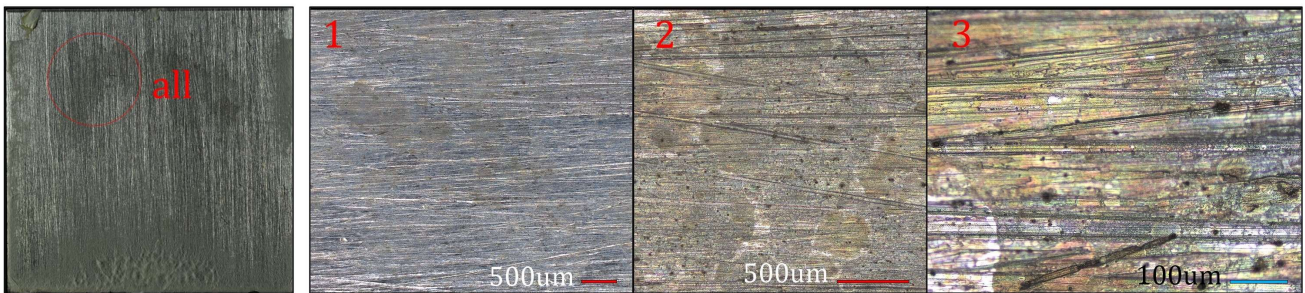
Al 7075
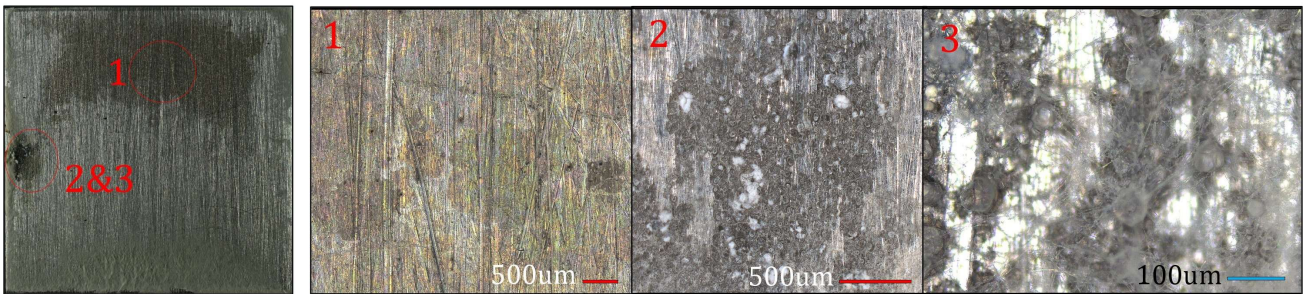
Al 6082
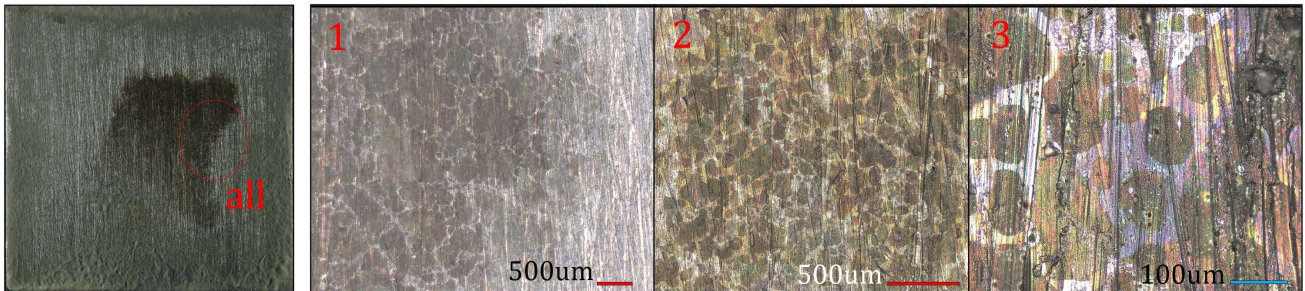
Figure 2.11 Corrosion features of 'degreased & grinded' aluminum surfaces taken after mycelial growth. The samples shown here for each alloy are representative of the population of 'degreased & grinded' aluminum plates in the food scarce setup.

2.3.3 Chemical structure & thermal degradation of the mycelium

The infrared spectrum of mycelial biomass obtained from one of the aluminum 6082 surfaces is shown in Figure 2.12. It is unclear how this biomass would differ when taken from different aluminum surfaces, or conditions, therefore this spectra is not necessarily representative of all the mycelia grown on aluminum in this work. The peaks present in this spectrum can be separated into three main categories: polysaccharides, proteins & chitin, and lipids & fatty acids. As discussed in the introduction, polysaccharides make up the majority of the fungal cell wall chemically. The large peak at 1034cm^{-1} is caused by C-O stretching [69-72], which is expected for *S. commune* fungi as it is glucan-based and has many C-O bonds along its alpha- and beta-glucan network. The nearby peaks at 1075cm^{-1}, 1103cm^{-1}, 1145cm^{-1}, and 1250cm^{-1} similarly represent C-X single bond stretching [69-72] of polysaccharides in the cell wall. The peaks at 1372cm^{-1} and 1554cm^{-1} may be caused by N-O stretching of nitro compounds [69-72], which are present in mycelial biomass in the form of amino acids and proteins. The peak at 1635cm^{-1} is commonly associated with N-H bending of primary amides and the peak at 1722cm^{-1} with C=O stretching of amides and/or esters [69-72]. These bonds are present in both proteins and chitin and thus these peaks represent the presence of both of those components from the cell wall. Finally, the peaks at 2850cm^{-1} and 2925cm^{-1} are both caused by H-C-H stretching [69-72], which is a type of vibration that would occur in lipids and long-chain fatty acids. These are present in the hyphal cell wall and are also part of their excretions [36]. The peak at 3300cm^{-1} broadly represents hydrogen-bonded O-H stretching [69-72], which can be obscured by absorbed water, so is difficult to interpret.
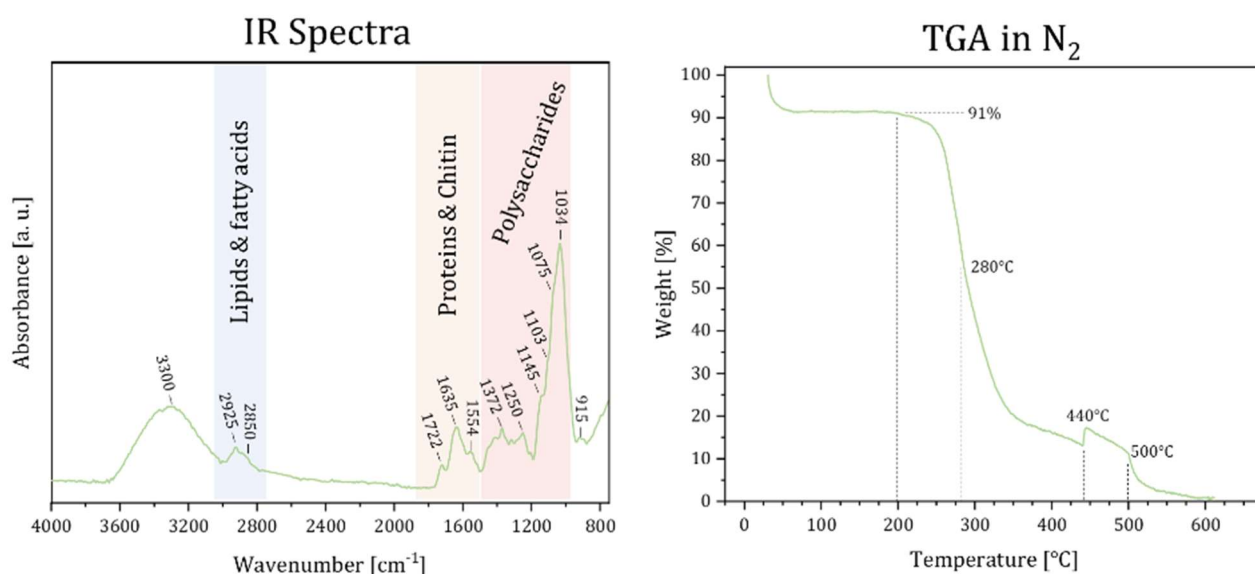
Figure 2.12 IR Spectra & TGA curve of mycelial biomass grown on aluminum. Both tests were performed on a small amount of biomass taken from mycelium grown in food rich conditions on aluminum 6082 in the 'degreased only' condition.

Another way to gain insight into the chemical composition of a material is by thermal degradation analysis. The weight-loss-on-heating curve in Figure 2.12 shows a two-step degradation process for mycelial biomass. First, the absorbed water content (~9%) evaporates at well below 100°C. Such low-temperature evaporation indicates that the water was mostly free-standing in the material, and not highly bound. The next step starts at around 200°C and represents the main degradation step of the organic material in the biomass. This step proceeds until 350°C, volatilizing approximately 80% of its weight. The next step is a slower degradation until complete volatilization at 600°C. This step likely represents the breakdown of more chemically complex molecules like chitin into simpler molecules that can be volatilized away. There is an interesting jump at 440°C indicating about 5% weight gain, though this is not likely to represent some kind of oxidation or chemical reaction accumulating more mass. It more likely is a testing error as the weight drops again rapidly at 500°C back to expected values.

2.3.4   The effect of nutrient availability on mycelial growth on aluminum

To delve deeper into how the availability of nutrients affects mycelial growth on aluminum, we grew mycelium using the 'inoculum on top' setup described in the methodologies. For this experiment, feeding blocks of agar-based SCMM were inoculated with solid-state-grown mycelia. The mycelia then grew off these feeding blocks onto the aluminum plate underneath as they searched for more food sources. By day 6, the aluminum surfaces appeared as shown in Figure 2.13. In almost all cases the mycelia had reached at least one edge of the plate by day 6. Exclusively underneath the aluminum plate was another block of agar-based substrate—which either contained distilled water (Set A&B) or SCMM (Set C&D). Further, the feeding blocks were of different sizes, which were previously reported in Table 2.1 Initial feeding block masses for experiment "inoculum on top" (Table 2.1). In this section, we will report how the changing variables of feeding block size, and the presence of food underneath affected mycelial growth. We split up the growth effects into two categories: growth extension and aluminum surface coverage.

Mycelial growth extension is the furthest distance that hyphae traveled radially along the aluminum plate. There are interesting differences between the sets regarding this characteristic (Figure 2.13). Firstly, there were three samples (Set B #2, #3, and Set C #1) that extended to shorter average distances than the others. It is unclear why this happened, though notice how the aluminum plate underneath Set B #2 & #3 appears a lighter shade of gray than the other aluminum plates. It is possible these aluminum plates had different surface properties than the others or corroded during growth in a more severe way. All the aluminum plates came from the same sheet metal and looked identical before the experiment. Due to the extensive growth of Set B #1, we could expect the difference in the growth of Set B #2 and #3 to be caused by surface properties and not by nutrient availability. Indeed, the samples with large feeding blocks in Set D grew ~7 to 8% further than samples with small feeding blocks in Set A and C. Keep in mind that this difference may have been even larger if the plates were larger, and mycelia had more space to grow. Further, there was no difference in the average extension of mycelia with small feeding blocks between Set A and Set C. This indicates that the presence of nutrients underneath did not affect mycelial radial extension. However, we cannot rule out that the presence of nutrients underneath may have influenced growth speed. Unfortunately, day 6 was the earliest day that photos of the surfaces were taken, so those results cannot be shown.
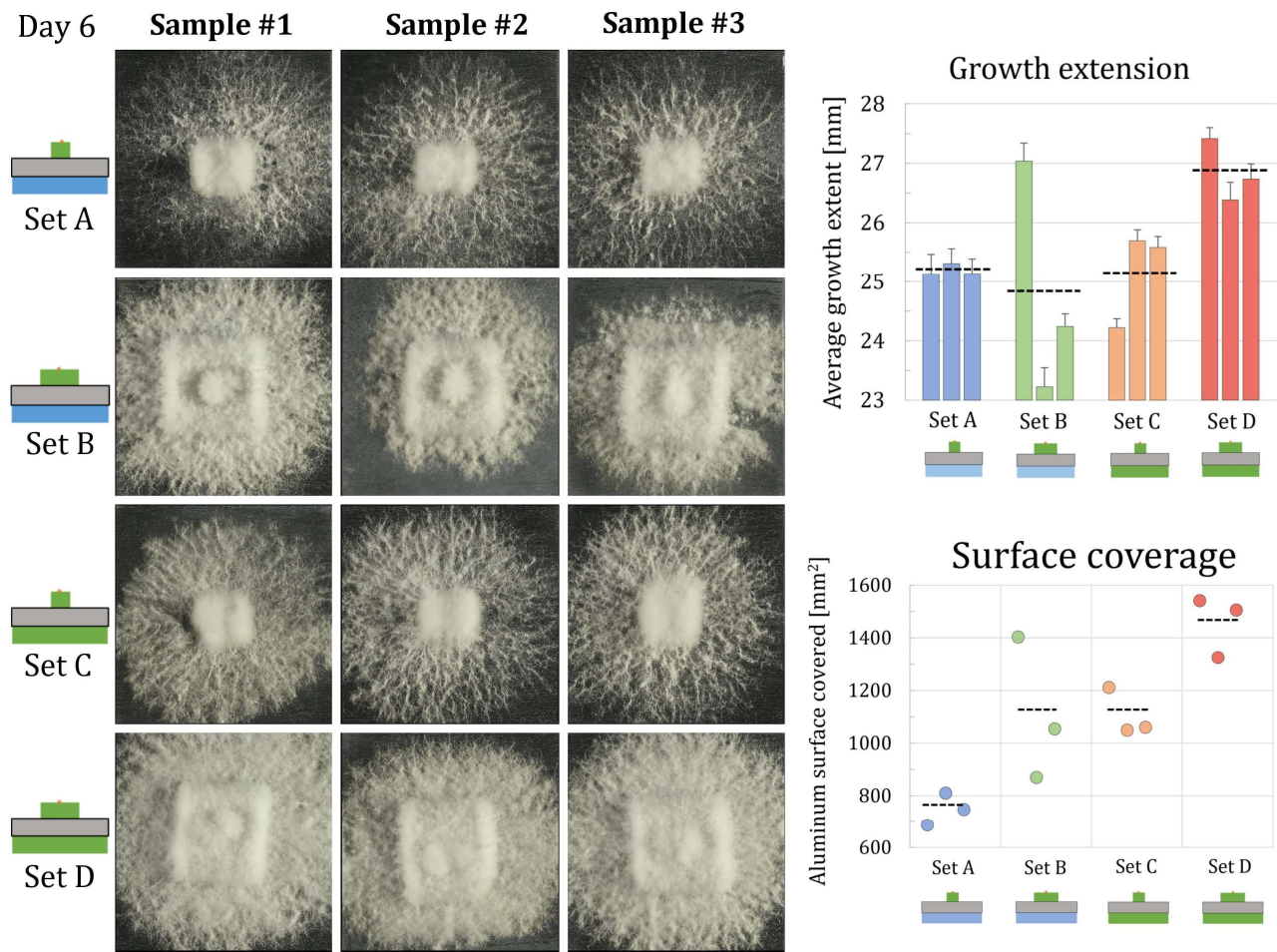
Figure 2.13 Growth of mycelia on aluminum plates: comparing how nutrient availability effects mycelial growth. The pictures shown are cropped out images of the aluminum plate surfaces at day 6 of growth. Growth extension was measured as the average radial distance extended by mycelium (average of 70 measurements). Surface coverage was measured by thresholding in ImageJ. The dotted black lines represent the average for each set.

Mycelial surface coverage represents a different physical phenomenon than growth extension—namely how densely the mycelium grows instead of how far. We analyzed samples for surface coverage using ImageJ processing and thresholding steps described in Appendix A. It is important to know mycelial growth density because it is possible for a mycelium to extend rapidly without branching much, or to extend slowly while branching frequently. These different types of growth would lead to various levels of surface growth density. There are interesting differences between the sets regarding mycelial surface coverage (Figure 2.13). Firstly, while Set A and Set C had similar growth extents, Set A has covered far less of the surface than Set C on average. This indicates that the presence of nutrients underneath the aluminum plate somehow

motivated the mycelia on samples of Set C to grow a denser network. There is also a distinction between the surface coverage depending on feeding block size. The mycelia grown with large feeding blocks always grew a denser network than those with small feeding blocks. In these cases, there does not seem to be much difference between those samples with and without nutrients underneath. The excess of nutrients available caused these mycelia to entirely blanket the surface, covering around 90-95% of the available aluminum surface.

Another interesting way to analyze the surface growth of mycelia on aluminum is to convert the images to grayscale and compare the grayscale histograms of the sets. This analysis is shown in Figure 2.14, and the details of it can be found in Appendix B. This analysis shows another perspective on the differences in growth density discussed before. Peak 1, at a grayscale value of between 40 and 50, represents the dark pixels in the image resulting from the aluminum plate.
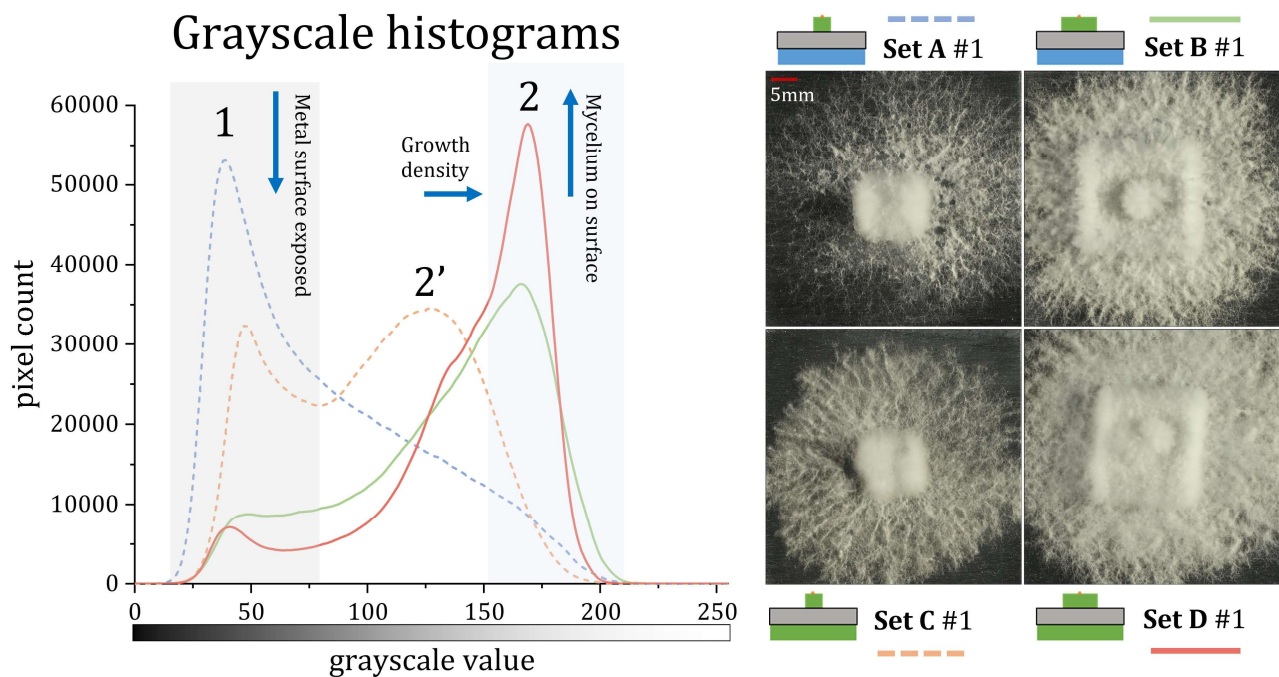
Figure 2.14 Grayscale value distribution of select samples from the three tested sets on day 6. For a detailed explanation of how this result was obtained, see Appendix B. Notice how 0 on the x-axis represents black, and 253 represents white, and everything between is on a spectrum from dark to light. It should be kept in mind that we showed here only one sample per set and not the average of all three samples per set. This was done to limit the confounding effect due to sample variability in Set B. The samples shown for other sets are representative of the other samples in their sets.

As expected, this peak is highest for Set A, then Set C, and is much smaller for Set B and D. This further iterates how much fewer dark values are coming through on the images for Set B and D due to the denser growth of white mycelia on the surface. It also drives home the point that mycelia grown with large feeding blocks in this experiment covered more of the surface available to them. Peak 2, at a grayscale value of around 175, represents the presence of white-colored mycelia on the surface. This peak is the largest for Set D, which is to be expected as it had a large feeding block and food underneath. Set B and Set C have similar heights at peak 2, indicating that they covered a similar amount of the surface. This interestingly indicates that mycelia with both small and large feeding blocks were able to cover the surface very efficiently. However, the fact that the peak of Set C occurs at a lower grayscale value than Set B tells reveals that it did not grow as densely. Because of that, more dark pixels appear in between the mycelial network, as opposed to Set B, which grew a dense network through which fewer dark pixels can show. This result suggests that although the size of feeding blocks used here did not affect the ability of mycelia to grow to cover the surface, the ones with larger feeding blocks were simply able to grow more biomass, which resulted in denser growth.

We followed the growth of mycelia on aluminum for this experiment through 14 days total. The evolution of surface coverage over time and the images of the aluminum surface through time for select samples are shown in Figure 2.15. The chart shows that mycelia from Set A already reached their maximum surface coverage by day 6. However, mycelia from all other sets continued growing at least to some extent. All samples from Set B increased in surface coverage between day 6 and day 9 and then stopped short of blanket coverage. The mycelia on these surfaces had large feeding blocks and thus plenty of food to support their growth for a few days more than the samples from Set A. For both Set C and Set D, the continued growth after day 6 was not a further extension of the colony on the surface, but a new extension from off the plate. This means that the mycelia on these surfaces reached the new food source underneath the plate, grew there, and then started to creep back onto the aluminum plates. Set C surface coverage increased until day 14, at which point it had not yet blanketed the aluminum. Set D, on the other hand completely covered the aluminum plate by day 9.
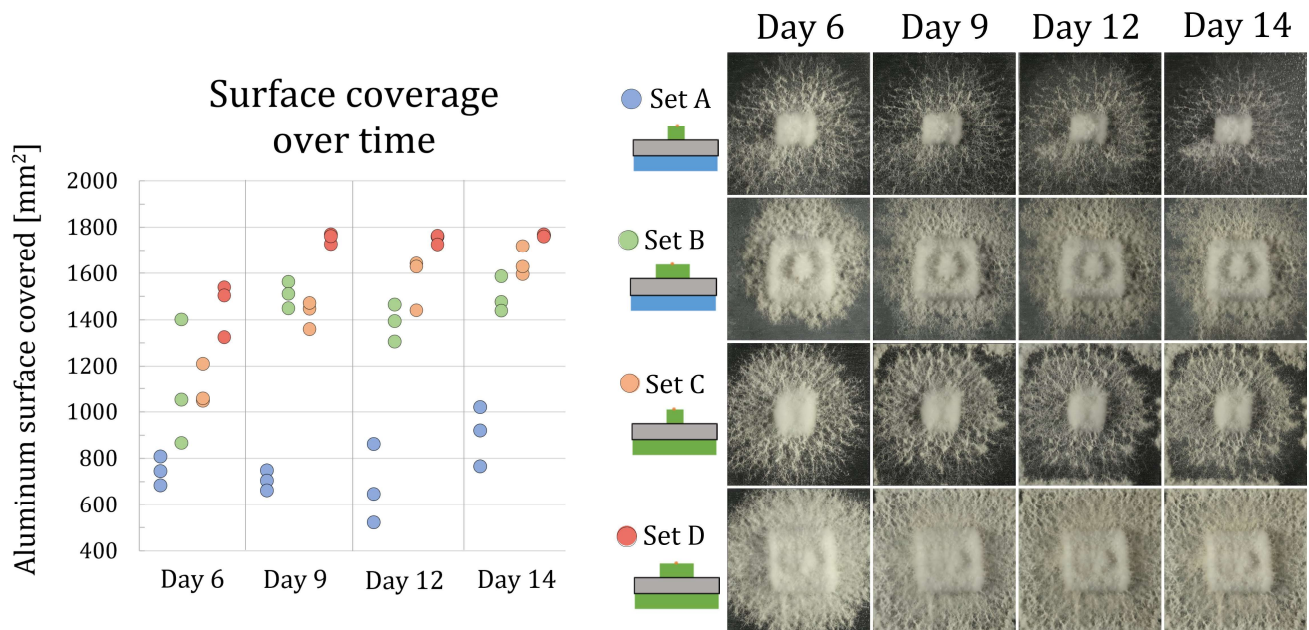
Figure 2.15 Evolution of mycelial surface coverage of aluminum through time: comparing the effect of nutrient availability. The surface coverage values were obtained by thresholding the grayscale-converted images to binary, and then measuring the area above the threshold. The select samples shown here were the following: Set A #2, Set B #2, Set C #3, Set D #3. We should note that the photo-taking conditions were variable between days—specifically between days 6 and 9 there was a change in the shutter speed, which may cause a change in image brightness.

2.3.5 The effect of aluminum surface grinding on mycelial growth

The next experiment was designed to shed light on how the surface properties of aluminum alloys affect the ability of mycelia to grow on them. The 'inoculum to the side' experimental setup described in the methodologies section was used for this. The first set of results describes the growth of mycelium on aluminum in food-scarce conditions. In this condition, the aluminum plates were surrounded by agar based SCMM on all sides, without any media on the surface or below the plate. In all cases for this setup, the mycelia grew on aluminum at least to some extent. In this section, we will go over the differences in growth extent and surface coverage of these plates based on the surface condition of the metal. The two surface conditions were 'degreased only', and 'degreased & grinded'. The degreased only surface was meant to simply remove dirt and grease from the surface, while the 'degreased & grinded' condition was meant to remove the near-surface deformed layer. The results for these growth sets are shown in Figure 2.16. The analysis method and steps as well as additional data are available in Appendix C.
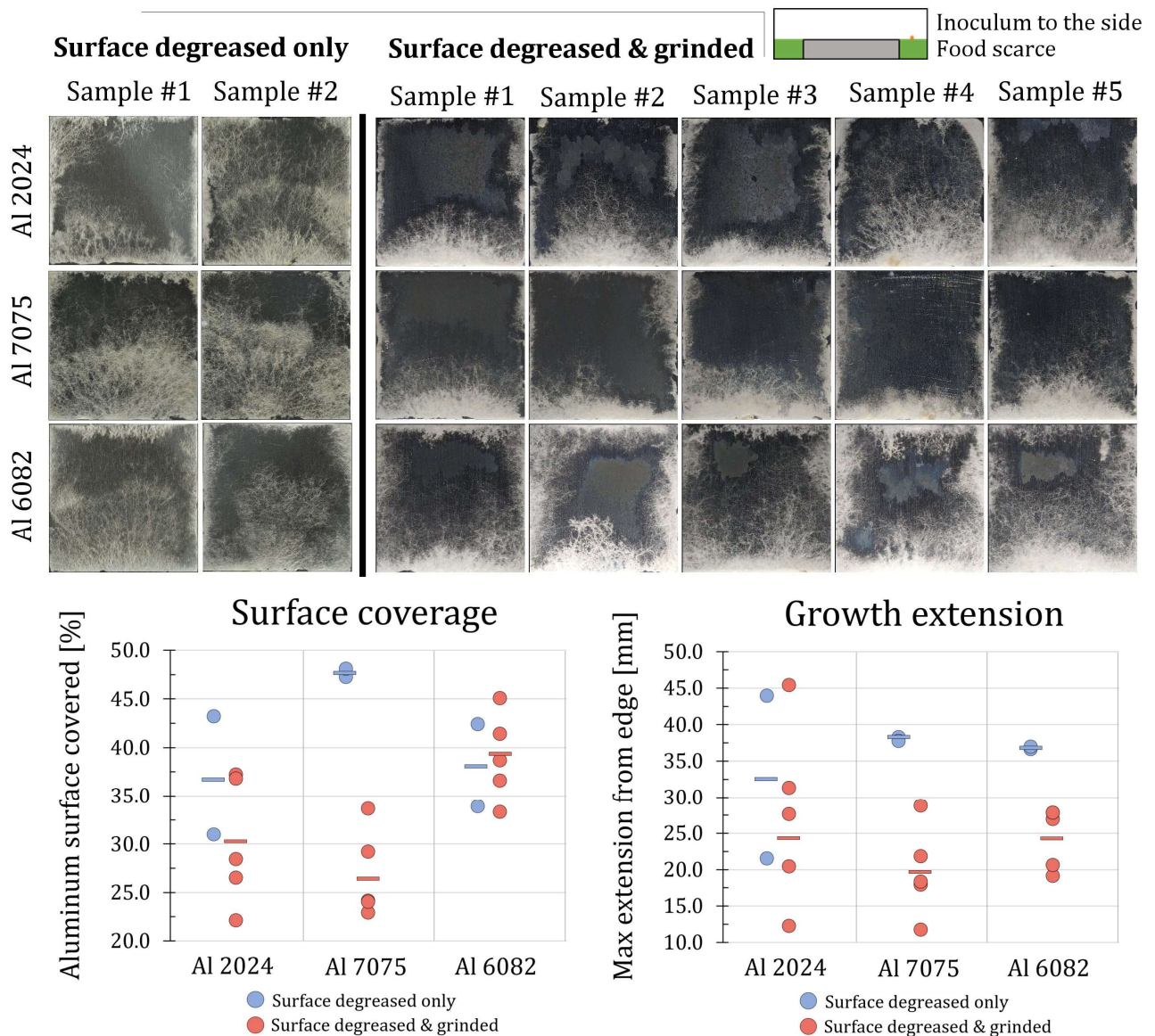
Figure 2.16 Surface coverage and growth extension of mycelium on aluminum alloy plates after 21 days of growth in food scarce conditions. Inoculum is represented by the orange dot to the side of the plate in the guide illustrations. Differences in metal color are artefacts of photographing, which took place under different conditions and with different cameras. Growth extension was measured as the furthest distance reached by the mycelium growing from the inoculum side (which is always oriented to the bottom in these images).

There are differences in the amount of surface covered of the three alloys, and also depending on if those alloys were grinded or not (Figure 2.16). Mycelia on 'degreased only' surfaces grew to cover between 30 and 48% of the surface after 21 days of growth. The sample size is low, but it seems that the mycelia grew to cover an additional ~12% more surface on Al 7075 compared to Al 2024 and Al 6082. Mycelia on 'degreased & grinded' surfaces grew to cover between 22 and 46% of the surface after 21 days. For Al 2024 and Al 7075, mycelia grew less on the 'degreased & grinded' surfaces compared to 'degreased only' surfaces, with ~6 and 20% less of the surface covered, respectively. However, mycelia grew to similar average coverage (37 to 40%) on Al 6082, regardless of surface condition. These results suggest that mycelia grow less on surfaces that were grinded, except Al 6082. Further, when the surface is 'degreased only', the mycelia grow most on Al 7075, and when the surface is 'degreased & grinded', the mycelia grow most on Al 6082.

The growth extension follows similar trends to the growth coverage (Figure 2.16). In this case, growth extension was measured as the further distance extended by hyphae from the inoculation side. Mycelia also grew onto the plates from the sides, after surrounding the metal and saturating the agar-based media. However, we are interested in how far the mycelia extended from only the inoculum side, as this hints at the ability of the mycelia to grow on that alloy. For growth extent, on average mycelia grew 7 to 17mm further onto the plate on 'degreased only' surfaces compared to 'degreased & grinded' surfaces, depending on the alloy. There is no clear difference between the averages of the alloys, other than in how variable the results were. On Al 2024, the mycelia grew extremely variably, extending on some samples up to 45mm, and others 10mm. On Al 7075, the mycelia extended almost 100% further onto the alloy when it was 'degreased only' compared to when it was 'degreased & grinded'. This is the largest difference among the alloys.

To further investigate how the surface condition of aluminum affects mycelial growth, we grew mycelia also in food-rich conditions. The results of this setup are shown in Figure 2.17. It is immediately obvious that mycelia grew far more densely in this food-rich condition compared to the food scarce condition. This is in line with the results from the previous section. On the 'degreased only' surfaces, there was high variability on Al 2024 and Al 7075, with mycelia in some cases only growing creeping onto the plate from the sides, and in other cases entirely blanketing the surface. For Al 6082, on average, mycelia grew to cover around 80% of the 'degreased only' surface. In the case of the 'degreased & grinded surfaces, all samples were nearly

completely covered, regardless of the alloy. Notice also how the mycelia on the 'degreased only' samples are a darker shade of orange, compared to the mycelia on the 'degreased & grinded' surfaces, which have a general white shade with some local yellowing.
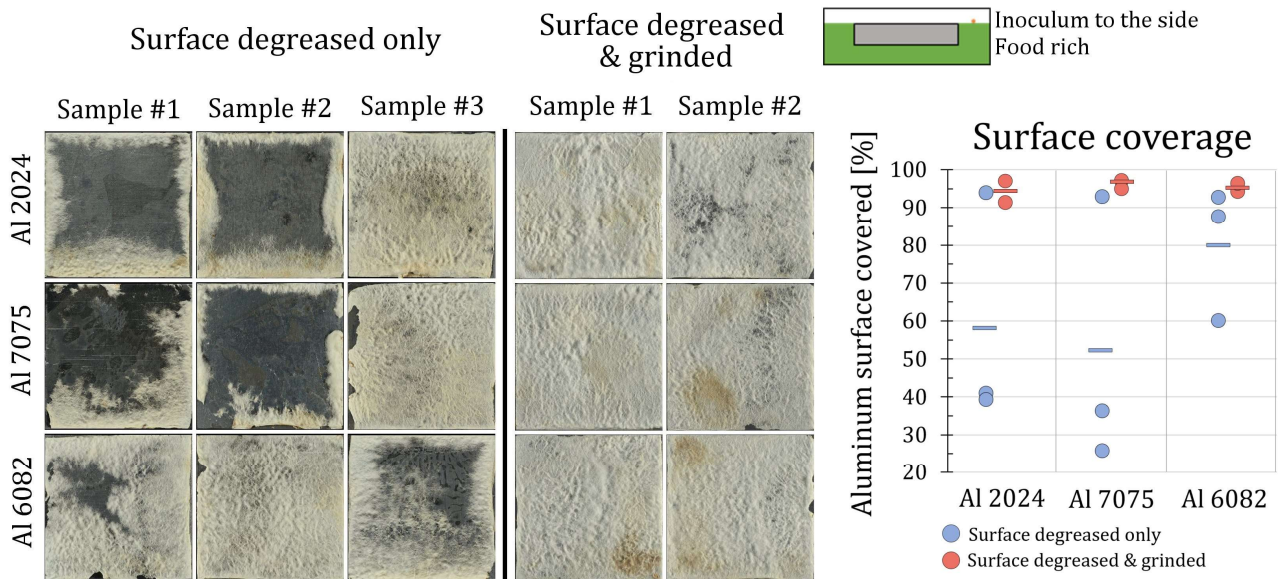
Figure 2.17 Surface coverage and growth extension of mycelium on aluminum alloy plates after 21 days of growth in food rich conditions. Inoculum is represented by the orange dot to the side of the plate in the guide illustrations.

2.4   Discussion

Mycelial colonization of an aluminum substrate under controlled conditions was demonstrated in this work for the first time. It is not entirely surprising that mycelia were able to grow on bare aluminum surfaces, as they can survive a large variety of environments. In many cases the mycelia grown here entirely covered the surface with solid biomass (Figure 2.17). However, in other cases the mycelia grew far less biomass at the surface. Since the aim of this work is to produce as much biomass as possible at the surface, it is interesting to try and understand how nutrient availability and metal surface characteristics were responsible for this. Firstly, blanket coverage was only reached by mycelia grown in the food-rich condition. It seems that the amount of food available to them in this condition was more than enough to support growth as far as 2.5cm from the nearest food source at the edge of the plate. This distance is quite far for a mycelium, which has hyphae with diameters ranging from 1 to 5µm. It is possible that long-distance transport of nutrients was supported by large cord structures of aggregated hyphae (Figure 2.7), that were present exclusively in this condition. In these structures, hyphae wrap around each other and fuse together by anastomosis [22]. Hyphal cords are known to transport nutrients across distances and nutrient-deficient substrates from areas where nutrients are plenty. This may have allowed mycelia to grow larger network on the aluminum surface, where there are no nutrients available.

The fact that some mycelia grown in food-rich conditions did not grow to cover the entire surface raises suspicions about mycelial interaction with aluminum. The surfaces were thoroughly degreased, so the cause is unlikely to be contamination or grease leftover from processing. It is possible that surface characteristics induced by rolling processes during sheet manufacturing are responsible. For example, hot-rolling creates a near-surface deformed layer at the top ~1 to 2µm of the aluminum, which has remarkably different metallurgical properties and microstructure than the bulk [67, 68]. These changes include deformed grains, elongated in the direction of rolling, up to 10x increased concentration of alloying elements like magnesium and copper, ultrafine and recrystallized grains, and grains more resistant to corrosion [73]. There have also been reports of Mg, Cu, Zn rich areas at the near-surface deformed layer [67]. Looking at Table 2.2, there are large concentrations of copper and zinc, in Al 2024 and Al 7075, respectively. Given that this NSDL is also present on the aluminum plates tested here, we can hypothesize that when mycelia encountered copper and zinc-rich regions, they were overdosed on metallic ions, and stopped growing in those areas. This would explain why mycelia grew to

blanket coverage on the grinded surfaces, of which the NSDL is removed, and only regular concentration of alloying elements is expected.

Table 2.2 Alloying compositions (by percent) of the aluminum alloys used in this thesis work. Values reproduced from:

"Wrought Aluminum International Alloy Designations & Chemical Composition Limits," *Teal Sheets*. 2018, [Online]. Available: https://www.aluminum.org/standards.

	Al	Si	Fe	Cu	Mn	Mg	Zn
Al 2024	~92-94	0.15	0.2	3.7-4.5	0.15-0.8	1.2-1.5	0.25
Al 7075	~87-90	0.4	0.5	1.2-2.0	0.3	2.1-2.9	5.1-6.1
Al 6082	~95-97	0.7-1.3	0.5	0.1	0.4-1.0	0.6-1.2	0.2

Confusingly, mycelia grown in the food-scarce condition showed the reverse pattern—they generally grew more on surfaces that were not grinded (Figure 2.16). This was not true only in the case of Al 6082, which is also the purest aluminum alloy used. That raises suspicions that the difference is still being caused by the alloying elements in Al 2024 and Al 7075. Notably, the surfaces which were grinded in the food-scarce condition experienced severe localized corrosion after mycelial growth finished. Further, this corrosion occurred only where the mycelia were not present, suggesting that the mycelia were either avoiding these regions or that more of those regions are present underneath the mycelial biomass. This kind of severe localized corrosion is expected for grinded aluminum alloys that have removed the near-surface deformed layer [73]. It is thus possible that this corrosion is what prevented the mycelia from growing more extensively on these plates. In that case, it is also possible that in the food-rich condition the mycelia are not so selective about where they grow, as they have plenty of resources to explore with. Again, it is not clear whether the food-rich grinded surfaces were also corroded, as the surfaces were entirely covered by mycelial biomass.

On closer investigation, the corrosion which occurred on both 'degreased only' (Figure 2.10) and 'degreased & grinded' (Figure 2.11) surfaces creates a structure resembling aluminum that has been etched for the purpose of microstructure imaging. The grain sizes are on the order

of hundreds of microns in diameter, which is similar to grain sizes reported at the NSDL in other work [67]. It is possible that the grain separation noticed across the board in the corrosion imaging is a result of acids/enzymes secreted by *S. commune* fungi [74], which enter solution on the thin water film on the surface and corrode away at the grain boundaries. This would explain the black color surrounding the grains being corroded metal.

Furthermore, the observation of yellowed mycelia (Figure 2.9) to at least some extent in all samples is a further hint at mycelia interacting with the metal surface. Literature explains that mycelia can and do absorb heavy metals and ions from their environment [30]. It is also known that these ions can be toxic at moderate concentrations. Pigmentation, or changing color, is a known effect of absorbing certain ions [75]. Due to the widespread presence of pigmented fungi, we can hypothesize that the hyphae were up taking metal ions that had been freed from the surface and released into the thin film of water at the surface. This may have been toxic to them and affected their ability to grow on the surface, though not in the food-rich condition. This further suggests that mycelia grown in food-rich conditions are extremely hardy and can survive these toxic metallic conditions.

A summary of the expected interaction of fungal hyphae with an aluminum surface is shown in Figure 2.18. This is a theory of what may be happening based on the results in this paper and supporting literature. Firstly, the aluminum plate becomes covered by a thin layer of condensed water, due to high-humidity conditions. Then, the hyphae release organic acids which enter solution in the water. S. commune is known to produce acids such as oxalic and citric acid, and chelating compounds (which bind metal ions) such as siderophores [74]. These organic acids chemically react with the aluminum, zinc, magnesium, and iron at the surface to oxidize these metals, resulting in release of metal salts and ions. These metal salts and ions enter solution in the water at the surface and are subsequently taken up by the hyphae through osmosis. If these metal ions enter the fungal cell in too high quantity, it may result in the slowing of biological function, or death of cells.

Our results showed that mycelia grow denser colonies in food-rich conditions, but that they nonetheless extend to similar distances regardless of how much food is available to them. Most of the extra growth occurs as aerial hyphal growth, as shown in Figure 2.6. In similar work of growing mycelia on wood, they found two kinds of growth: bio-film growth at the surface of the substrate, and aerial growth above the substrate to obtain oxygen [18]. We can hypothesize that the biomass grown on aluminum has a similar structure. Large-diameter, sparsely grown

hyphae at the aluminum surface, supporting a mass of small-diameter aerial hyphae growing above the surface. Our results of increasing mycelial density without increasing coverage, suggest that most extra growth is aerial mycelia biomass above the surface. This is significant for making coatings or thin films out of the biomass grown at the surface.
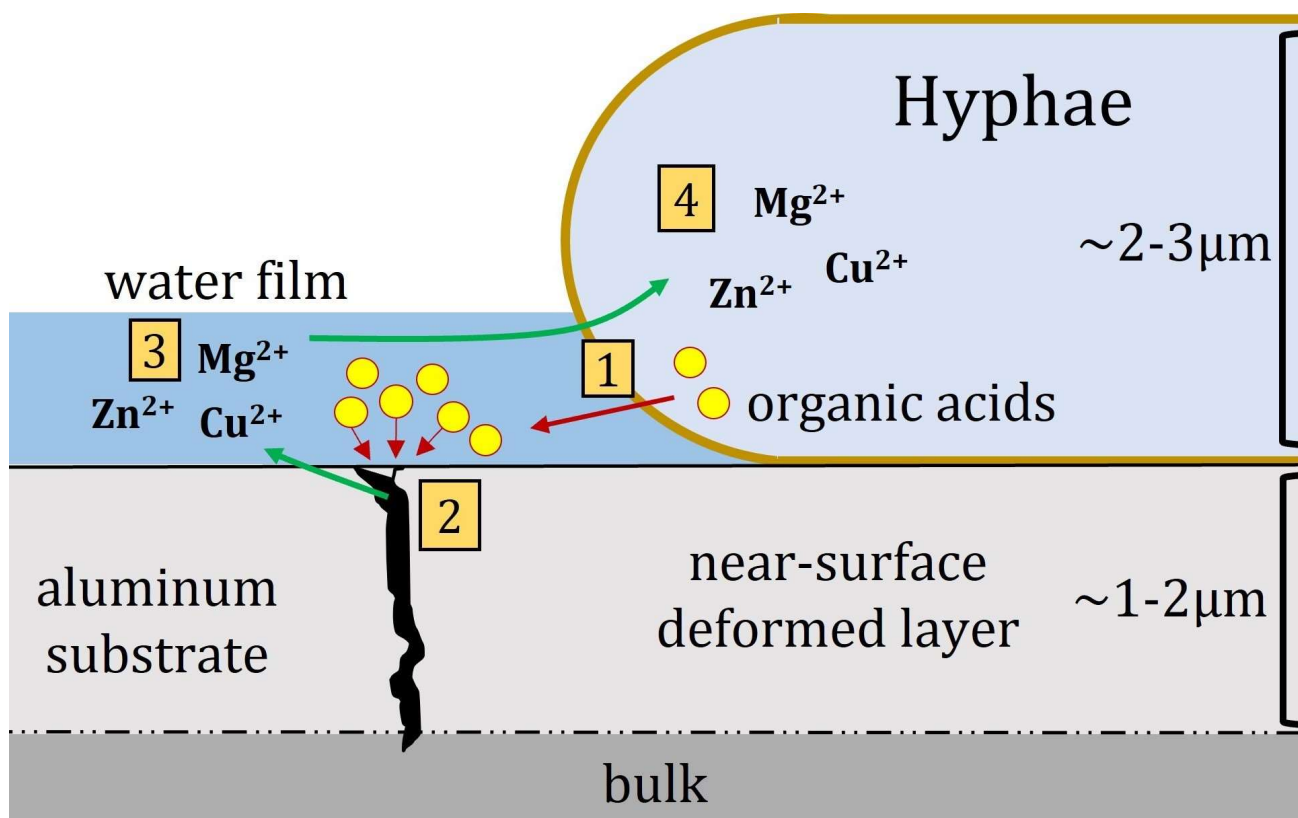
Figure 2.18 Illustrative theory of how a fungal hypha may interact with an aluminum surface. The yellow circles indicate organic acids produced by *S. commune* fungi, which are released into solution. [1] organic acids released into a thin water film at the surface of aluminum in saturated humidity conditions. [2] organic acids corrode and etch the surface. [3] metallic ions from the aluminum alloy get released into the thin water film due to oxidation of the surface. [4] fungal hypha uptakes ions in solution by osmosis, at potentially toxic concentrations.

Now that we have theorized about how mycelia grow onto and interact with aluminum surfaces, we return to the original point of this investigation. Based on these results it is possible to grow mycelium to completely envelop an aluminum surface and thus "coat" it. However, this is not any sort of engineering coating. The mycelial biomass is non-adhesive and easily scratches off with a bare finger. Furthermore, the microstructure of the mycelia is thick, extremely porous, and fibrous, not the kind of structure we look for in thin-film barrier coatings. Overall, having the biomass on the surface is not useful from a coating perspective, unless it can be processed in-situ to achieve a less porous, more adhesive thin film.

2.5 Conclusions

In conclusion, our work shows that mycelia can be grown to cover plates of aluminum alloys under certain conditions. When there is an excess of food available for the mycelia, they grow to cover nearly 100% of the plate. Mycelia seem to grow more extensively on Al 6082 compared to Al 7075 and Al 2024. Thus, there seems to be a strong effect of alloying composition on fungal growth. This effect is even stronger when the surface is grinded, which indicates that the near-surface deformed layer may be playing a role. One of the reasons for inhibited mycelial growth on the surface could be the presence of Zinc or Copper-rich regions on the 'degreased only' surfaces. These elements may be toxic to the fungi at the high concentrations that could be expected at a corroding near-surface deformed layer. When mycelia are grown in food-rich conditions, they seem to be less vulnerable to these surface properties of the alloys. Thus, this work proves that it is possible to grow fungal material in-situ at the surface of aluminum, and that the growth there is highly dependent on the surface properties of the metal. The most biomass can be grown when the surface is grinded and there is a large amount of food available. Unfortunately, the biomass which is leftover after the mycelia have dried out on the surface is not currently suitable for use as an engineering coating, due to its porous and non-adhesive structure.

3 MYCELIAL CULTURE EXTRACTS AS COATINGS FOR ALUMINUM
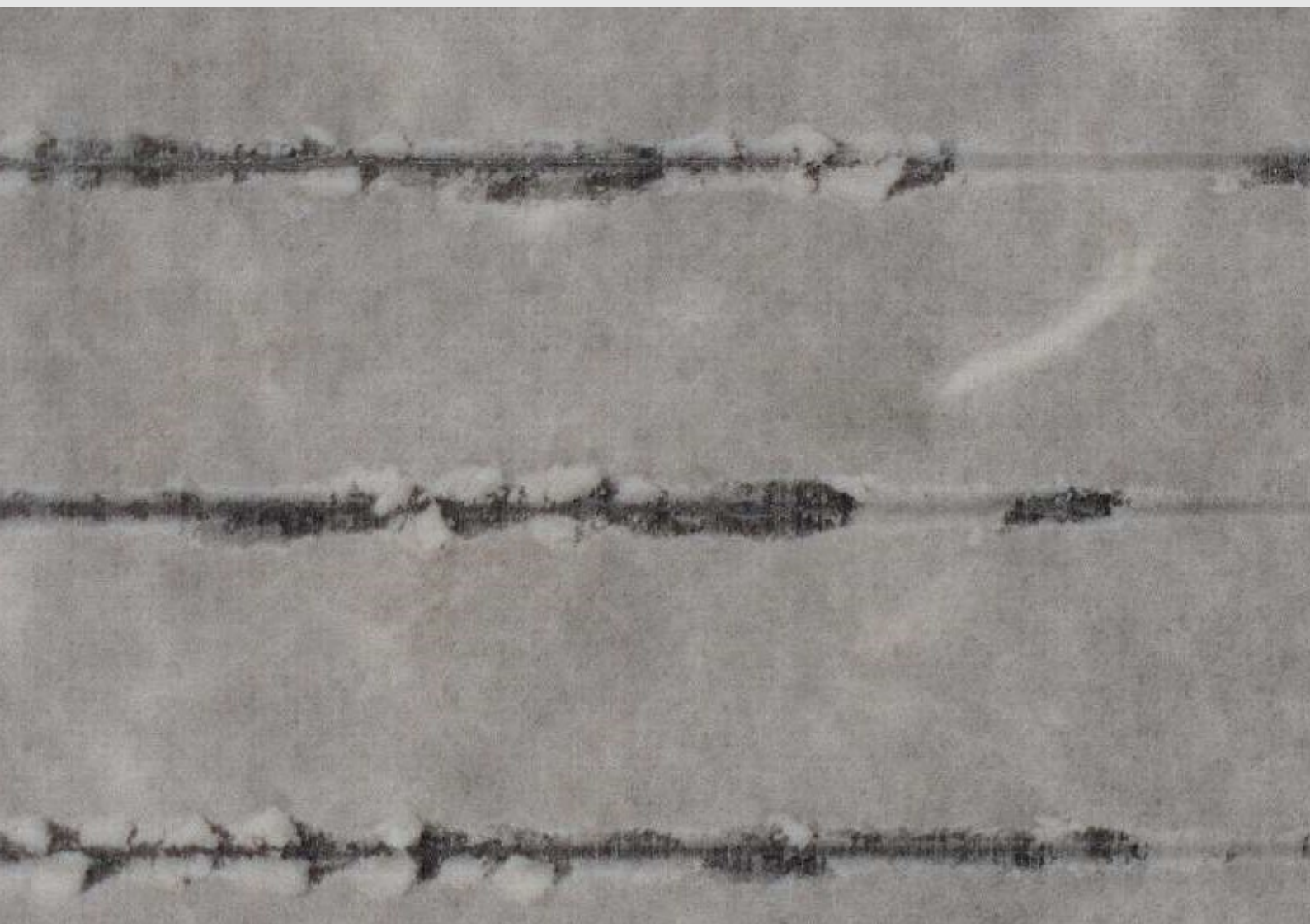
3.1   Introduction

After finding that mycelial biomass grown on aluminum was porous, structurally unstable, and non-adhesive, we were interested in exploring alternate routes. Exploratory work during the initial phase of this thesis work revealed the possibility of drying mycelium films onto aluminum to form an adhesive layer (Figure 3.1a). However, this layer was thick (>100μm), difficult to process, and did not resemble an engineering coating in any way. Nevertheless, it piqued our interest in the adhesive potential of mycelium to aluminum. Soon after, we found a simple means to extract mycelial biomass from liquid culture onto aluminum in a more controlled way. With this method, mycelial biomass could be consolidated onto aluminum resulting in something resembling a conventional coating (Figure 3.1b). Further, it was possible to extract schizophyllan biopolymer from the growth media and form it into a coating on the surface (Figure 3.1c). The techniques for forming coatings of mycelial extract onto aluminum are presented in this chapter for the first time in literature.

Mycelium film on Al	Processed mycelium on Al	SPG extract on Al
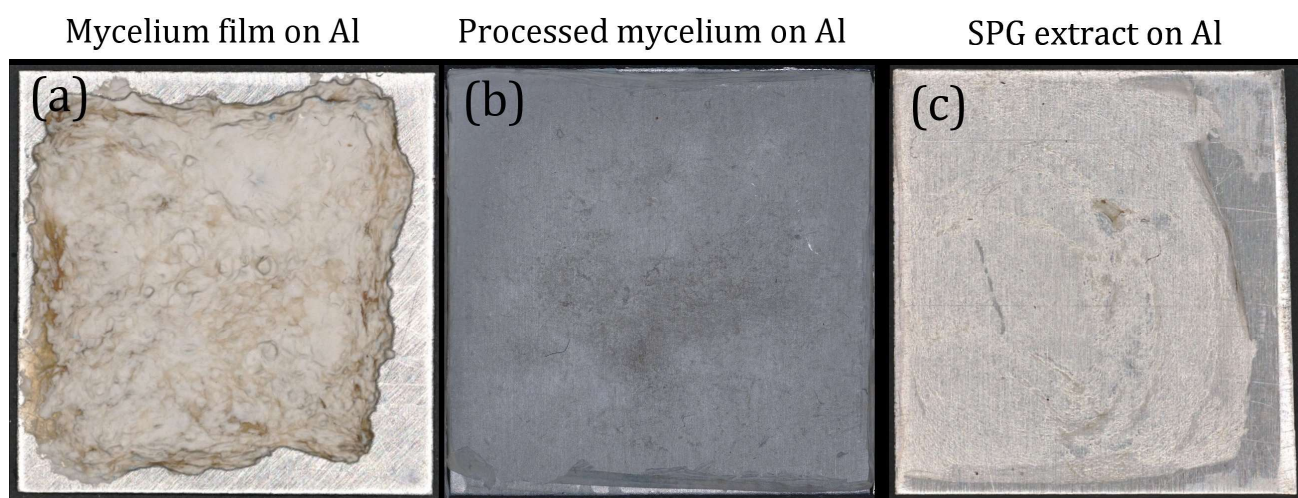
Figure 3.1 Comparison of mycelium film on aluminum to processed liquid culture extract on aluminum. (a) mycelium film obtained by vacuum-filtering liquid culture biomass into a wet filter cake, and then drying onto aluminum. This film is equivalent to mycelium films from ALC reported in literature, with the new step of drying on aluminum. (b) mycelium coating on aluminum obtained by drying processed liquid culture on the surface. (c) SPG coating on aluminum obtained by drying processed extract from liquid culture on the surface. Each sample shown has a 20x20mm plate of aluminum 6082 as the substrate.

3. Mycelial culture extracts as coatings for aluminum

This chapter will describe first the materials and methods used to create mycelium coatings on aluminum (Section 3.2), and then describe their structure and properties in a combined results & discussion section (3.3 Results & discussion). Further, we will directly relate how the processing of the liquid culture—by blending and washing—affects the structure and properties of the resultant coating on aluminum. The results include analysis of microstructure by SEM, chemical composition by TGA, FTIR, and adhesiveness by micro-scratch testing. The adhesiveness of mycelial biomass to aluminum by micro-scratch testing is a novel application of an old technique, that is reported here for the first time in literature. Finally, conclusions on the major results and the usefulness of such coatings are drawn (3.4 Conclusions).

3.2 Materials & methods

This section will explain all the methods involved with growing liquid culture, processing them, and extracting mycelial biomass onto aluminum. Then, the methods for preparing the aluminum plates which were coated are shortly discussed. Finally, we will explain the methods we used to test the mycelium material. These include SEM, TGA, FTIR, and micro-scratch testing for adhesion strength to aluminum.

3.2.1 Growing the liquid cultures

S. commune fungi were grown by a liquid culture method developed by the microbiology research team at the University of Utrecht [65]. The general procedure is to inoculate a sterilized minimal media with homogenized inoculum and then grow at 200rpm stirring for 7 days. For the results shown in this chapter, we used mycelia from three separate cultures, simply due to running out of mycelium. The differences in growth conditions for the cultures may affect growth morphology, quantity, and structure of the biomass grown. Thus, it is important to keep in mind from which culture each coating was formed. The different growth conditions, and the difference in solids content of the cultures, are listed in Table 3.1. The first culture was grown in Utrecht using the methods developed there and donated for this work. This culture was more precisely three cultures (Figure 3.2a), combined into one. To explain, Culture 1 is the mycelia of 3 separate 1.2L flask cultures, filtered out and resuspended into 1.2L of filtrate (Figure 3.2b). That was done simply to transport the mycelium back to Delft, but it is important to consider how that higher concentration of mycelia may impact the properties of the material.

Table 3.1 Culture growth conditions. *Solids content was measured by drying a controlled volume of culture and measuring the dry mass. For culture 2, that is an average of 5 measurements, and for culture 3 it is an average of 8 measurements.

	Grown at	Inoculum volume [ml]	Grow time	* Solids content [mg/ml]
Culture 1	Utrecht	-	7	-
Culture 2	Delft	4ml	10	6.24 +/- 0.67
Culture 3	Delft	7ml	10	8.32 +/- 1.00

The next two cultures were grown in the lab at TU Delft (Figure 3.2c). We mixed this media in-house using the ingredient list provided by our collaborators. After mixing, we sterilized the minimal media 2.4L at a time in a kitchen-grade pressure cooker. Media was in the pressure cooker at 0.65bar pressure for a minimum of 30 minutes. After sterilizing, phosphate buffer was added to the media through a 0.45-micron filter with a syringe, since the phosphate buffer can't be pressure cooked. The SCMM was then transferred into two 2L Erlenmeyer flasks—with 1 liter going into each—that would be the flasks in which the mycelium grew. Those flasks had been previously dry heat sterilized in the oven at 180°C for 2 hours. All transfers were done under semi-sterile conditions near an open flame and after wiping down all surfaces with 70% ethanol.
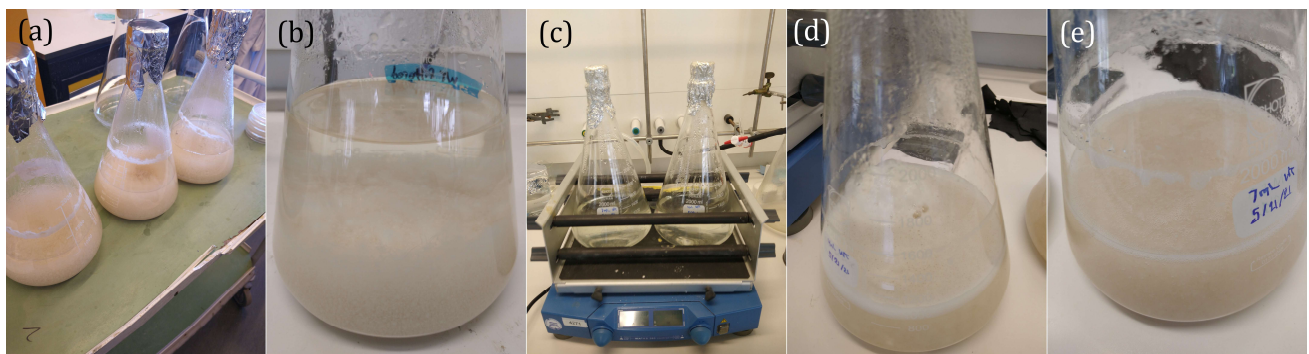
Figure 3.2 Images of *S. commune* liquid culture growth. (a) Three *S. commune* liquid cultures grown in the Microbiology lab at the University of Utrecht for 7 days. These cultures were filtered down into 1.2L of culture, thus increasing concentration 3x. The resulting culture (b) is referred to as Culture 1 in the remainder of this work. Notice how the mycelia have settled to the bottom of the flask. (c) Cultures 2 and 3 secured into the shaking platform, on the first day of growth. (d) Culture 2 after 10 days of growth. (e) Culture 3 after 10 days of growth. Notice the difference in amount of foaming between Culture 2 and Culture 3. Culture 3 was more pulp-like, and Culture 2 was more discretely pelleted.

Immediately after transferring SCMM to the growing flasks, mycelium inoculum was added. Mycelium inoculum was in the form of an old liquid culture that had been homogenized in a blender, mixed with glycerol at 10:1 volume ratio, and frozen at -3°C for two weeks. This inoculum was thawed at room temperature, and 4 or 7ml of it was added to the freshly sterilized SCMM near an open flame. Directly after inoculating, a flask stopper made of cork-like

(breathable) material—which had also been dry heat sterilized—was put into place on the flask. Aluminum foil covered the top of the flask, and then it was ready to start growing.

The freshly inoculated media was immediately secured into a shaking plate, which shook the culture flasks at 200rpm at room temperature for 7 days (Figure 3.2c). The temperature was monitored and stayed within the range of 22 to 25°C for the duration of growth. Light conditions were not controlled, so the fungi experienced the lighting cycles of the lab. After 10 days, when the presence of foaming was notable, growth was halted by removing the flasks from the shaking plate and placing them—still sealed—in the fridge at 9°C. At this point, growth had reached a maximum, and the cultures could now be preserved for a further time before testing took place. The differences in inoculum size resulted in different dry yields for Cultures 2 (Figure 3.2d) and 3 (Figure 3.2e), with Culture 3 growing more mycelium in it by day 10 due to having a larger inoculum. Further, the effect of inoculum size on the structure and how mycelium grows in agitated liquid culture has been described elsewhere [22]. More precisely, Culture 2, with less inoculum than Culture 3, may have exhibited more discretely pelleted growth.

3.2.2   Processing the cultures

Two processing steps—blending and washing—were used on the fully grown cultures in attempts to improve their film forming ability. Blending was done using a process called homogenization, which is typically used for preparing liquid inoculant [64, 65]. Cultures were homogenized using a Model E8122 Waring two-speed laboratory blender base (Figure 3.3a) made available by our collaborators at Utrecht. The blender has two settings, 21,500 and 24,500rpm. The blender was used at the high setting for most operations, and we note where that was not the case. Liquid cultures were filled into an E8580 stainless steel semi-micro blending container with press fit lid, shown in Figure 3.3a&b. The container had a custom blending assembly with four flat-edged blades warped slightly up or down (Figure 3.3b). After homogenizing, the cultures were placed in new containers and stored in the fridge until further use. Cultures were washed by straining through a cheesecloth until drips were more than 20s apart. Next, the strained mycelial biomass was re-dispersed into distilled water of the same volume, stirred for 60s seconds, and allowed to soak for 5 minutes. This process was repeated a total of five times to obtain the 'washed 5x' condition. The filtrates of each subsequent wash were saved for further analysis.
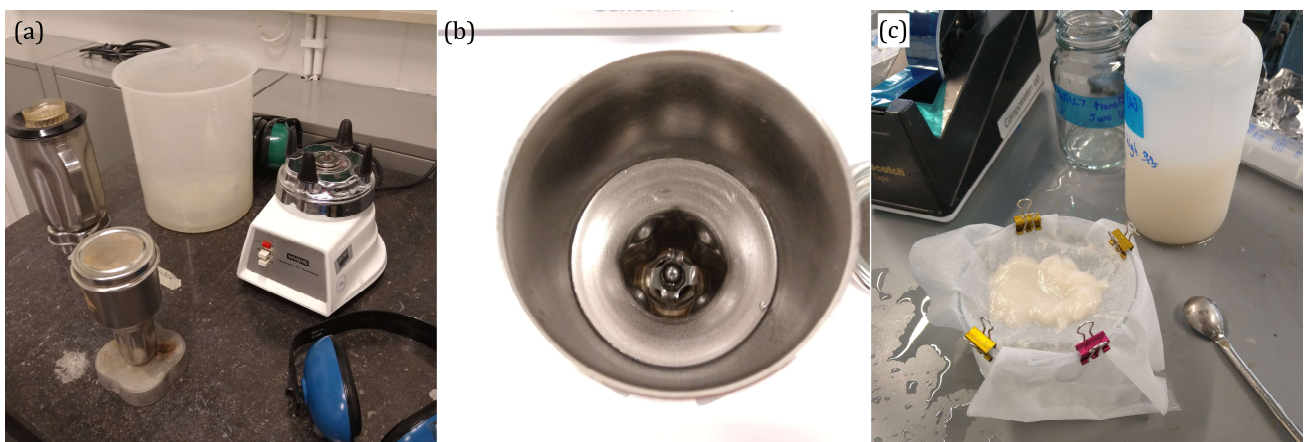
Figure 3.3 Images of equipment used to blend and wash *S. commune* liquid cultures. (a) blending setup showing the separated blending base and container. (b) up close image of the blending container, illustrating the shape of the blades. (c) Image of the setup used to wash liquid cultures in distilled water. In this image a blended liquid culture has been poured onto the cheesecloth and allowed to drip for 60+ seconds to form the some wet mycelial biomass, which we sometimes refer to as "dough".

3.2.3   Extracting Schizophyllan

Schizophyllan is a water-soluble polysaccharide excreted by *S. commune* fungi into liquid cultures during growth. We were curious about the properties of this material, so we extracted it from filtrates of the liquid cultures using established ethanol extraction methods [76, 77]. The filtrates derived from washing the liquid cultures were used as the basis for extraction. First, 100% ethanol was added at a 1:1 ratio by volume to the filtrate. This was mixed shortly so that the ethanol could be well dispersed through the filtrate. Then, the solution was left in the fridge at 9°C for 1 hour. This gave time for the SPG to precipitate out of solution and rise to the top (Figure 3.4a). At this point, the precipitate was removed using a metal spoon (the SPG was very sticky & cohesive and stuck readily to the spoon) and moved into 50ml of 50:50 ethanol plus distilled water solution. This mixture was again mixed and then left to precipitate in the fridge for an hour. After that, the mixture was centrifuged at 4400rpm for an hour so that the SPG accumulated at the bottom of the test tube (Figure 3.4b). The solution was poured off the top, and the SPG was collected, then re-added to another 50ml of ethanol plus distilled water mixture. The centrifuging process was repeated 3x to aid in purifying the SPG. After the final centrifuging and pouring-off, the SPG was stored in a still-wet state in the fridge at 9°C in a sealed container (Figure 3.4c).
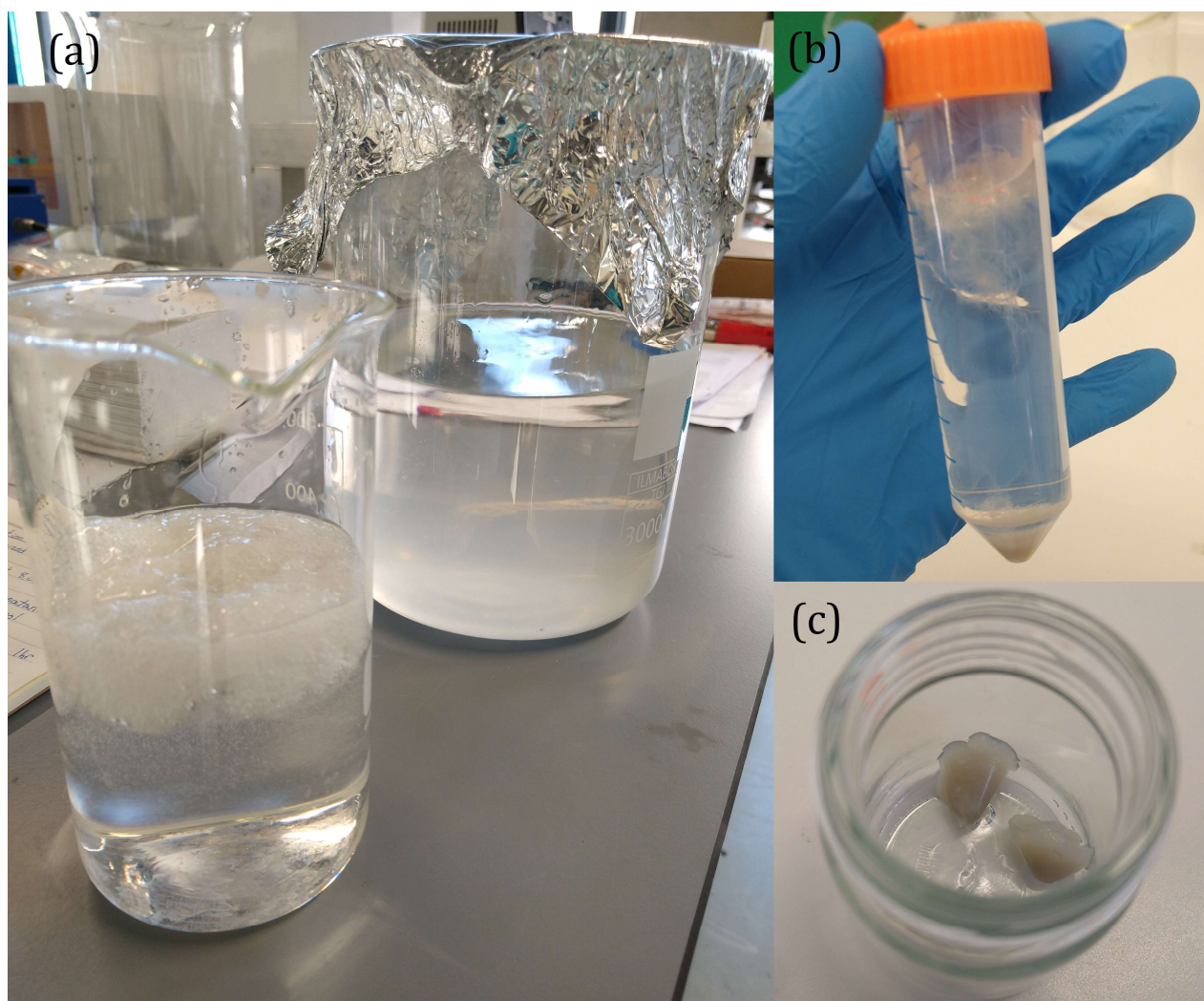
Figure 3.4 Images of SPG extraction process. (a) *S. commune* filtrate in the background in the large container, and precipitating SPG (the bubbles) in the forefront. (b) SPG migrating to the bottom of the tube, after 30 minutes of centrifuging. (c) Condensed SPG that was recently removed from the centrifuge. In this form the biopolymer is cohesive and still wet.

3.2.4   Consolidating mycelia onto aluminum

We consolidated mycelia onto aluminum using a simple method of air-drying mycelium suspended in liquid culture above the surface of the aluminum (Figure 3.5). This was done using a 2ml pipette, very carefully dropping 0.5-1.0ml of culture onto each plate, so that the surface tension of the water held the mycelial biomass in suspension above the plate (Figure 3.5a). Before pipetting the culture, it was shaken vigorously to mix up the mycelial biomass inside more evenly. Slowly, as the water evaporated at room temperature, the particles of the mycelia dropped to the surface of the aluminum plate and adhered there. Plates were left to dry for approximately 24 hours, after which they formed thin, coating-like films on aluminum (Figure 3.5b). After full drying, plates were stored securely in air-tight plastic bags at room temperature and humidity. We expect that the temperature and humidity during drying influence how the film dries to the aluminum, but we did not investigate that in this study. The temperature in the lab was between 20 and 25°C, and humidity was between 40 and 55%.
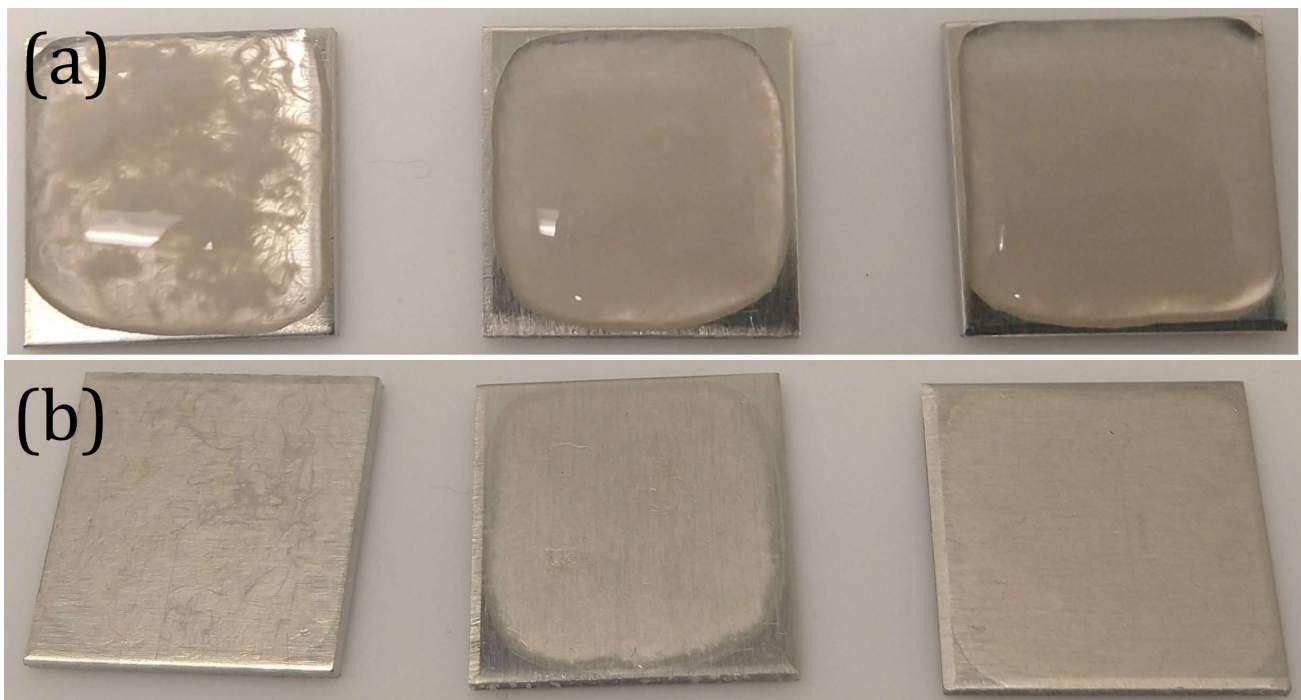
Figure 3.5 Images of mycelial biomass consolidation onto aluminum. (a) *S. commune* liquid culture (unblended, blended 30s, and blended 60s, left to right) in suspension above the surface of aluminum. (b) dried mycelial biomass ("coatings") on aluminum after 24 hours of drying at room temperature and humidity.

3.2.5   Aluminum surface preparations

Three kinds of aluminum surface treatments were used, with the aim of understanding the how differences in aluminum surface condition affect adhesion to aluminum. The three surface conditions were termed: 'degreased only', 'degreased & grinded', and 'pseudoboehmite' (Figure 3.6). The 'degreased only' surface (Figure 3.6a) was prepared by wiping the surface with acetone, and then ultrasonicating in acetone for 5 minutes at the medium setting. The 'degreased & grinded' surface condition (Figure 3.6b) was prepared by first grinding and subsequently degreasing the surface as for the previous condition. The surface was grinded to a rough consistency using 3 steps. First with 320 grit sandpaper in water, then with a 3M Scotch-Brite coarse-grade industrial hand pad in water, followed by the same Scotch-Brite pad in ethanol. Grinding was done by hand, until the entire surface reached an even consistency. The intention was to create a rough surface in which hyphal filaments from the mycelial biomass dried on aluminum could get trapped, creating physical adherence. The pseudoboehmite treatment (Figure 3.6c) was prepared according to previous work [78], by first grinding and degreasing the surface, and then dipping aluminum plates into 2M NaOH for 10 seconds and then letting them air dry. This process destroys the natural oxide layer and reforms a more homogenously distributed oxide layer, which is typically advantageous for adhesion thanks to enhanced hydrogen bonding potential.

In the 'degreased only' condition, the surface at higher magnification (Figure 3.6d) shows parallel striations that may be artefacts of the rolling production process. In the 'degreased & grinded' condition, the striations are less visible, and the surface is a more homogenous color. At higher magnification (Figure 3.6e), scratches of 5 to 20µm width are present across the surface in random directions and orientations. In the 'pseudoboehmite' condition, some brown coloration and spots appear on the surface. At higher magnification (Figure 3.6e) of the pseudoboehmite-treated surface, it appears that the surface is covered by a transparent film, especially when compared to the 'degreased & grinded' surface. This could be the pseuboehmite which has formed on the surface. In that case this image implies that it did not form homogenously across the entire surface, though it is unclear why.

Degreased only   Degreased & grinded   Pseudoboehmite
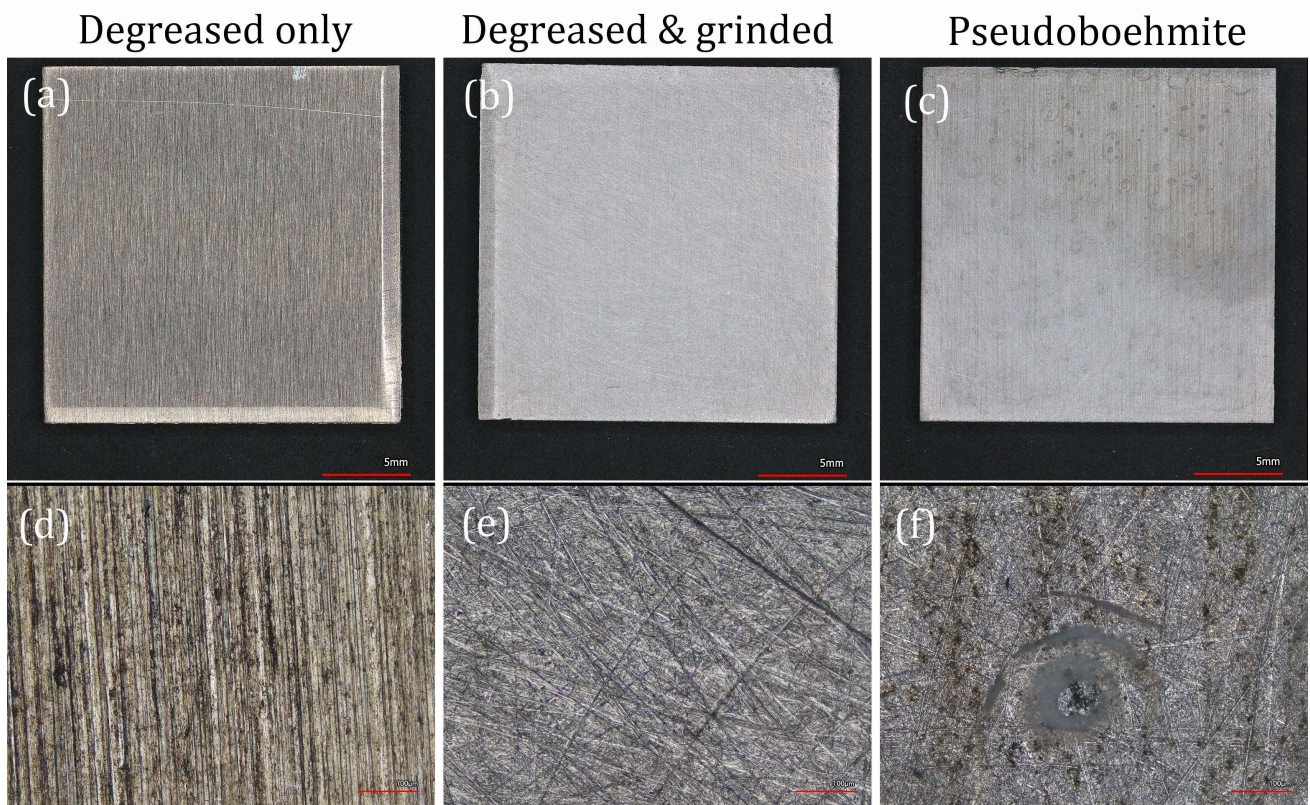
Figure 3.6 Images of surface preparations for consolidating mycelial biomass on aluminum. (a) degreased only, (b) degreased & grinded, (c) pseudoboehmite surface condition of aluminum plates. All plates shown here are 20x20mm and 2mm thick Al 6082. (d,e,f) 20x magnified surface images obtained using a laser scanning microscope, which show the surface condition above them in higher detail. Red lines in (d,e,f) represent 100µm.

3.2.6   Microstructure by SEM

Scanning electron microscopy was used in this work to generate view of the tops of mycelium coatings on aluminum, and cross-section views of free-standing representative mycelium films. The SEM used for this work was a JEOL JSM-7500F. The SEM was set to LEI and either LM or SEM mode, depending on the magnification needed. Since mycelium is not particularly conductive, samples were sputtered with a 10nm layer of gold using a Quorum Q300T sputtering machine. For cross-section imaging, films were dipped into liquid nitrogen for 10 seconds, and then immediately shattered to produce a cross-section. This avoids the creation of a smeared cross-section which occurs when cutting ductile films like these. These films were

wrapped in regular tape to aid them to stand up straight inside the SEM. Unfortunately, due to warped and uneven samples, and samples not standing perfectly straight inside the SEM, it was difficult to produce proper cross-sectional views of the films. Further, the SEM used operated under a vacuum, which may have caused micro-structural changes in the unstable mycelial biomass.

3.2.7 Chemical composition by FTIR and thermal analysis by TGA

The equipment and methods for obtaining IR spectra and thermal degradation curves were the same as those previously described in Section 2.2.7. The analysis was carried out on representative mycelium films (Figure 3.7) as it was not possible to test the biomass on aluminum. Six samples were used for TGA analysis: 'unblended, unwashed mycelium film' (Figure 3.7a), 'unblended, washed 5x mycelium film' (Figure 3.7b), 'blended 30s, unwashed mycelium film' (Figure 3.7c), 'blended 30s, washed 5x mycelium film' (Figure 3.7d), dried SPG extract (Figure 3.7e), and dried filtrate from liquid culture (Figure 3.7f). The films were intended to be representative of the mycelial biomass dried onto aluminum. They were created by pipetting 5ml of their respective cultures onto release film and air-drying for 24 hours. The films were like dried leaves, extremely fragile and brittle. A film of SPG extract was obtained by simply air-drying the wet SPG shown previously in Section 3.2.3. Dried culture filtrate was obtained by air-drying 50ml of filtrate from the 1st washing cycle of Culture 2. This resulted in a yellow, sticky, goo which was collected with a razor blade and smeared onto the FTIR crystal. Approximately 3mg of each sample was used for TGA analysis, and a small amount for FTIR analysis.
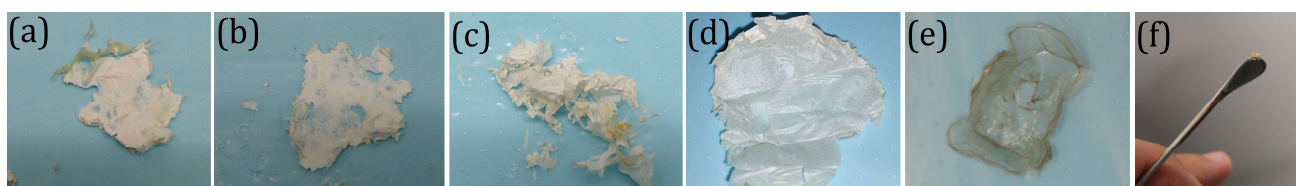
Figure 3.7 Free-standing mycelium films and other samples used for FTIR and TGA analysis. (a) unblended, unwashed mycelium film, (b) unblended, washed 5x mycelium film, (c) blended 30s, unwashed mycelium film, (d) blended 30s, washed 5x mycelium film, (e) SPG film, (f) dried filtrate from Culture 2 at the tip of a stirrer.

3.2.8 Film adhesion to aluminum by scratch testing

Micro-scratch testing is a technique that is often used to measure the adhesion strength of coatings by measuring critical loads of certain failure events like cracking or delamination [79]. The setup is shown in Figure 3.8. In this test, a spherical scratch tip applies force to a coating, and then starts moving in one direction thus scratching the surface. This movement causes crack spreading due to compressive and transverse force enforced onto the coating. At a specific load, the damage is extensive enough to be noticeable by imaging techniques. This load is considered the critical load of coating failure, which is an alternate way of measuring coating adhesion. Mycelium coatings on aluminum were scratched using a Micro-combi tester from CSM instruments (Figure 3.8a). A 200µm diameter diamond stylus was used as the scratch tip (Figure 3.8b). This stylus was checked for damage before use and found to be in good condition. 20x20mm aluminum plates with mycelial biomass consolidated on top were scratched as shown in Figure 3.8c. Ten constant load scratches, going from 0.1 to 1.0N of 3mm length each were scratched at 10mm/min scratch speed. After that, 5 repeats of a progressive load (0.03 to 1.0N) scratch were performed along 5mm on the other side of the sample, also at 10mm/min. Data on normal force, penetration depth, and residual depth were collected by the machine. For this, samples were both pre- and post-scanned with a load of 0.03N, though that was not found to cause any damage to the mycelium. Scratch tracks were imaged directly after scratching using a laser scanning confocal microscope, stitching together at 20x magnification.
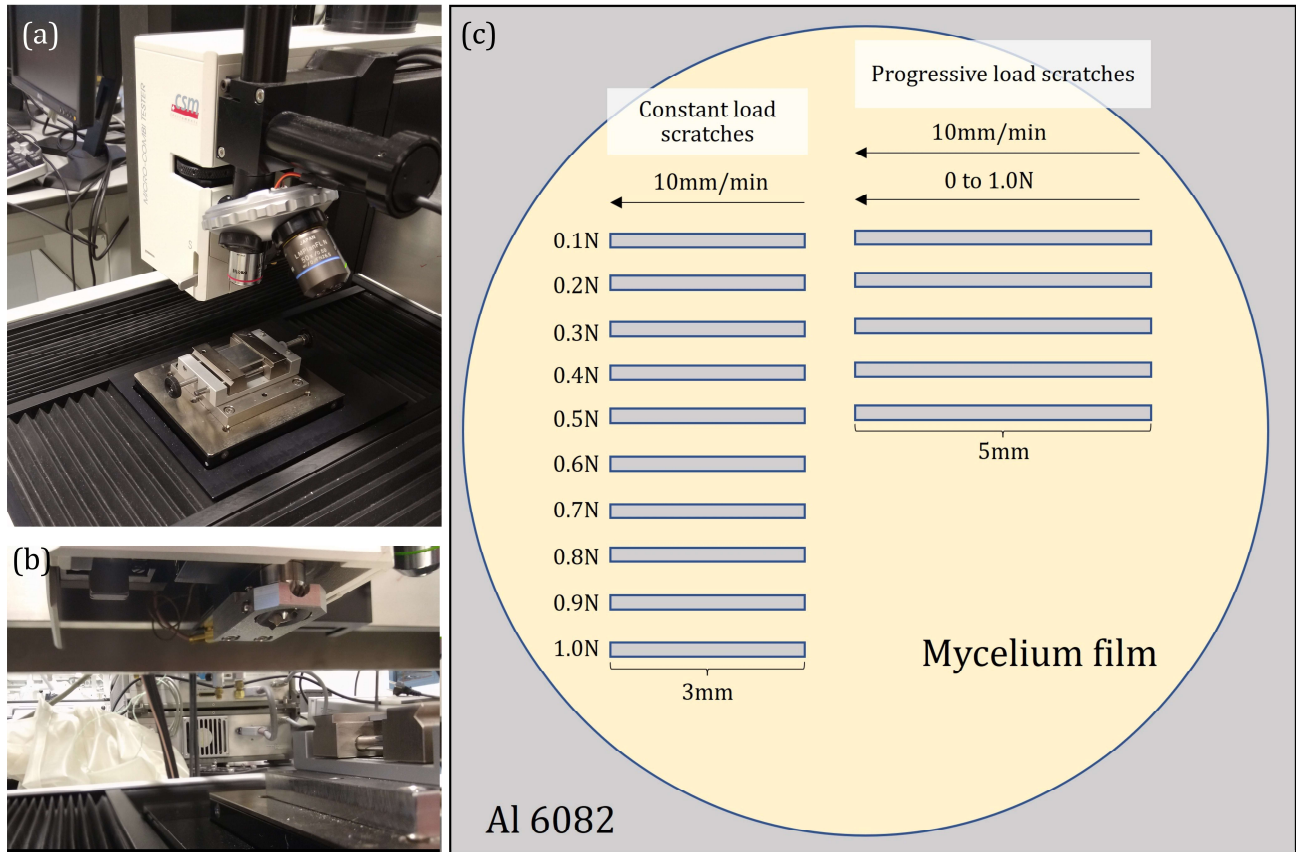
Figure 3.8 Images and illustration of the micro-scratch testing setup. (a) image of the Micro-combi scratch tester, with an aluminum plate in the sample holder. (b) close-up image of the scratch tip. (c) illustration of how the scratches were placed on the coating on aluminum. Scratching was performed sequentially starting with the five progressive load scratches, and then ten constant load scratches from 0.1 to 1.0N.

3.3   Results & discussion

3.3.1   Homogenizing the mycelium

To have a proper protective coating for aerospace applications, the material should be providing a barrier against oxidative and reductive species as well as water. At a minimum, this would require even distribution of mycelium on the surface of the aluminum. As shown in Figure 3.9a&b this is not possible with the culture "as-is". This is because the mycelium grows in the form of pellets in the ALC. These pellets are large aggregations of hyphae that form dense-packed structures to facilitate oxygen and nutrient distribution [22]. As shown in Figure 3.9a, the rope-like aggregates of hyphae are more than 100µm in width, with hyphal growth becoming sparse further from the center of the structure. When drying on aluminum, these "ropes" maintain their structure (the white threads in Figure 3.9b), creating a deposit with extensive structural and thickness heterogeneity. This deposit is useless as an engineering coating due to the uncontrolled structure and difficulty measuring properties.

Homogenizing of mycelium is common practice in microbiology to create smaller pieces of inoculum which means more nucleation sites for growth, and a faster-growing culture. For deposition of mycelia onto aluminum, we can also take advantage of this process to create more homogenous films. Figure 3.9c shows what a culture homogenized for 30 seconds looks like under an optical microscope. Notice that the "ropes" of hyphal aggregation are not present. Those large-scale structures have been disentangled/broken down by the blender, leaving behind smaller aggregations of hyphae. Those clumps are still present in the film formed from this culture Figure 3.9d, however, it is apparent how much more homogenous the film is compared to the "as-is" film. After blending that culture for another 30 seconds (60s total), the mycelia appear to be even less aggregated (Figure 3.9e), and the film formed from this culture is free of large white spots indicating clumps Figure 3.9f.

Based on these images we can hypothesize the homogenization step to be doing two things: (1) destroying large-scale pellet structures, and (2) chopping up hyphae into smaller segments. Since the blender used for homogenization had 4 sharp blades and was spinning at 24,500rpm we assumed that the length of hyphae would be reduced by chopping/grinding. This appears to have been a correct assumption, notice in Figure 3.9c&e that some hyphae are only 100µm in length or even shorter. In the "as-is" culture, we can't tell the full length of the hyphae, but they are hundreds of microns at a minimum. Having shorter hyphal segments would aid in

disentangling the mycelium, which is key to producing a structurally homogenous fibrous material. The fact that the homogenized films are translucent suggests a reduction in light scattering interfaces in the film. This could be due to hyphae in the homogenized films being more closely packed as their movement is less restricted by large-scale structures and entanglements. Therefore, we can use a homogenization step to deposit mycelia onto aluminum in a way that more closely resembles engineering coatings, at least in appearance.
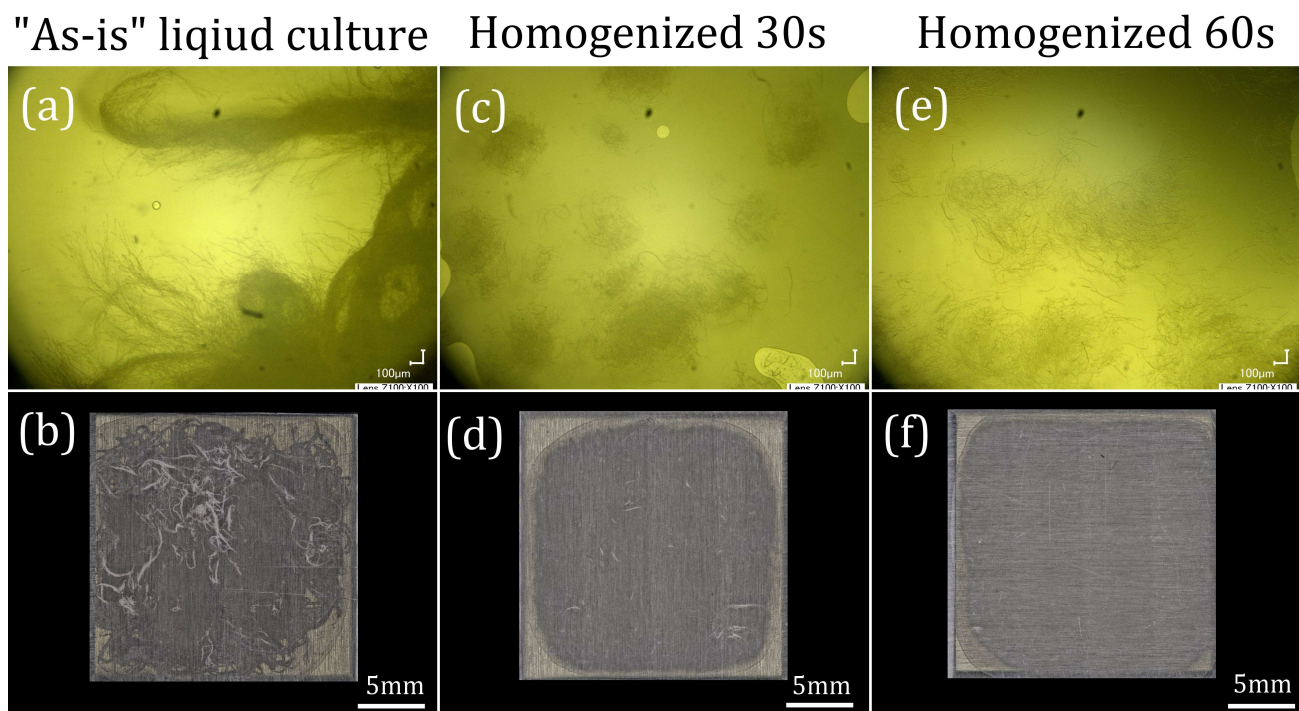
Figure 3.9 Optical microscopy illustrating the effect of blending on mycelium culture, and the difference in resultant films on aluminum. (a) unblended agitated liquid mycelium culture, (b) blended 30s culture, (c) blended 60s culture. Blending done @24,500rpm. Images (a)-(c) were obtained by pressing one drop of liquid mycelium culture between two glass microscope slides. (d)-(f) show the corresponding films made of the mycelium cultures that are above them. These films were consolidated on Al 6082, in the 'degreased only' condition by dropping 0.5ml of culture with a pipette and slow-drying at standard lab conditions.

3.3.2   Washing the mycelium

A liquid mycelium culture is composed of many elements other than mycelium. For one, the unconverted chemicals that made up the nutrient source like glucose and inorganic salts. Also, water-soluble EPS (extracellular polymeric substances), proteins, and lipids excreted by the mycelium during growth would be floating around in solution. Since these chemicals may block efficient packing of hyphal in the resultant film by taking up hydrogen-bonding sites [64] and by physical interference, it has been suggested that removing them may create a denser, more uniform film [11, 65]. In this work, we would like to create a film that is both structurally "bulky" and non-porous. Thus, we intended to explore if washing mycelium cultures would indeed have a positive effect on the structural uniformity of films they form.

The processing step of washing the mycelium was very simple. Cultures were filtered through cheesecloth and then mixed back into the same amount of distilled water as culture that was filtered out. This process was repeated five times; by the third wash, there was negligible solid matter left in the filtrate (see Appendix D for a test of solids content in the sequential filtrates). Figure 3.10a-c show images of an unwashed culture, one washed 3x, and the dried filtrate of the first wash, dried onto glass microscope slides. The cultures in these images were all homogenized post-growth for 20 seconds. In the unwashed culture, aggregates of hyphae appear as white spots on the slide (Figure 3.10a). These aggregates are not present in the washed culture (Figure 3.10b), which appears a uniformly translucent, white color. This effect is visually similar to the effect that homogenization had on the culture. This suggests that washing also reduces aggregation among hyphae and promotes a more uniform film. The first filtrate, when dried onto a glass slide (Figure 3.10b) forms a barely visible, but mostly homogenous film. We could expect this filtrate film to be present in the unwashed film, and not present in the washed film, though that is not clear from these images.

Zooming in on those glass slides under a microscope confirms the presence of aggregates in the unwashed mycelium (Figure 3.10d), and the reduced number of aggregates in the washed mycelium (Figure 3.10e). Aggregates appear to be either circular or elongated in shape, which matches the form of aggregates seen in 30s blended liquid culture in Figure 3.9c. Having such dense chunks of hyphae scattered throughout the film obstructs efficient hyphal packing. Another interesting characteristic is the "bubble" that surrounds the mycelium, which is present in both the washed and unwashed versions. This could be the same film as in the dried filtrate (Figure 3.10f), though in that case, we might expect it not to be present in the washed culture,

which it is. The dried filtrate may be important for adhesion, as it includes water-soluble proteins that adhere by hydrophobic interaction and EPS that is chemically adhesive [80, 81]. Notice the crystal patterns present in the dried filtrate, suggesting the presence of sugars. From a material property perspective, we would like to see good adhesion between mycelium and aluminum. We can compare adhesiveness between an unwashed and a washed culture, to find if the presence of the water-soluble components in the culture aids adhesion.
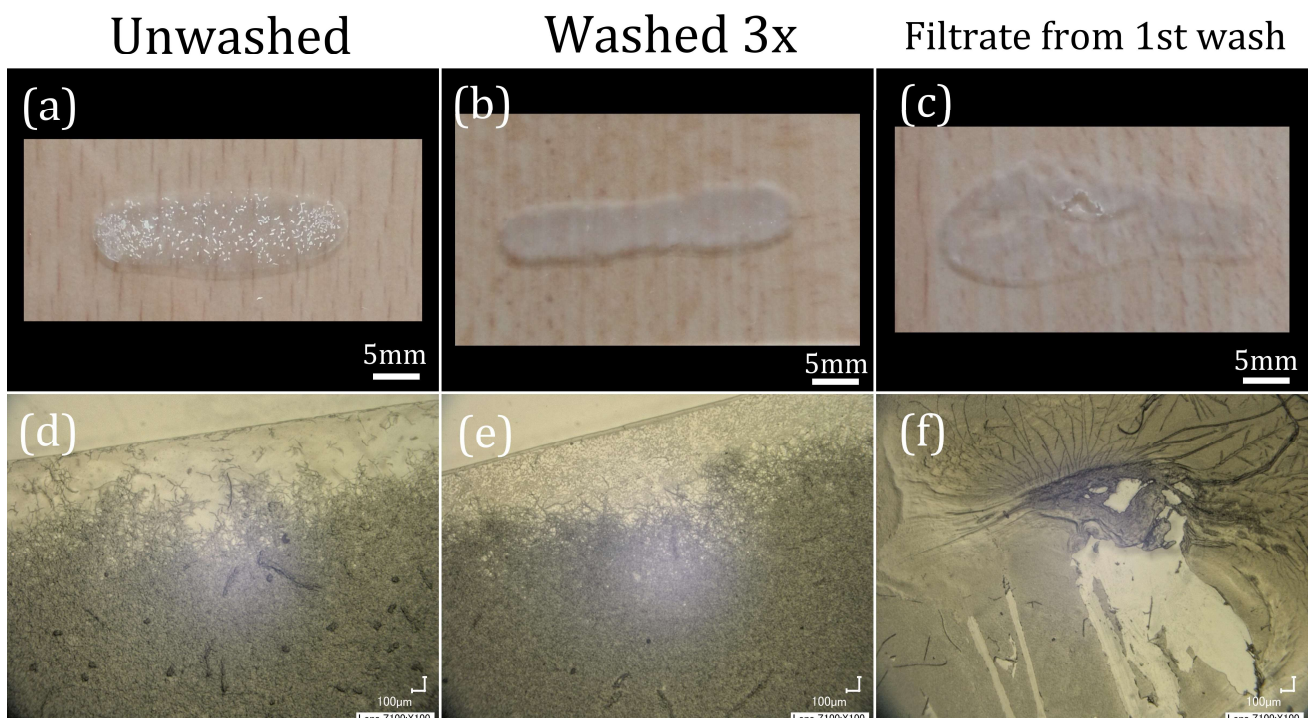
Figure 3.10 Optical microscopy illustrating the effect of washing on mycelium culture, and the difference in resultant films on aluminum. Images of (a) unwashed, blended 20s mycelium, (b) washed 3x, blended 20s culture, (c) dried filtrate from first wash. Cultures blended at 24,500rpm. Images (a)-(c) were obtained by pressing one drop of liquid mycelium culture between two glass microscope slides. (d)-(f) show microscopic images of the slides shown above them.

3.3.3   Top-view microstructure analysis

To help understand the effect of processing on structure, we investigated the microstructure—both top-view and cross-section—of the mycelium films by scanning electron microscopy. First, we will review select images of the tops of mycelium films on aluminum and relate processing to structure. Since the top-view doesn't provide a complete picture of the internal structure of the film—we must also investigate the cross-section. However, this was not possible for the films already on aluminum, so we will show cross-section images of free-standing films representative of those on aluminum.

In the unblended and unwashed state, a colony of mycelium grown in stirred liquid culture is composed of large, intertwined threads of hyphae. These features are preserved in the microstructure of the respective film consolidated on aluminum. Figure 3.11a shows a top view of such a film from a low magnification. Notice three distinct features present from the surface of this film, as marked on the image. Region 1 marks an area of the film with high porosity, where the hyphae have not stacked efficiently onto each other. Region 2 marks an area of the film where those long threads of entangled hyphae are present, thus causing thickness heterogeneity and porosity in that region. Region 3 is an area of the film where porosity is low, and thickness is relatively homogenous. For creating a film with barrier properties, this kind of low porosity structure is a requirement.

At higher magnification, some more details emerge about the film structure—namely the flatness of hyphae, and the appearance that they are embedded in a matrix. In Figure 3.11b the different morphologies of hyphae are shown at a higher magnification view of the film at a high porosity region. Two details of note from this image are [1] fully flattened hyphae, and [2] hyphae which have maintained at least some structural integrity. As discussed in the introduction, hyphae maintain their tubular shape through turgor pressure driven by osmoregulation. The hyphae which have been completely flattened are those that have lost all of their water content, and thus have no way to maintain their weight. The cell wall of hyphae is very thin, so it easily collapses. Interestingly, these collapsed hyphae seem to stack better and form a more continuous (bulky) material with fewer pores. Notice how the hyphae which have maintained some structure are present at the areas of thickness inhomogeneity and porosity. The hyphae width distribution seems to lie between 1 and 5μm, which is supported by previous work [32]. We should expect that the flattened hyphae would seem to be wider than the inflated hyphae, which does seem to be the case, with some flattened hyphae approaching 7 or 8μm width. There are

large differences between the flattened and pressurized hyphae, which we expect to influence the mechanical properties of the film. Since this culture was consolidated onto aluminum as-is, this flattening of hyphae is likely to have occurred during the drying step in an uncontrolled/random manner. Another important feature to notice in this image is the transverse cracking failures of hyphae circled in red. This occurs exclusively on flattened hyphae, suggesting that in this state their resistance to stresses is lowered.
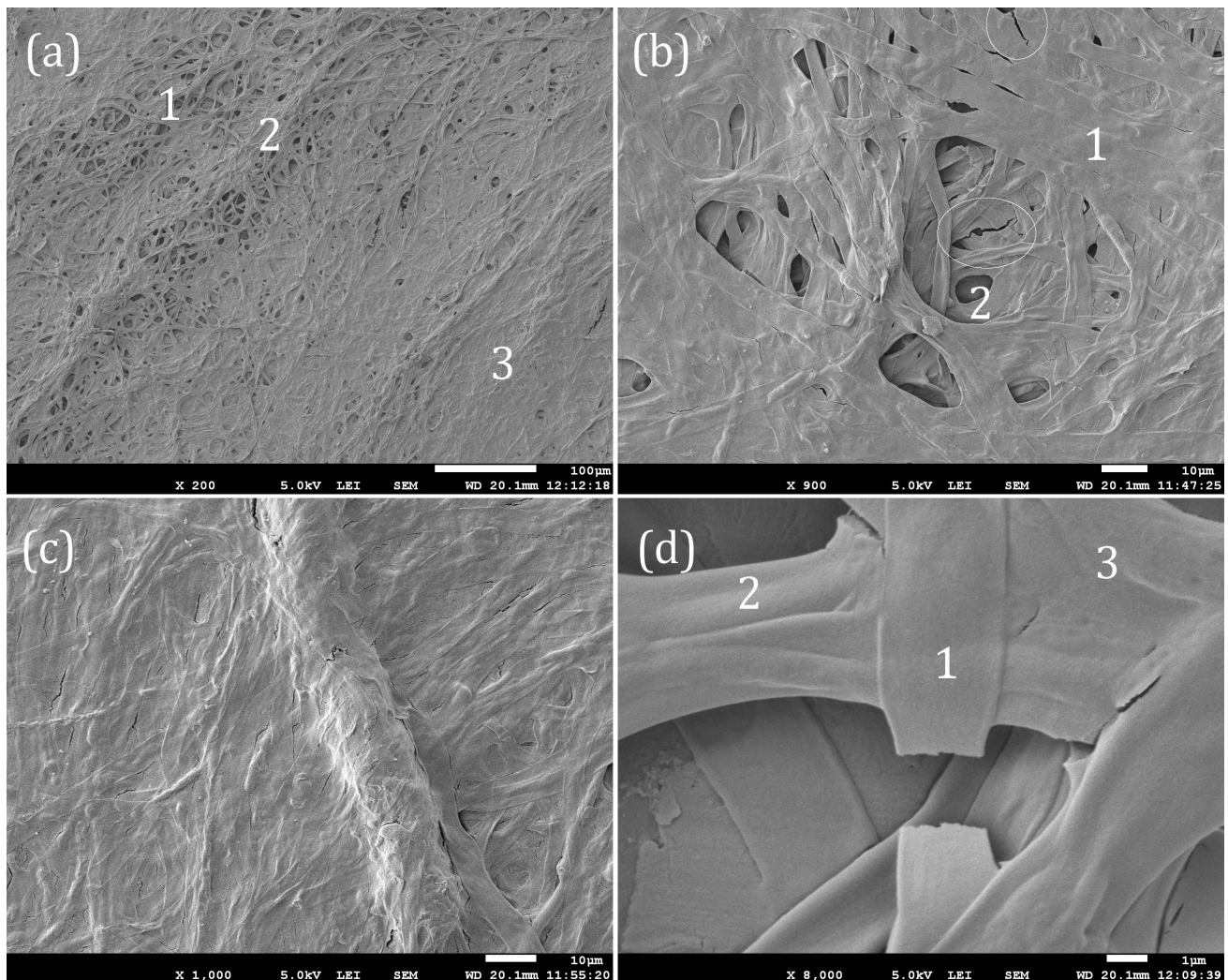
Figure 3.11 Top-view SEM images: unblended, unwashed mycelium on aluminum. All images are of the same sample, at various magnifications: (a) 200x, (b) 900x, (c) 1,000x, (d) 8,000x. The film was consolidated on Al 6082, in the 'degreased only' condition, though the surface is not visible in these images.

A higher magnification view of a large thread of entangled mycelium running across the image top to bottom is presented in Figure 3.11c. This thread has a width of about 10μm and rises a few microns above the rest of the film. This thread/rope is one of those discussed in the previous section, in which a large number of hyphae are tightly entangled. These possibly exist as nutrient transporting highways, since they can transport nutrients in one direction more effectively this way. From a materials standpoint, this structure could get in the way of creating a homogenous, continuous film of even thickness. In this case, however, the structure is embedded in the surrounding film with hyphae running through and across it. Indeed, it seems very much as if the hyphae in this image are embedded in a matrix of some kind. It is possible that the spaces between the hyphae are being filled by some biopolymer excretion. This biopolymer could be schizophyllan, a broadly studied excretion of *S. commune* fungi. This indicates that the mycelium grown this way form a composite microstructure: with hyphae acting as fibers, and biopolymer acting as the matrix. However, the large presence of cracks running parallel to the hyphae suggests that the interface between these hyphae and matrix is not stronger than the hyphae. In materials science, we highly prefer fiber failure to interfacial failure, as those fibers are meant to reinforce the matrix and they cannot do that without a proper interface.

Figure 3.11d shows a zoomed-in view of a few hyphae, illustrating their failure modes. From the lower magnification images, we identified two failure modes: transverse hyphae failure, and interfacial failure between hyphae and matrix. The flattened hyphae [1] running across the middle of the image has failed in tension, in a ductile fashion—evidenced by necking on both failed ends. This suggests that the flattened hyphae are at least somewhat elastic, which is supported by other research [32]. On the other hand, the inflated hyphae [2] shows cracking at its interface with hyphae 3 and 4. This makes sense if there is some matrix holding these hyphae in contact with each other. Again, it seems that the interface is not able to properly transfer load between biopolymer and hyphae, so the inflated hyphae—which could have withstood more pressure—do not get a chance to carry that load. This image supports the idea that inflated hyphae may be stronger in tension than flattened hyphae. Though it is not certain, as it is also possible that hyphae 1 in this instance just had more load on it, due to the heterogenous nature of the sample.

Blending the mycelium culture for 60s seems to have some effect on the microstructure of the resultant film. The top-view of this blended film is shown in Figure 3.12a. Compared to the

unblended film, this one has fewer large inhomogeneities and interruptions in structure. This is because the large ropes of hyphae were separated into many individual hyphae during the blending process. It also appears that porosity has been reduced, as hyphae are able to stack together more closely. The higher magnification view Figure 3.12b reveals the presence of both flattened and inflated hyphae. As with the unblended film, the problem areas of the film seem to be those where the hyphae have not been entirely unentangled, like in region [1]. Region [2] shows a far more uniform, continuous, and well-stacked hyphae structure. It's also interesting to note that the hyphae—in terms of length and width—do not seem to have been affected by blending. At most the hyphae have been unentangled, but there is no evidence that they have been chopped or grinded to smaller pieces.
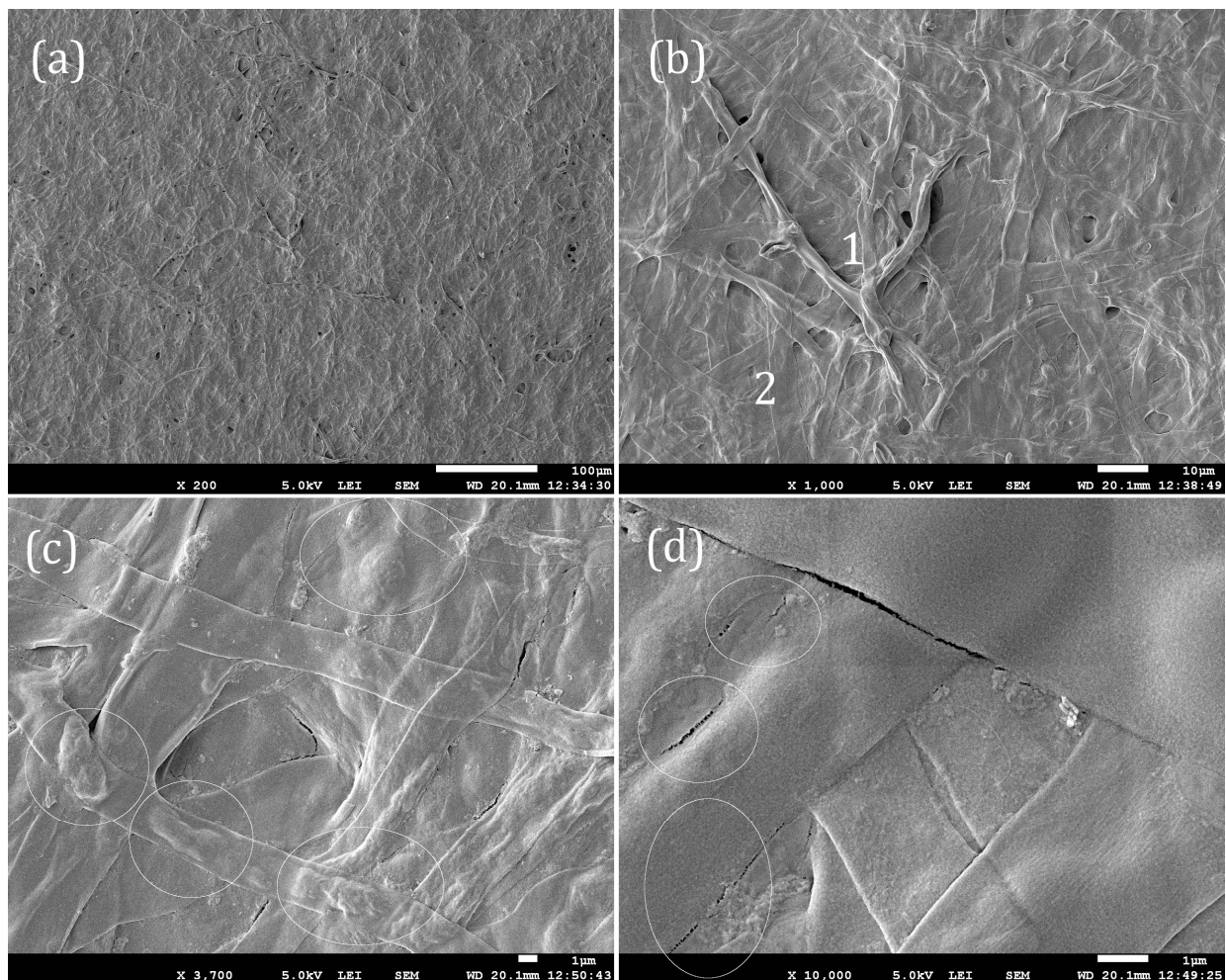
Figure 3.12 Top-view SEM images: blended 60s, unwashed mycelium on aluminum. All images are of the same sample, at various magnifications: (a) 200x, (b) 1000x, (c) 900x, (d) 8000x. The film was consolidated on Al 6082, in the 'degreased only' condition, though the surface is not visible in these images.

Zooming in further on the film (Figure 3.12c) reveals the composite structure of the film. The outlines of the flattened hyphae are visible, as well as widespread interfacial cracking. Of interest are the chunks of material pointed out by the circled areas. These chunks seem to be stuck within the hyphae, which could suggest that they are cytosolic contents of the fungi, which were not released. There are also some chunks outside of the hyphae, suggesting that some cytosolic contents escaped the hyphae through openings, but still stuck to the film. This cytosolic material is not useful from the perspective of creating a barrier film for aluminum, so it would be ideal to remove it entirely. In Figure 3.12d the interfacial failure discussed earlier is present in greater detail. The red circles highlight where this failure is occurring. Notice how the matrix separates from the hyphae with some strands of matrix still bridging the gap. This suggests progressive interfacial failure, and further suggests that the matrix is physically adhesive.

Washing the mycelium is a step that we could expect to remove water-soluble cytosolic contents and other water-soluble chemical components of the films. It is therefore interesting to see how the microstructure of the film changes after washing. Figure 3.13 compares an unwashed film to one that was washed 5x. In the low magnification image of the unwashed film in Figure 3.13a, there are again two distinct morphologies; porous regions where hyphae are randomly arranged in a fiber network free of matrix, and dense regions where hyphae appear weaving in and out of some matrix which they are embedded in. Interestingly the porous regions are far less prevalent in this section of the washed 5x film (Figure 3.13b). That is not to say that there are no porous regions in the washed sample, however, those large-scale heterogenous fiber bundles are not present to the same extent. Looking at the higher magnification images (Figure 3.13c&d), it seems that the hyphae are more often flattened and more tightly packed in the washed film. This corresponds to results found for free-standing mycelium films [11, 65] that hyphae densify upon being put through a water soak. The structure formed by the washed 5x film is more bulky than fibrous. A bulky structure is useful for creating barrier coatings due to lowered porosity and more even interfacial contact with surfaces, which could aid adhesion.

There are a few reasons why hyphae may collapse more in the washed 5x condition. Firstly, mycelium was stirred around during washing, which may have caused more cytosolic content to be removed from inside the hyphae. This is not entirely clear from the images above, however, it is logical that if hyphae are washed while they are open, then the water-soluble cytosolic contents will be removed. In both films, the chunks within the hyphae pointed out previously are also visible here. A more intensive washing process or longer water soak may have removed these

final bits of cytosolic content from the washed film. Another reason why the hyphae are more tightly wrapped in the washed film is due to the removal of water-soluble proteins and polysaccharides that are occupying space on the outside of the fungal cell wall. When these components are removed during a wash, more physical space and new hydrogen bonding sites are available for hyphae to pack closer together.
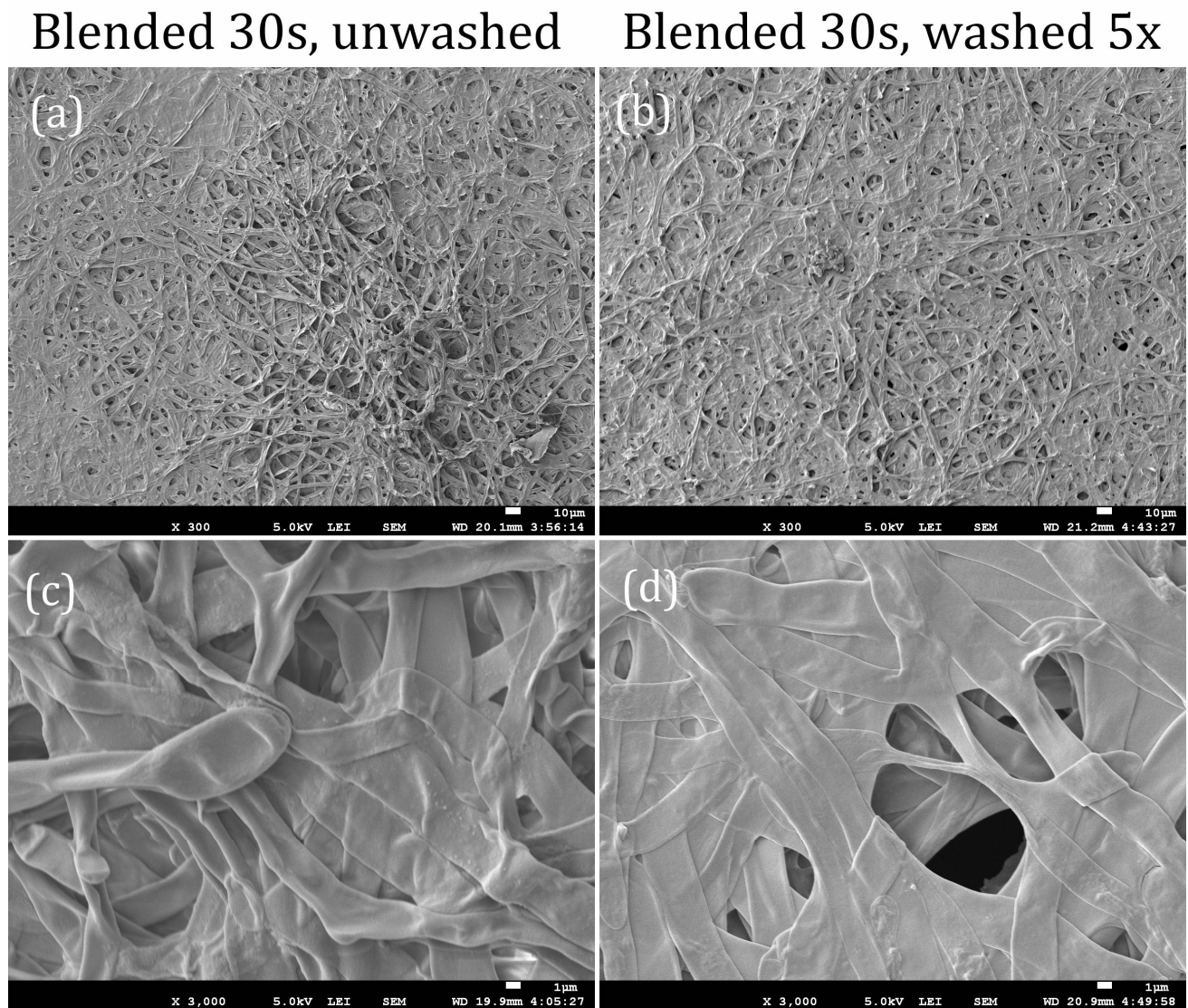
Figure 3.13 Top-view SEM images: unwashed vs. washed 5x mycelium on aluminum. (a) blended 30s, unwashed film at 300x and (c) 3,000x. (b) blended 30s, washed 5x film at 300x and (d) 3,000x. These films were consolidated on Al 6082, in the 'degreased only' condition, though the surface is not visible in these images.

3.3.4   Cross-section microstructure analysis of free-standing films

To understand further the microstructure of the mycelium films, we look at their cross-sections. However, it was not possible to create a cross-section of the films on aluminum. Instead, we created free-standing films using the same method used to consolidate them on aluminum. These films could be frozen in liquid nitrogen to embrittle them, and then split in half. The fracture plane could then be looked at under the SEM to gain some insight into what the inside of the film looks like. Due to warping, and difficulties creating an even profile, the cross-section images are shown in Figure 3.14 are not perfect, but they still provide valuable insight into the internal structure of these films. It is important to keep in mind that there may be structural differences between these free-standing films and those consolidated on aluminum. Figure 3.14a-c shows that the top/bottom surfaces of these films display the same porous fiber network structure as the films on metal. Further, notice how the samples which were blended for 30s exhibit severe warping compared to the unblended sample which is relatively flat. Also, notice the difference in thickness of these films—although the same volume of culture was used to create each. The unblended film is around 50µm thick, while both blended films are closer to 10µm thickness. This already suggests that the blended films are stacking more efficiently while drying than the unblended film. In the future, it would be important to make nicer films—more geometrically controlled size/shape—to be able to geometrically measure density and be able to prepare a nice cross-section.

In the high magnification look at the inside of the unblended and unwashed film in Figure 3.14d, the porous, chaotically arranged structure is evident. Some hyphae are running towards the fracture plane, while others are running parallel to it. Further, most hyphae have are at least partially inflated. It is not clear from this image whether there is a difference in the structure from the top of the film to the bottom. We could expect that hyphae may be more flattened near the bottom due to the pressure of hyphae above, but that doesn't seem to be the case. Further, we see many impurities and clumps on the outside of the hyphae. Also, a huge gap is present between the layers/planes of hyphae, where it seems that hyphae are completely absent. This suggests the possibility of large internal voids caused by structural inhomogeneities. Further, most hyphae seem to be fractured cleanly transversely, but there are instances of some that are entirely crushed/exploded.

Unblended, unwashed   Blended 30s, unwashed   Blended 30s, washed 5x
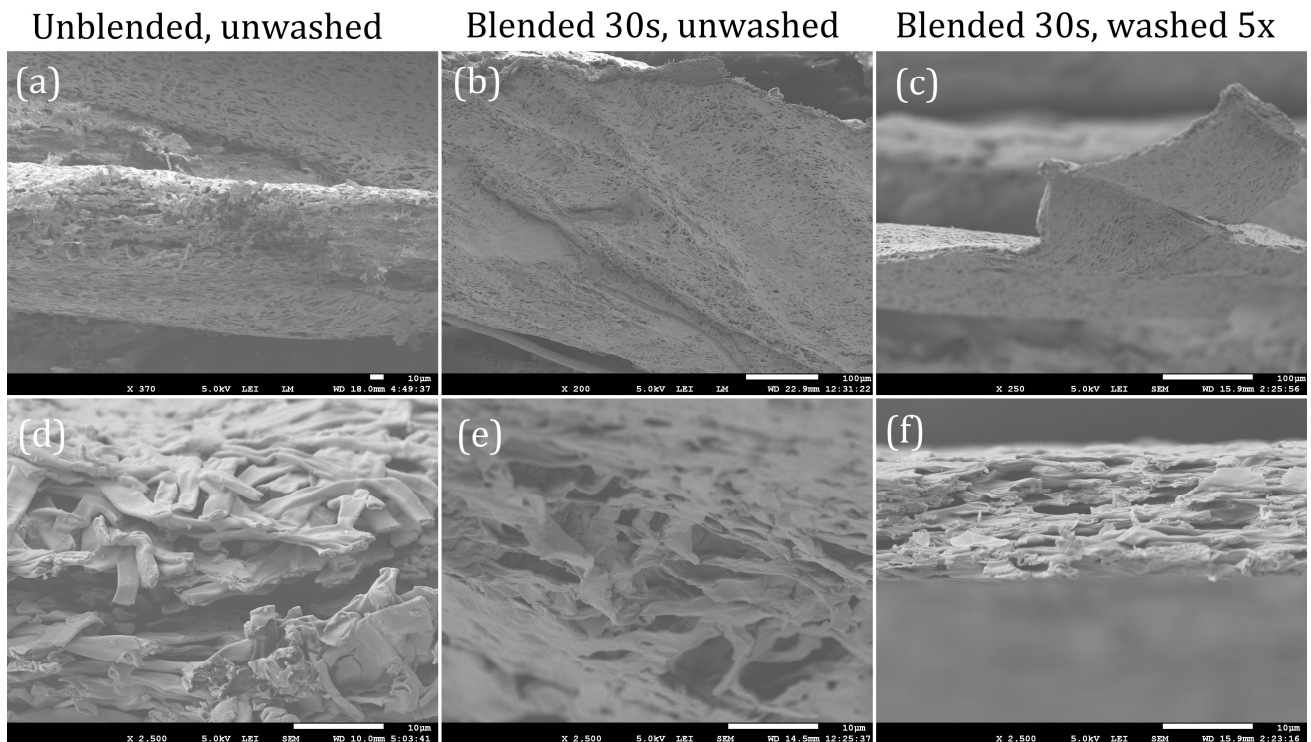
Figure 3.14 Cross-section SEM images of free-standing mycelium films. (a) brittle fracture plane of the unblended, unwashed mycelium film at 370x and (d) 2,500x. (b) brittle fracture plane of the blended 30s, unwashed mycelium film at 200x and (e) 2,500x. (c) brittle fracture plane of the blended 30s, washed 5x mycelium film at 250x and (f) 2,500x.

In the cross-section of the blended 30s, unwashed film in Figure 3.14e, the random and porous structure seems similar to the unblended, unwashed film. The main difference appears to be the presence of more flattened/disfigured hyphae. This, of course, could be explained by the blending process, which may open up more hyphae, allowing their contents to spill out. Still, there is scant evidence in this image to support that this film is denser. On the other hand, the blended 30s & washed 5x film (Figure 3.14f) shows a more neatly arranged microstructure. The hyphae in this film are mostly flat and pressed tightly onto each other. The structure seems like sheets of hyphae layered on top of each other. There still are voids inside the film, but they are less between hyphae and more between layers of hyphae.

As discussed in the introduction, *S. commune* fungi secrete a polysaccharide-based biopolymer called schizophyllan (SPG). This biopolymer has important functions, including aiding mycelial adhesion, and coating/protecting the mycelium. Since this molecule is water-soluble, it is reasonable to expect a difference in its level of presence in a washed or unwashed

film. The "matrix" we have pointed out in the previous SEM images of mycelium films may be composed at least partly of SPG. Figure 3.15 shows SEM images of a film of SPG extract that has been separated from the mycelium. This film (Figure 3.15a) is not fibrous, like the mycelium films shown before, but rather it is bulkier, like a polymer. Figure 3.15b shows the cross-section of this film, notice that pores are large and running parallel to the fracture plane. This is in contrast to the regular porosity of the fibrous mycelium structure. SPG may form a sort of layered structure due to its cohesiveness. Also notice in Figure 3.15c how the fracture plane of this film is clean, suggesting brittle failure. Further, there is no regular porosity visible, just material heterogeneities at the fracture plane.
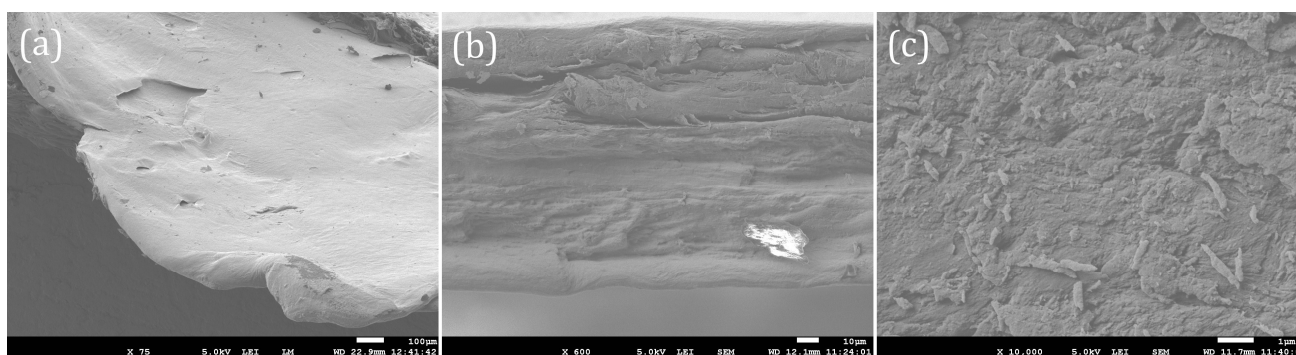
Figure 3.15 Cross-section SEM images of Schizophyllan film. All images are of the same sample, at various magnifications: (a) 75x, (b) 600x, (c) 10,000x.

3.3.5 Film thermal properties

The weight-loss-on-heating curves of select mycelium films in Figure 3.16a indicate a 2 or 3-step degradation process. The first step happens between 30 and 200°C—it represents the evaporation of water. Films which were created from blended 30s culture may contain slightly more water (2 to 3%) than those from unblended culture. At the same time, that water evaporates faster, suggesting that the water is more strongly bound in the unblended mycelium film. This follows logic, as the unblended film contains the large pellet structures which may have entrapped water within. There doesn't appear to be any difference in water content between the unwashed and washed 5x mycelium for each blending condition. This is interesting, as we did expect that the washed 5x samples may absorb some water during the short soak cycles. Apparently, the soaking time of 30 seconds was too short to lead to significant water absorption.

In other works, mycelium films are known to absorb water at a fast pace when immersed, however that does not necessarily seem to be the case when the raw biomass is soaked instead of the film. The extract from culture seems to contain more, and more strongly bound water than the other films. This suggests that the water in the schizophyllan film contains hydrogen bonded water molecules, rather than simply absorbed water trapped in pores.
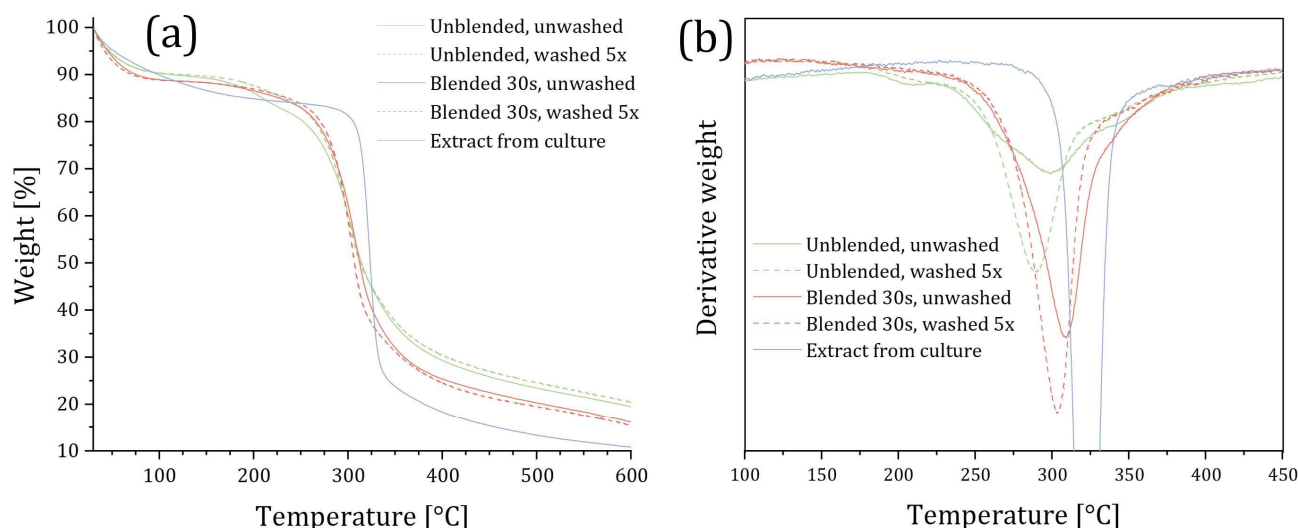
Figure 3.16 TGA degradation curves of select mycelium films and extract. (a) mass loss on heating, and (b) derivative of mass loss curve. Mass of ~5mg of material was used for each test run. Samples were heated from room temperature to 600°C at 10°C/min in air.

The next step is the main one during which most organics—proteins, lipids, and polysaccharides—degrade. This degradation starts around 200°C and reaches its maximum rate at around 300°C. When the degradation rate slows, and the final percentage of carbon char left over, varies depending on the type of film. A look at the derivative weight loss curves of this degradation step in Figure 3.16b provides more information on the differences. The first visible step happens around 210°C and is most prominent in the films from unblended cultures. This degradation step may represent the evaporation of strongly bound water or cytosolic water still inside the hyphae. We would expect there to be less cytosolic water trapped inside the hyphae in the blended films, as those would have more open hyphae which have already released their cytosolic contents. Therefore, we can hypothesize that blending and/or washing the culture reduces the amount of cytosolic content and water entrapped inside the hyphae.

The main degradation step is a single, sharp peak in the derivative weight loss curve (Figure 3.16b) for each sample except for the film from unblended, unwashed culture. That sample has multiple peaks obscuring each other. This result indicates that blending and washing the culture results in a more chemically homogenous material. Further, the peak derivative of weight loss increases for films from blended and washed cultures. This follows the logic that blending the culture increases homogeneity and that washing removes water-soluble compounds, further homogenizing the resultant films. Interestingly, the extract from culture film has by far the highest peak derivative at around 320°C —which also occurs at ~10 to 20°C higher than the mycelium films. This indicates that the extract has a more chemically homogenous and thermally stable composition than the other films. Compared to conventional polymers, like epoxy, this degradation temperature is quite high. This effect is even more evident when compared to biodegradable polymers like PLA, which has a melting temperature of around 160°C.

There is one final degradation step between 325 and 350°C, which is slightly overlapping with the main degradation peak. This could represent the degradation of the most thermally stable organic compounds in the fungal cell wall, such as chitin. That peak is not visible in the extract film, which is expected, since the extraction process does not remove chitin from the culture. The final difference between the samples is the amount of carbon char left over at 600°C. For the films from unblended culture the amount of residue is ~20% by weight. For the films from blended culture, the amount of char leftover is slightly less, indicating that more of the organic matter in the film could be degraded. For the films from extract, the amount of residue was around 10%, indicating less undegradable carbon-containing material.

3.3.6   Film chemical composition

Broken down chemically, mycelium is composed mostly of polysaccharides, proteins, and lipids. Unsurprisingly, the absorption ranges that show up on the IR spectra in Figure 3.17 correspond to those chemical components. The broad absorption band between 2600 and 3600cm^{-1} corresponds to hydrogen-bonded O-H stretching [69-72]. This could indicate the presence of carboxylic acids (2400 to 3400cm^{-1}) or phenols and alcohols (3100 to 3600cm^{-1}) [69-72]. Carboxylic acids may be present in the form of fatty acids or carboxyl groups on amino acids. Alcohol groups are present in the form of alpha and beta-glucans, while phenols could represent some bioactive molecule produced by the fungi. In the extract sample, the prevalence of the alcohol peak is likely due to ethanol leftover in the film from the extraction. The presence

of absorbed water also shows up in this region as an increase in peak intensity. Because of that, increase in peak intensity of the dried filtrate only tells that this sample was more wet when being measured than the other films.
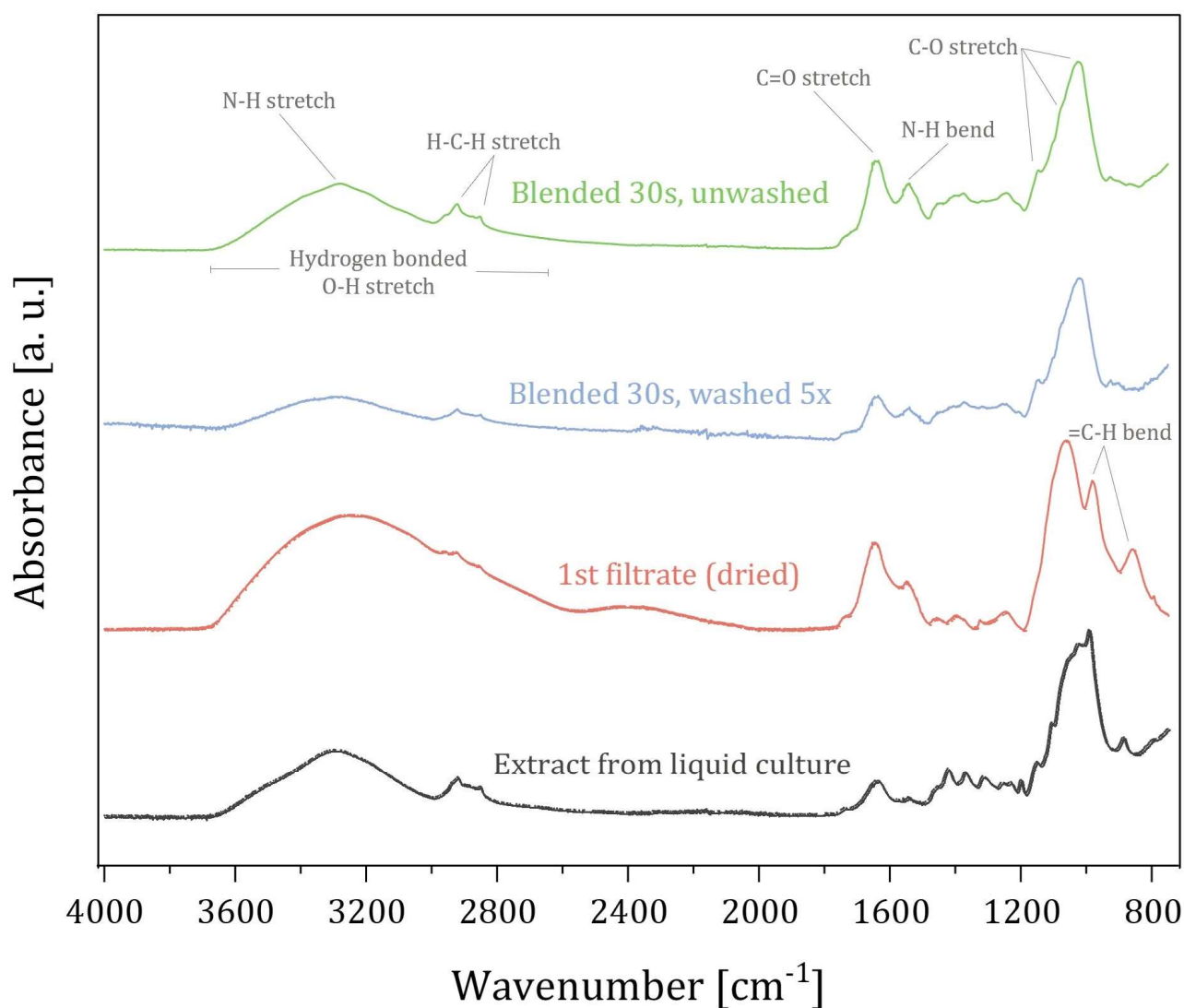
Figure 3.17 IR spectra of select mycelium films, filtrate, and extract. Films were compressed with a value of 50 to achieve a better signal. Still, not all samples had the same strength of signal. The curves shown here are normalized to the highest peak in their own curve. Thee absolute values of the peaks are not comparable here. For the purpose of this work it will be sufficient to compare the ratio of peak heights in a single spectra, between the samples.

A sharper peak at between 3100 and 3500cm^{-1} represents N-H stretching that is associated with amines or amides [69-72]. This could indicate the presence of proteins (amines) and/or chitin (amides). Since the prevalence of this peak decreases between the unwashed and washed 5x film, it is more likely to represent proteins—which are water-soluble and would be washed away during that process. This peak is not clearly visible in the extract or filtrate samples, though it may be obscured under the broad hydrogen-bonding peak. The C=O stretching peak at 1600-1670cm^{-1} and the N-H bending peak at 1550-1640cm^{-1} both indicate the presence of amines or amides [69-72]. As before, the presence of amines and amides relates to the presence of proteins and chitin in the films.

The peaks between 2800 and 3000cm^{-1} represent H-C-H stretching of alkanes [69-72]. Alkanes are present in fungi as fatty acids and phospholipids. These peaks are present in all the samples, so washing and extracting likely don't effect these molecules. The other peaks that can be linked to lipids are those at ~850 and ~990cm^{-1}. These both indicate =C-H bending of alkenes [69-72], which is commonly present in unsaturated fatty acids. Those peaks are present in the dried filtrate, indicating that these fatty acids are removed in the 5x washing process. These lipids may also be present to a smaller extent in the schizophyllan film. In short, these spectra indicate that washing effectively removes lipids and proteins from the mycelium film. This adds further evidence to the hypotheses that simple washing of the mycelium causes hyphae to stack more tightly together. If the proteins and lipids are not present, there is more space for the cell walls of the hyphae to bind with one another.

The last type of macromolecule present in these IR spectra are polysaccharides. Of course, polysaccharides are the main constituent of the film. The main indicator of these is the sharp peak between 900 and 1200cm^{-1}. This peak includes at least three distinct peaks which are overlapping, and all three peaks indicate C-O stretching [69-72]. This type of bond is present in alpha and beta -glucans, as well as chitin. Therefore, the peaks in this region represent the presence of polysaccharides. As we could expect, these peaks are present in all samples. However, we can't compare their absolute peak height to any effect. It is only possible to compare the ratios between peaks in each individual curve. The ratio of peak height between N-H bend and C-O stretch peaks, indicate that washing 5x decreases the presence of proteins in the resulting film.

These differences in chemical composition are relevant to creating an engineered film/coating out of mycelium. Firstly, we want to reduce the concentration of proteins and lipids in the film, which could be around 10% by mass of the film [35]. These do not add any structural

value and may be responsible for heterogeneities and porosity in the film. On the other, proteins and exopolysaccharides may serve adhesive function to the mycelium, which would be a useful property for a bio-coating. Therefore, it is possible that a tradeoff might exist, where washing the mycelium results in a more homogenous and less porous film, but at the same time results in a less adhesive film. We will now investigate this more in the next section.

3.3.7 Films on aluminum

In this section we demonstrate a novel method for quantifying mycelium adhesiveness to metal, which is to our knowledge a new addition to the field of mycelium research. Traditionally, adhesion of mycelium to substrates is measured by counting cells, solidifying in agar, removing the agar, and then counting how many cells are left [81]. This is sufficient, but not a very quantitative method. In this work we wanted to measure the adhesiveness of mycelium to metal in a way that we could compare results to conventional coatings materials. Thus, we used micro-scratch testing to determine critical failure loads, similar to how it is done for other materials. This section will show some insights on how strongly mycelium adheres to aluminum, and how it fails under an applied scratch load. Further, we will see how the surface condition of the aluminum affects this adhesion, and how washing and/or blending the mycelium may impact it further. To investigate these differences, we created the samples shown in Table 3.2.
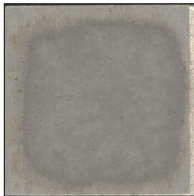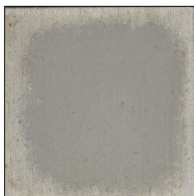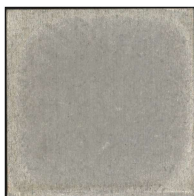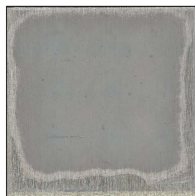
Due to time and material constraints, it was not possible to create the ideal samples that were exactly similar to each other. Most of the mycelium films came from culture 2, however the "blended 80s, unwashed" sample came from culture 3. This presents a possible huge source of variety in material behavior, as we discussed previously the differences between the cultures. Culture 2 was inoculated with 4ml of mycelium, while culture 3 was inoculated with 7ml. In literature, it has been reported that larger inoculum sizes cause more distributed growth rather than discrete pelleted growth [22]. Since the pelleted growth causes large heterogenous structures in the film (as shown in the SEM images), we could hypothesize that culture 3 would result in more homogenous films. We will see further if that is the case later in this section.

The volume of culture dropped onto the aluminum surface, and the resulting mass of mycelium film that formed there, were also variable. The sample that was washed 5x had about 35% less mass on the surface than the unwashed culture, which means that a lot of material was being removed in the wash. As discussed previously, this is all of the water-soluble glucans, proteins, lipids, and other loosely-bound cell wall material [36]. The variability in the other

masses of mycelium from culture 2 is due to randomness from the culture. Though the culture was stirred before pipetting, it was still a heterogenous suspension, so even pipetting the same volume will result in a different mass of mycelium. The "blended 80s, unwashed" sample from culture 3 had less mycelial mass on the surface because less volume of culture was used (0.5ml vs. 0.7ml), simply because a 0.7ml drop would not sit stably on the surface. The reason for that could be that the highly blended mycelium is very particulate and doesn't hold together cohesively enough to resistant wetting the surface. Further, there is a peculiar difference between the mycelium on different aluminum surface preparations. The samples treated to the pseudoboehmite condition seem to be missing that thin clear film surrounding the films dried on degreased only conditioned surfaces. It is unclear why this might be, though it could be with the way that the mycelium culture forms hydrogen bonds more effectively between mycelium-water-surface in the pseudoboehmite condition, when the surface is full of functional Al-O groups ready for hydrogen bonding.

Table 3.2 Select mycelium films consolidated on aluminum: micro-scratch test samples. Mass of mycelium on the surface was measured after 24 hours of drying. Thickness was measured using a laser scanning microscope, which provided a height map where the aluminum surface could be used as a reference.

	Blended 30s, unwashed	Blended 30s, unwashed	Blended 30s, unwashed	Blended 30s, washed 5x	Blended 80s, unwashed
Culture	Culture 2	Culture 2	Culture 2	Culture 2	Culture 3
Volume dropped	0.7ml	0.7ml	0.7ml	0.7ml	0.5ml
Mass of mycelium	4.1mg	3.6mg	3.5mg	2.3mg	3.0mg
Aluminum surface treatment	Only degreased	Degreased & grinded	Pseudoboehmite	Pseudoboehmite	Only degreased
Thickness of mycelium	15 to 30μm	~10 to 25μm	~15 to 30μm	10 to 20μm	~20 to 35μm

The last important physical feature of these films to discuss is their thickness. It was not possible to precisely determine thickness because of the material heterogeneity on the surface. In some locations, the material could be piled up to 35μm, while in other cases as low as 10μm. These values given are meant to be taken as a range of thickness values along the surface of the films, where the films could be anywhere between that depending on how much material was distributed there. For the most part, the ranges of thickness are similar, between 10 and 30 μm. In the future, it would be necessary to design a processing method which more evenly distributes material on the surface. These thickness variations could certainly have an effect on the micro-scratch testing results, which we will discuss next.

3.3.8   Progressive load micro-scratch testing

Micro-scratch testing is a conventional test to determine adhesion of coatings to substrates [82]. A typical setup for measuring adhesion of ceramic coatings is shown in Figure 3.18. A scratch tip (diamond stylus) applies a set compressive force to the sample, and then moves along the surface of the coating, maintaining that force, or increasing progressively. As the stylus scratches the sample, the combined compressive and tangential forces induce damage into the coating, which eventually cause it to de-adhere from its substrate. The point of adhesive failure is called the critical load (Lc), and is based on a subjective choice of consistent, reproducible damage, such as initiation of crack propagation, or initiation of spalling. With enough scratch repetitions the Lc determined in this way represents a point at which the coating fails. There are two ways to perform such a test to determine a critical load: with progressive loading and with constant loading. Progressive load scratches start from a low load and proceed to a load known or expected to be above the failure load of the material. The point along the scratch track where a reproducible damage event occurs is taken as the point for Lc determination. For the case of our material, preliminary results showed that we could expect failure at less than 1N force. Therefore, we loaded our samples from 0.03N to 1N. We chose a scratch speed of 10mm/min as we were time limited, and slower scratch speeds took too long.
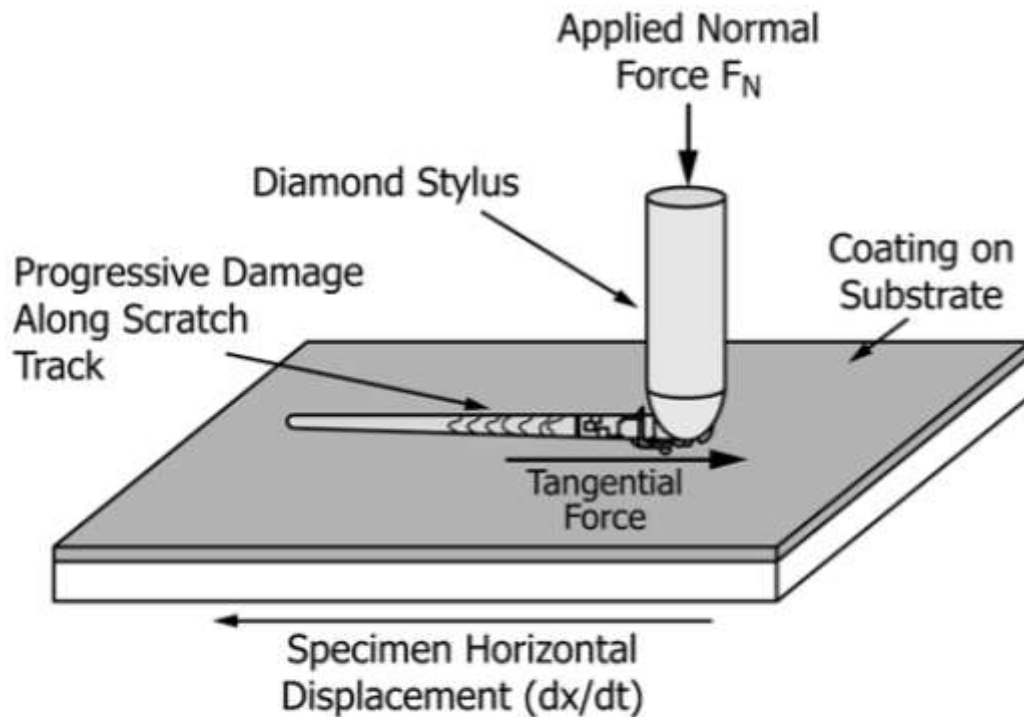
FIG. 1 Test Method Schematic

Figure 3.18 Schematic representation of micro-scratch test for coating adhesion. Source: ASTM C1624-05(2015), "Standard Test Method for Adhesion Strength and Mechanical Failure Modes of Ceramic Coatings by Quantitative Single Point Scratch Testing".

The scratch tracks for all five of the films with their five repetitions each, are shown in Figure 3.19. The gray color appearing from under the film is the exposed metal, where the mycelium film delaminated. For most samples, the film delaminated from its substrate early along the scratch track. Interestingly, in many cases film delamination was not exactly progressive. For example, some films delaminated first locally, and then only again at a higher load. This behavior highlights the heterogeneity of the films, which delaminate when the scratch tip encountered weak points in the film. As mentioned previously, the mycelium films were between 10 and 35µm in thickness. The scratch tip reached a penetration depth of about 3 µm by the end of the scratch track, so it never actually touched the metal. The compressive and tangential forces imposed by the scratch tip was what caused the damage to the mycelium film. The kind of irregular material removal present in these scratch tracks is expected for 'brittle and weak' materials, which have low tensile strength and ductility [83]. Based on the free-standing

83

films created earlier in the study for IR and TGA testing, weak and brittle is a suitable description of this mycelial material. Such materials are expected to exhibit earliest signs of damage at very low loads, and exhibit extensive cracking, crazing, void-formation, and delamination at higher loads [83].
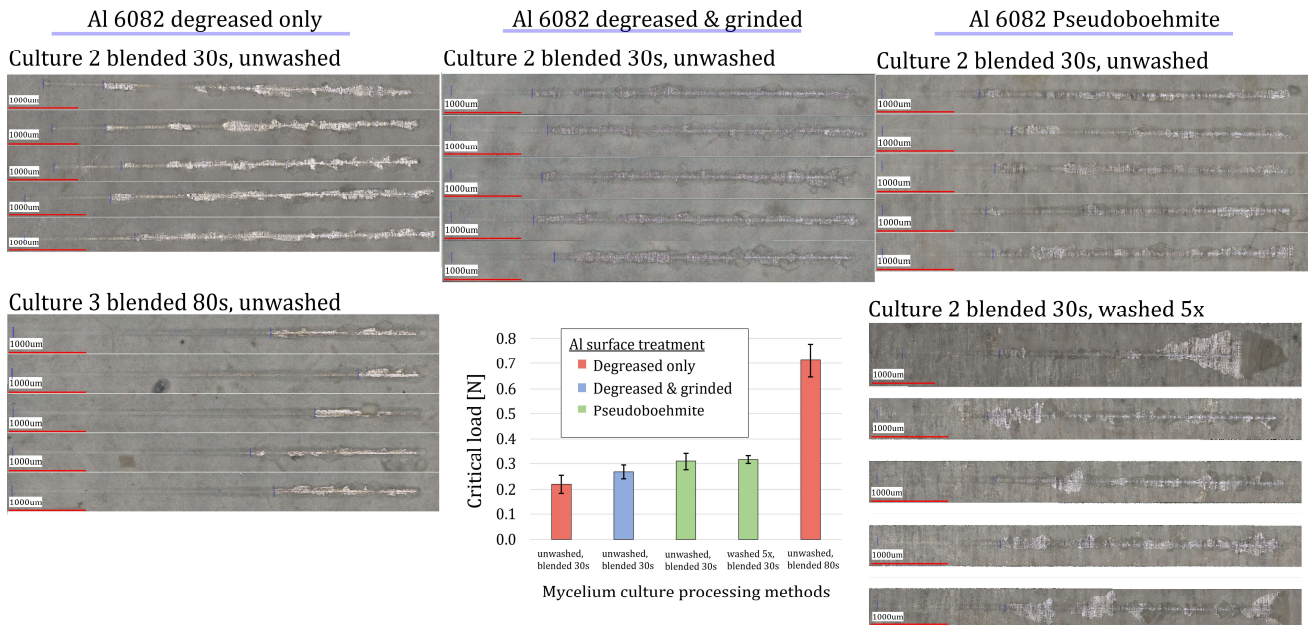
Figure 3.19 Compilation of progressive load micro-scratches for select mycelium films on aluminum 6082. The scratches in all cases proceed from left to right.

Cracks form at the mycelium-metal interface due to the applied compressive load. These cracks spread to behind the scratch tip, fully separating the compressed film from the bulk [82, 83]. This mechanism is well known and is illustrated in Figure 3.20. As the scratch tip continues forward, the material—in this case mycelial biomass—is pushed forward by the scratch tip. This mechanism is what causes the films to delaminate and is responsible for the pile-up of material seen at the end of the scratch track for many of the samples. Mycelium films which were more adhesive, or regions in a film that were heterogeneously more adhesive, were able to resist the sliding force imparted by the scratch tip and stay adhered to the aluminum substrate below. Since it was not possible to investigate more deeply the precise mechanisms of crack propagation using SEM analysis, the working theory shown in Figure 3.20 will be the basis for analysis of scratch testing in this work.
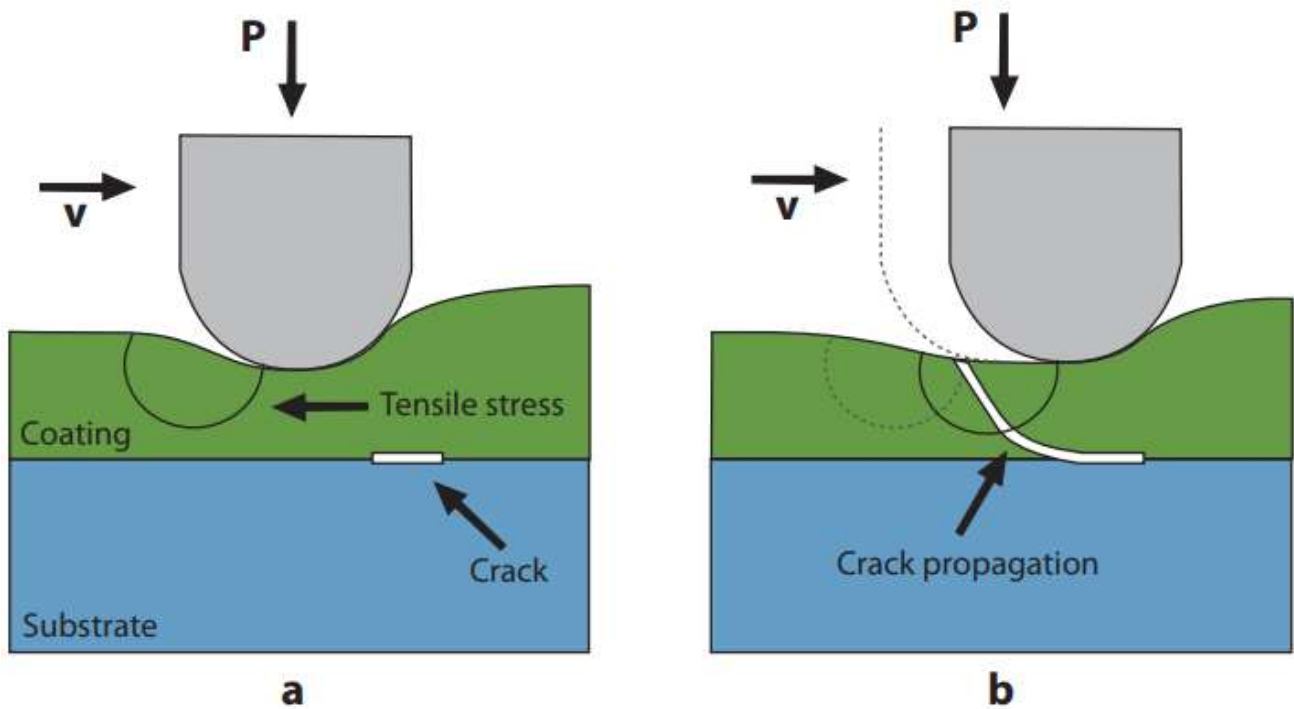
Figure 3.20 Schematic of how cracks spread during micro-scratch testing of polymeric films. Source: G. L. Guerriero, "Thermotropic Liquid Crystalline Thermosetting Polymers as Protective Coatings for Aerospace," PhD, Technische Universiteit Delft, 2012.

The conditions being compared in Figure 3.19 are the aluminum surface condition, and the effect of blending and washing the culture. The adhesiveness of mycelial biomass in these various conditions was compared by determining Lc averages of all the progressive load scratches for each sample. Critical load was chosen as the first point along the scratch at which the metal substrate is visible due to mycelium delamination. In polymer coatings, this is typically the known as the point of coating failure, where buckling due to high compression loads a crack propagation causes exposure of the substrate [84]. Other forms of damage typically found in polymeric coatings such as marring, spalling, and crack propagation [83] were not noticeable in these films due to their semi-transparent appearance. It was not possible to investigate by SEM, as the films delaminated from aluminum upon being exposed to a vacuum. spalling and crack propagation were not possible to determine in a reproducible way. The points along the scratch track chosen as the distance at which Lc occurred are marked by blue lines in Figure 3.19, and are recorded in Table 3.3.

Table 3.3 Critical loads of select mycelium films on aluminum from progressive load micro-scratch testing. Distances shown here are the average distances in mm from scratch start to first point of delamination along the scratch. Critical load is the average load applied on the coating at that distance, which was calculated individually for each sample.

| | Degreased only | | Degreased & grinded | | Pseudo-boehmite | | Pseudo-boehmite | | Degreased only | |
	Culture 2		Culture 2		Culture 2		Culture 2		Culture 3	
	Blended 30s		Blended 30s		Blended 30s		Blended 30s		Blended 80s	
	Unwashed		Unwashed		Unwashed		Washed 5x		Unwashed	
	Distance [mm]	Critical load [N]	Distance [mm]	Critical load [N]	Distance [mm]	Critical load [N]	Distance [mm]	Critical load [N]	Distance [mm]	Critical load [N]
Average	1.04	0.22	1.22	0.27	1.42	0.31	1.48	0.32	3.50	0.71
STD	0.21	0.04	0.17	0.03	0.17	0.03	0.07	0.01	0.33	0.07

The average critical load differs based on aluminum surface treatment and mycelium culture processing. Grinding the surface as opposed to simply degreasing, increases average Lc from 0.22N to 0.27N. This may be in part thanks to hyphae becoming entrapped or physically entangled in the grinding scratches on the surface. Performing the pseudoboehmite surface treatment further increased Lc to 0.31N. This is significantly higher than the average Lc of mycelial biomass on the 'degreased only' surface treatment. This can be better understood by first explaining what the pseudoboehmite treatment is. Pseudoboehmite is finely crystalline version of boehmite, which itself is an aluminum hydroxide mineral [85]. The chemical composition of pseudoboehmite is AlO(OH) [85]. When an aluminum plate is dipped in NaOH the following etching reaction produces sodium aluminate and hydrogen gas [86]:

$$2Al + 2NaOH + 2H_2O \rightarrow 2NaAlO_2 + 3H_2$$
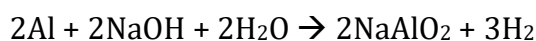
After washing under running water for a few seconds, the reaction proceeds to produce sodium hydroxide and aluminum hydroxide, which is deposited at the surface of the plate:

$$NaAlO_2 + H_2O \rightarrow NaOH + Al(OH_3)$$
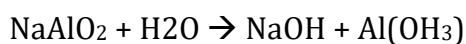
While slow-drying in air, the aluminum hydroxide deposited at the surface converts to aluminum oxide:

$$2Al(OH)_3 \rightarrow Al_2O_3 + 3H_2O$$

There is no loss of material at the surface [86], rather the oxide layer is reformed. This process destroys the native aluminum oxide layer and deposits a new oxide layer more homogenously across the surface. When that layer is hydrated, the chemical structure At that point, H-bonding between the aluminum oxide layer and -OH or -CH groups from the β-glucan chains of *S. commune* biomass may be more effective than before. An illustration for how β (1-3)-(1-6)-glucan may hydrogen bond to an aluminum oxide layer is shown in Figure 3.21. Compared to a 'degreased only' surface with the heterogeneous native oxide layer, there are more sites for hydrogen bonds to form between negative-dipole oxygens from the aluminum oxide and positive-dipole hydrogens from the glucan network. In case the aluminum oxide layer is hydrated, the glucan network of the fungal cell wall could form strong hydrogen bonds to the bound water at the surface. Since hydrogen bonding is the main proposed mechanism for adhesion of mycelial biomass, increasing the density of hydrogen bonding could be expected to increase adhesion. Thus, increased H-bonding potential may explain the 40% increase in Lc for the biomass adhered to the 'pseudoboehmite' aluminum surface condition compared to the 'degreased only' condition.

On aluminum plates with the 'pseudoboehmite' condition, there is no difference between the average critical load of an unwashed or washed 5x film (Table 3.3). The washed 5x mycelium film has Lc of 0.32N, compared to the unwashed mycelium film with Lc of 0.31N. However, this is only referring to the onset of damage in the film. The severity of delamination seems to be much higher in the film that was washed 5x (Figure 3.19). Further, it appears that cracks spread much further laterally from the scratch track on the washed 5x film. This suggests that the mycelial biomass that is washed 5x forms a more structurally brittle film. This can be tied back to the film microstructure in the SEM images, which showed a more collapsed and densely stacked hyphal arrangement. In this microstructure, there may be less space for hyphae to elastically deform when encountering the scratch tip, thus causing permanent deformation and crack propagation.
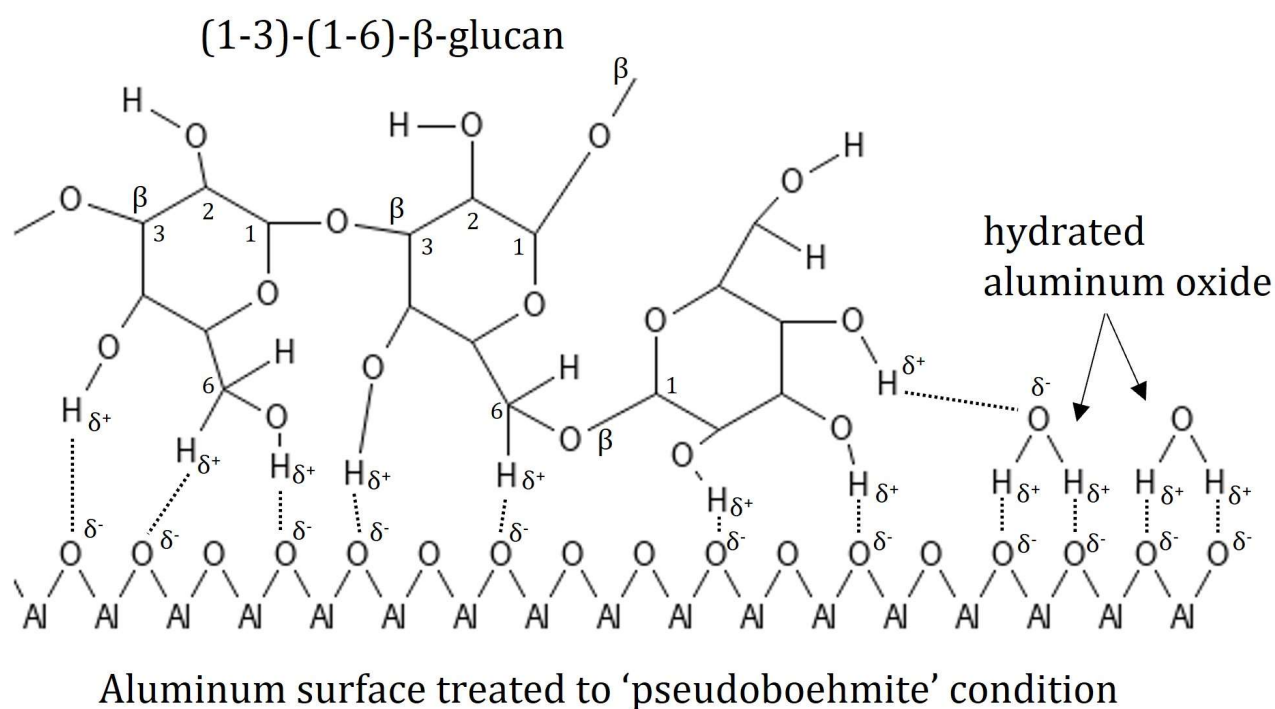
Figure 3.21 Illustration of possible H-bonding interactions between mycelial biomass and aluminum surface in 'pseudoboehmite' condition. This image does not represent the true chemical structure of fungi since it consists of more than just β-glucans. The purpose is to show that the main structural component of the fungal cell wall has many opportunities for H-bonding with a reformed aluminum oxide layer. Even when the oxide layer is hydrated, the β-glucans can hydrogen bond to the bound water in a similar way.

Further, IR spectra of washed and unwashed mycelial biomass suggest a smaller presence of proteins and lipids after washing, which may play a role in adhesion. Particularly, proteins called hydrophobins have been found to play an important role in adhesion of *S. commune* fungi to hydrophobic substrates like Teflon [81]. Bare aluminum plates are hydrophilic, with water contact angle around 80° [87]. Thus, it is unclear how these hydrophobins would interact with the surface of an aluminum alloy. Further, it is unclear how much water-soluble schizophyllan is removed during the wash, and how that could be expected to influence adhesion. According to these results, there is not a significant different in Lc between washed and unwashed mycelial biomass. However, the results also suggest that microstructure changes induced by washing indeed have a strong influence on the mechanical properties of the resulting film. This is in accordance with previous work which found that mycelium films washed 5x became 5x stiffer,

4x stronger, and twice as dense, while becoming slightly more brittle [11]. Further, it is important to note that the washed 5x film had less biomass than the unwashed film on the surface (2.3mg vs 3.5mg, Table 3.2), as well as overall lower thickness. In ceramic coatings, thicker coatings may produce lower Lc values due to higher residual stresses on the coating/substrate interface [88]. In polymeric coatings, higher coating thickness leads to higher critical loads, up to a point after which the effect levels off [84]. Since it is unknown how coating thickness affects scratch behavior of mycelial biomass, it is not possible to draw conclusions about its effect.

To test the effect of blending extent on the liquid culture, a sample of Culture 3 was blended for 80s, and consolidated on Al 6082, in the 'degreased only' condition. This sample compares to the sample of mycelial biomass for Culture 2, blended for 30s, and also consolidated on Al 6082, in the 'degreased only' condition. The mycelium film from Culture 3, blended for 80s had an average Lc of 0.71N, as opposed to 0.22N for the film from Culture 2, blended for 30s. This 220% increase in critical load seems to be an effect of the properties of the liquid culture from which the biomass came, and also the extent of blending. Firstly, Culture 3 was inoculated with 7ml of liquid inoculum, as opposed to Culture 2, which was inoculated with 4ml of liquid inoculum. This led to greater solids content in Culture 3 (8.32 vs. 6.24mg/ml, Table 3.1). Further, high inoculum size may favor dispersed growth, as opposed to growth as discrete pellets in culture with small inoculum volume [22]. However, other research shows the opposite, that in liquid culture growth of *P. ostreatus*, a 5x increase in inoculum volume leads to minor increases in pellet size by the end of growth [89]. Research on *S. commune* has found that inoculum size in low-nitrogen conditions is correlated to the density of biomass grown, and amount of SPG (schizophyllan) produced [90]. Thus, the larger inoculum size of Culture 3 led to a denser biomass, with possibly more SPG dissolved in the medium, and possibly more homogenously distributed growth.

A more homogenously distributed culture could lead to increased adhesion by increased surface contact of mycelium and metal at their interface. The SEM images in Figure 3.11 and Figure 3.12 support the idea that a culture blended for 60s results in a film on metal that is less porous and more uniformly deposited. Thus, increased blending time could increase adhesion by homogenizing the biomass and increasing surface contact for hydrogen bonding. Further, if there is indeed more SPG in the film from Culture 3—due to larger inoculum size—we could except a microstructure of hyphal filaments embedded in an SPG matrix like that shown in Figure 3.15. This could potentially aid mycelial adhesion to metal by increasing surface contact. Further, SPG may help to transfer loads more evenly between the hyphae, which could lead to greater
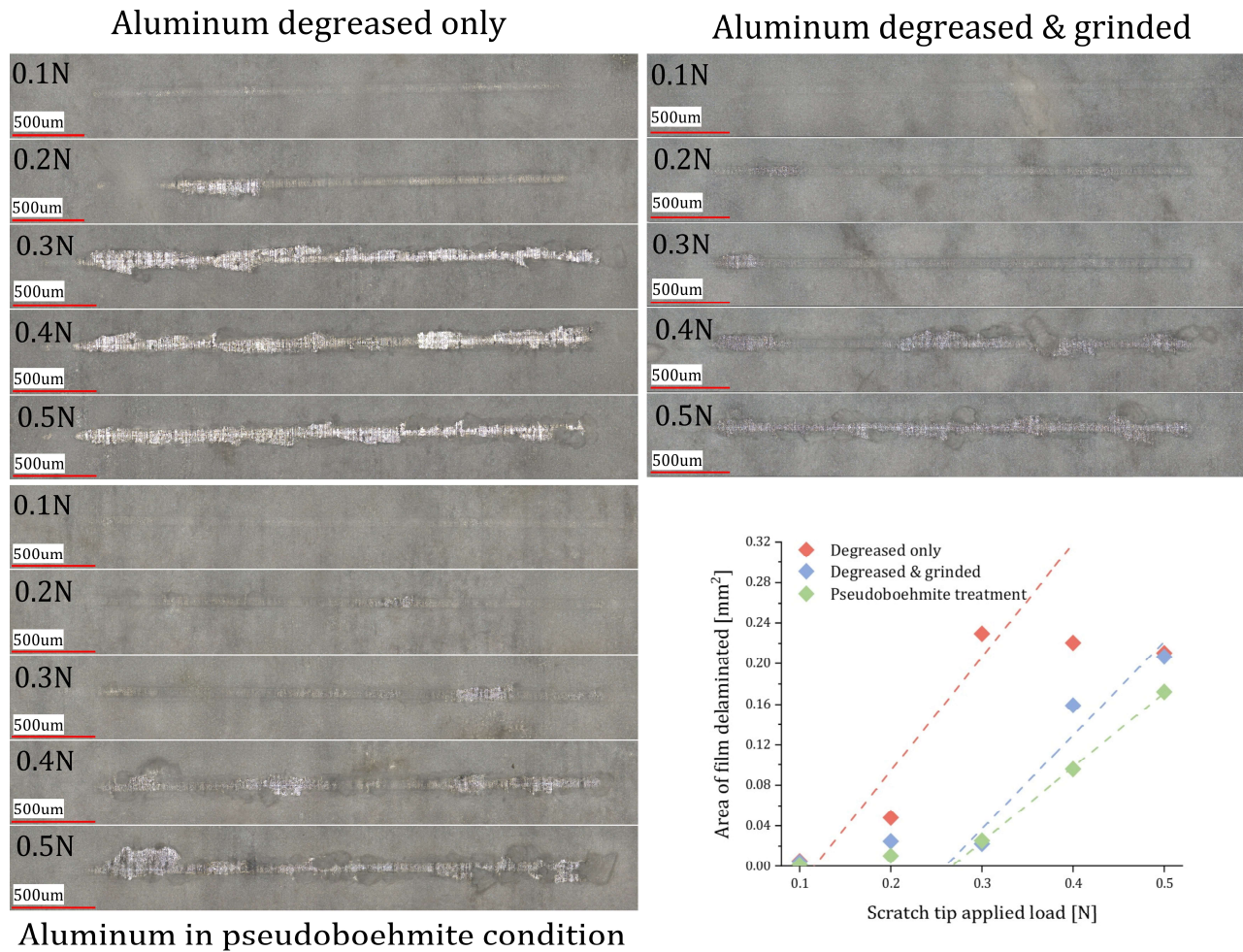
compressive strength, and thus greater scratch resistance. However, this is mostly theorizing since these specific properties were not tested for in this work. Thus, it is not possible to determine exactly what caused the 220% increase in Lc between the blended 30s film from Culture 2, and the blended 80s film from Culture 3. Nevertheless, based on literature it appears to be some combination of the effect of inoculum size on resulting culture morphology, greater SPG production for Culture 3, or longer blending time.

3.3.9   Constant load micro-scratch testing

Another way to analyze adhesion by micro-scratch testing is through constant load testing. Constant load micro-scratch testing involves scratches the surface at discrete loads to see what kinds of damage occur at specific loads. This can be used to compare how mycelium films in different conditions suffer damage differently at the exact same applied scratch load. In this section, the constant load scratch test results for the five mycelium shown in Table 3.2 are compared to determine the effect of aluminum surface condition, culture washing, and blending on mycelium film adhesion to aluminum. Based on progressive load testing, constant load scratches were chosen to go from 0.1N to 1.0N at 0.1N increments.

The first set of results compares the scratch response of mycelium films on three common and simple aluminum surface preparations. The scratch images and analysis are shown in Figure 3.22. The same kind of delamination failure is present in these scratch tests as in the progressive load tests. In all three films, local failure is clearly evident during the 0.2N and 0.3N scratch test. These early, local failure points represent the weakest areas of the film. The weak points could be caused by material, structural, or thickness heterogeneities, which all are present in these mycelium films on metal. Mycelium consolidated on the 'degreased only' surface delaminated entirely along the scratch track by 0.3N, while that didn't occur for mycelium on the other 'grinded' or 'pseudoboehmite' surfaces until 0.5N.

Aluminum degreased only

Aluminum degreased & grinded

0.1N
500um

0.1N
500um

0.2N
500um

0.2N
500um

0.3N
500um

0.3N
500um

0.4N
500um

0.4N
500um

0.5N
500um

0.5N
500um

0.1N
500um

0.2N
500um

0.3N
500um

0.4N
500um

0.5N
500um

Aluminum in pseudoboehmite condition

Figure 3.22 Area of film delaminated under constant loads around Lc: effect of Al surface condition. All films shown here are from Culture 2, blended for 30s and not washed.

The area of film delaminated can be measured by ImageJ thresholding and plotted to get an estimate of Lc—in a different way than with the progressive load scratches. The linear regression of the three points-of-increase to large-scale delamination can be used to determine an estimate of the load at which delamination started. This analysis shows that mycelium on 'degreased only' surface delaminated at just above 0.12N, whereas the 'degreased & grinded' and 'pseudoboehmite' surfaces started delaminating around 0.26N. This result indicates the just grinding the surface resulted in the mycelium films having more than 2x greater adhesiveness to aluminum, compared to the 'degreased only' surfaces. This contrasts with the results from progressive loading, which showed only a 0.04N difference in Lc between mycelium films on 'degreased only' and 'degreased & grinded' surfaces. This is mainly due to Lc being much lower for mycelium on 'degreased only' condition by this constant loading delamination analysis

compared to the progressive scratch analysis (0.12N vs. 0.22N). In any case, this result cements the finding that mycelial biomass adheres more strongly to aluminum surfaces after surface grinding, or pseudoboehmite treatment.

To investigate in greater detail the effect of grinding vs. pseudoboehmite treatment, analysis of delamination at the loads above Lc are necessary. At higher constant loads (Figure 3.23) the films have delaminated along the entire length of the scratch track. However, the amount of film that delaminates to the side of the scratch track is variable. As the scratch tip moves along the sample, it is compressing a certain area of the film depending on its penetration depth into the film. If the area of film delaminated is greater than the area of the film under compression, then the damage induced into the film was spreading past the scratch track. This indicates very weak adhesion where the internal forces generated by film cracking were enough to cause further spreading film delamination from the surface. This is the case for the "degreased & grinded" film on aluminum. However, the "pseudoboehmite treatment", except at 0.8N, experienced damage less than that of the compressed are of the film. This result indicates that mycelium films consolidated onto aluminum in the pseudoboehmite condition are more resistant to the compressive forces induced by the scratch tip. As discussed previously, this could be due to increased H-bonding density between the polysaccharide material in the mycelial biomass and the aluminum reformed aluminum oxide layer. When the scratch tip compressed the film, the higher density of hydrogen bonds created an interface that was more capable of resisting the induced normal forces that would de-adhere the film.
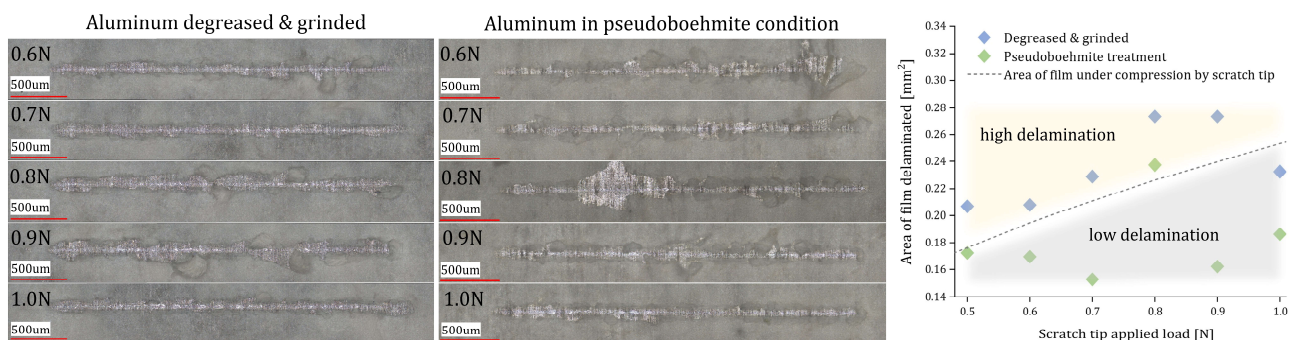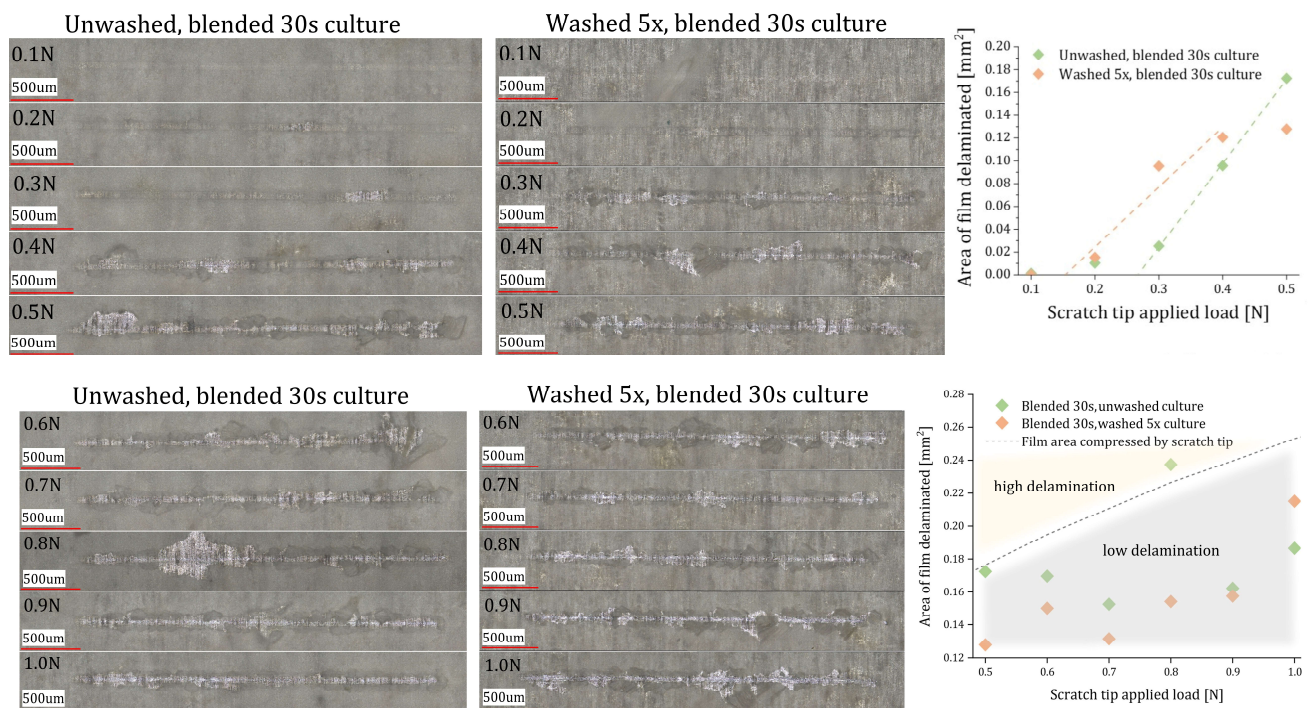

Figure 3.23 Area of film delaminated under constant loads above Lc: effect of Al surface condition. The degreased only condition is not shown in the chart of the higher loads, as that data was not collected.

It was also possible to compare the effect of washing the culture on constant load film delamination. Comparing an unwashed mycelium film to one washed 5x (Figure 3.24), both start to delaminate by 0.3N. However, the unwashed film delaminated only 0.03mm², compared to the washed 5x film which delaminated 10mm². For this reason, the linear regression analysis showed that the washed 5x mycelium starting delaminating at 0.15N as opposed to the unwashed mycelium, which started delaminating just below 0.3N. This result suggests that mycelia washed 5x are only half as adhesive to aluminum as mycelia that are not washed. This contrasts to the averages from progressive load scratch testing, which showed that washed unwashed films adhered similarly to aluminum. This discrepancy may be caused by material heterogeneities in the film, as progressive load scratches were taken from a different side of the film than constant load scratches. At higher loads (Figure 3.24Figure 3.24) the area of film delaminated is below the compressed area of the film for both samples. This indicates that this behavior may be dominated by surface conditions—pseudoboehmite treatment—in this case. Based on these results, it is inconclusive if there is a difference in adhesiveness between a washed and unwashed film of mycelium consolidated on aluminum.
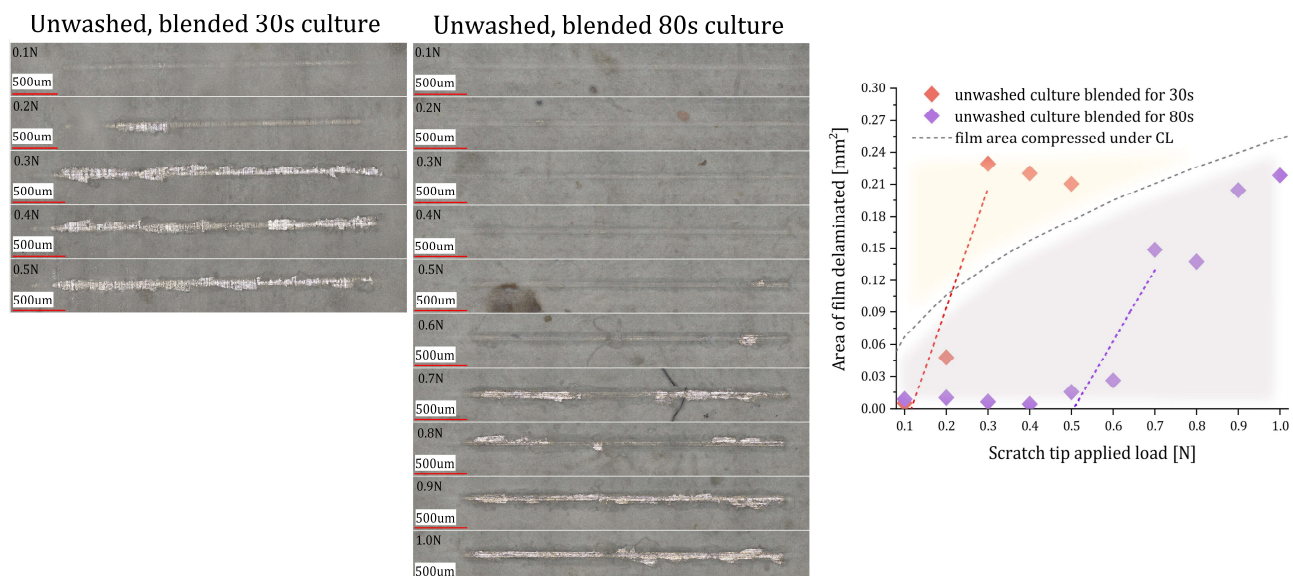

Figure 3.24 Area of film delaminated under constant loads: effect of washing the culture. Both films are consolidated on Al 6082, in the 'pseudoboehmite' condition.

Another processing step which may influence mycelium adhesion to aluminum is blending. When mycelium is blended, the hyphae that are entangled and roped together become less-so, and some hyphae may also become chopped into smaller fractions. This would help create a more homogenous film of which more surface area can make contact with the surface of the aluminum, and thus promote adhesion. The constant load scratch results shown in Figure 3.25 support this hypothesis. Local delamination in the blended 80s sample doesn't start until 0.5N, which is 316% higher than the 0.12N at which local delamination was already occurring for the film blended for only 30s. Global delamination doesn't happen until 0.9N, which is 300% greater than global delamination of the blended 30s culture. This result is in agreement with the progressive load scratches, which showed a 220% increase in Lc for the blended 80s mycelium film. These results suggest that properly homogenizing the mycelial biomass is a key factor determining adherence of mycelium to aluminum.

Figure 3.25 Area of film delaminated under constant load: effect of blending the culture. Both films are consolidated on Al 6082, in the 'degreased only' condition. The unwashed, blended 30s culture is the same shown previously for comparing aluminum surface treatments. The unwashed, blended 80s culture is from culture 3, not culture 2, which may also have a significant effect on scratch behavior.

Compared to other adhesive coatings reported in literature, even the best mycelium coating on aluminum was far inferior in terms of scratch resistance. The comparisons are shown in Table 3.4. The highest critical load (representing adhesive coating failure) achieved in this work was for the blended 80s, unwashed mycelium on Al 6082, in the 'degreased only' condition at 0.5 for constant load scratches, and 0.7 for progressive load scratches. Compared to that, chromium nitride ceramic coatings of more than 10x less thickness on steel began to show first signs of damage at 2N [88]. A more accurate comparison is to polycaprolactone (PCL), which is a fully biodegradable polymer. Coatings of PCL with approximately 50µm thickness have Lc around 3.7N on magnesium [91], or more than 5x higher than progressive load critical scratch average of the most adhesive mycelium film to aluminum. Acrylic coatings on steel with 36 µm thickness show first onset of damage at 18N and adhesive failure at 27N, which is around 38x higher. The most adhesive PVD DLC ceramic coatings on steel don't show damage until 54N [88], and polycarbonate and epoxy resins show first signs of damage around 70 and 75N, respectively [83]. These comparisons show that more development is required for mycelium to compare with traditional coating materials, in terms of adhesion to substrate.

Table 3.4 Values of Lc for onset of damage and adhesive failure for various adhesive coatings in literature.

Material	Substrate	Thickness (µm)	Onset of visible damage (N)	Coating adhesive failure (N)
Blended 80s, unwashed mycelium	Al 6082	20-35	-	0.5 (CL), 0.7 (PL)
PVD CrN (ceramic) [88]	Steel	1.9	2	-
PCL (biodegradable polymer) [91]	ZM21 Magnesium	49-52	-	3.7
Acrylic coating (polymer) [84]	Steel	36	18	27
PVD DLC (ceramic) [88]	M42 Steel	2	54	-

3.4   Conclusions

In conclusion, this segment of the work demonstrates that mycelial biomass can be consolidated onto aluminum to form films resembling coatings. When unprocessed, the biomass retains the microstructure it forms in liquid culture, resulting in a clumpy mass of fibrous material on the surface which has no resemblance to a coating. However, the inherent structure of the mycelium can be broken up by a minimum of 30s of high-speed blending. This step results in a culture which is more particulate—consisting of aggregations of hyphal filaments—which forms a more homogenously distributed film on aluminum. Washing such a blended culture in distilled water reduces hyphal aggregations and further homogenizes the resulting film. These blended and washed mycelial cultures form semi-transparent, thin films on aluminum, which more closely resemble engineering coatings, at least in appearance. In microstructure, the processed mycelium films are fibrous networks of thin filaments. It does appear that homogenizing the mycelium lowers porosity in the film microstructure. Unfortunately, porosity could not be eliminated entirely, as the fibrous structure of mycelium was preserved to some extent.

Despite its unsuitable microstructure for protective coating applications, mycelial biomass was adhesive to aluminum. This was investigated by micro-scratch testing, which revealed critical loads of adhesive coating failure between 0.2 to 0.7N depending on surface treatment, and mycelium culture processing. Compared to model epoxy resins, the scratch resistance values for mycelium films are remarkably low (more than 100x lower). Our mycelium films compare more favorably to other biodegradable polymer coatings like PCL, however still with critical load more than 5x lower. Nevertheless, this work demonstrated the possibility of improving mycelial biomass adhesion to aluminum by homogenizing the culture through blending. Further, both grinding and treating the aluminum surface with pseudoboehmite led to increases in adhesion. In conclusion, mycelial biomass is not significantly adhesive to aluminum using the methods described in this text. Nevertheless, this fungal material is easily processed, and further improvements in both structure and adhesion can be expected if optimizing the processing conditions demonstrated in this work.

4 CLOSING THOUGHTS & FUTURE PERSPECTIVES

The work was an investigative one, meant to explore the possibility of using filamentous fungi as protective coatings for aerospace aluminum alloys. In pursuit of this goal, we found that it is possible to grow *S. commune* mycelia in-situ on bare aluminum surfaces. In some cases, the mycelia grew to cover the entire surface with fibrous, mycelial biomass. This is a unique manufacturing method which takes advantage of the living aspect of fungi to grow material with minimal energy input directly to the surface. The biomass left on the surface after drying is a thick layer of micron-sized filaments, arranged as a random fiber network. Due to its porous and unstable microstructure, and its lack of adhesion to its aluminum substrate, this biomass has no current use in place on the surface as a protective coating. This severely limits its applications and research potential. Still, industry work on creating leather alternatives from mycelial biomass have shown that many post-processing steps are available to improve properties of this kind of fungal material. It could be interesting to try these post-processing steps—such as soaking the biomass-coated aluminum plate in glycerol water—to see if the biomass can be processed into a more interesting coating in-situ on the metal.

In the second half of our investigation, we investigated the possibility of extracting bio-based coating material from mycelial liquid culture. As these cultures have been used in literature to produce cohesive thin films, we were interested to see if those films could be formed on aluminum as protective coatings. The result was similar to the result of the in-situ growing mycelia on aluminum. After some processing the films could be made to look like conventional synthetic coatings, however their structure and properties could not. Issues of porous microstructure and weak adhesion to aluminum also severely limit the application potential of such films on metal. Looking towards the future, it would be necessary to process the material or hybridize it to densify the structure and improve adhesion to aluminum.

Our results showed that blending the mycelial culture, results in a more homogenous material distribution onto aluminum, and a more than 2x increase in adhesion to aluminum. Future investigations could be planned to determine the precise amount of blending time that yields the most benefit to microstructure and adhesion. Further, our results indicated that mycelial adhesion to aluminum was weaker when it was washed, due to the removal of adhesive substances like SPG. Future research could focus on forming adhesive thin films out of SPG extract and testing the scratch resistance. It is possible that hybridizing mycelial biomass with additional SPG could result in a film that is both less porous, and more adhesive. Indeed, one of the biggest issues with these films is their porosity due to fibrous microstructure. To solve that problem, mycelium could be hybridized with any number of biodegradable polymers, or biopolymers like SPG to produce a composite system in which mycelium forms the cohesive structure, and the polymer embeds its and creates a barrier.

One particular reason to be interested in fungi as bio-based coating platforms, is due to their living aspect. Figure 4.1 illustrates a theorized method to take advantage of fungi in a self-healing coating system. Fungi could be kept in statis inside a coating by limiting their access to oxygen or water, both which they need to grow. The fungi would be enveloped in a soft matrix, for example a bio-compatible polymer like fungal EPS. Upon receiving damage like a scratch, nutrient pellets inside the matrix would burst, and oxygen and water would be available, thus creating all the conditions needed for fungal growth. Fungi would then grow, restore the property, and close the site of damage again by forming a hard outer skin, which has been associated with mycelium materials [9]. For this aspect, mycelia could be grown at the surface as demonstrated in Chapter 2, and then post-processed to create this system.
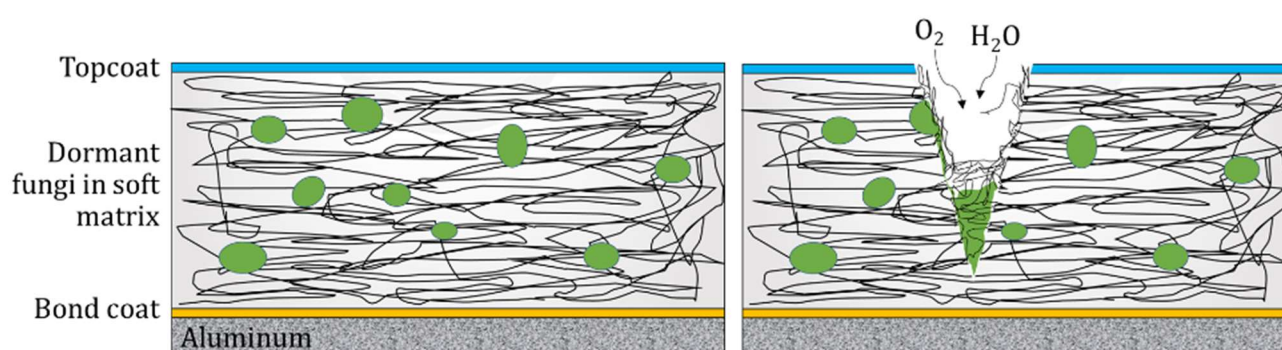
Figure 4.1 Illustrative theory of a protective mycelium coating for aluminum. The green circles represent pellets of nutrients encased in a hard shell, which breaks on suffering damage.

References

[1]   X.-S. Yi, X. Zhang, F. Ding, and J. Tong, "Development of Bio-Sourced Epoxies for Bio-Composites," *Aerospace,* vol. 5, no. 2, 2018, doi: 10.3390/aerospace5020065.

[2]   V. Montano, A. Smits, and S. J. Garcia, "The bio-touch: Increasing coating functionalities via biomass-derived components," *Surface and Coatings Technology,* vol. 341, pp. 2-14, 2018, doi: 10.1016/j.surfcoat.2017.10.073.

[3]   O. Weizman, A. Dotan, Y. Nir, and A. Ophir, "Modified whey protein coatings for improved gas barrier properties of biodegradable films," *Polymers for Advanced Technologies,* vol. 28, no. 2, pp. 261-270, 2017, doi: 10.1002/pat.3882.

[4]   P. J. Denissen and S. J. Garcia, "Cerium-loaded algae exoskeletons for active corrosion protection of coated AA2024-T3," *Corrosion Science,* vol. 128, pp. 164-175, 2017, doi: 10.1016/j.corsci.2017.09.019.

[5]   K. Nishchitha, M. K. Deepa, B. G. Prakashaiah, J. N. Balaraju, and B. E. Amitha rani, "Effect of Surface Treatment on Bio-corrosion in Aluminum Alloy 2024-T3," *Journal of Materials Engineering and Performance,* vol. 27, no. 11, pp. 5778-5787, 2018, doi: 10.1007/s11665-018-3671-5.

[6]   C. Balagna *et al.*, "Antibacterial coating on polymer for space application," *Materials Chemistry and Physics,* vol. 135, no. 2-3, pp. 714-722, 2012, doi: 10.1016/j.matchemphys.2012.05.049.

[7]   M. Jones *et al.*, "Waste-Derived Low-Cost Mycelium Nanopapers with Tunable Mechanical and Surface Properties," *Biomacromolecules,* vol. 20, no. 9, pp. 3513-3523, Sep 9 2019, doi: 10.1021/acs.biomac.9b00791.

[8]   V. Meyer *et al.*, "Growing a circular economy with fungal biotechnology: a white paper," *Fungal Biol Biotechnol,* vol. 7, p. 5, 2020, doi: 10.1186/s40694-020-00095-z.

[9]   E. Elsacker, A. Søndergaard, A. Van Wylick, E. Peeters, and L. De Laet, "Growing living and multifunctional mycelium composites for large-scale formwork applications using robotic abrasive wire-cutting," *Construction and Building Materials,* vol. 283, 2021, doi: 10.1016/j.conbuildmat.2021.122732.

[10]   F. V. W. Appels and H. A. B. Wösten, "Mycelium Materials," in *Encyclopedia of Mycology*, vol. 2, Ó. Zaragoza and A. Casadevall Eds.: Elsevier, 2021, pp. 710-718.

[11]   J. G. v. d. Brandhof, "Mycelium Design," MSc Thesis, Bio Inspired Innovation, Utrecht University, Utrecht, NL, 2018.

References

[12]   M. Jones, A. Gandia, S. John, and A. Bismarck, "Leather-like material biofabrication using fungi," *Nature Sustainability,* vol. 4, no. 1, pp. 9-16, 2020, doi: 10.1038/s41893-020-00606-1.

[13]   A. Gandia, J. G. van den Brandhof, F. V. W. Appels, and M. P. Jones, "Flexible Fungal Materials: Shaping the Future," *Trends Biotechnol,* Mar 26 2021, doi: 10.1016/j.tibtech.2021.03.002.

[14]   W. M. F. W. Nawawi, "Renewable Chitin Based Nanomaterials from Fungi," Doctor of Philosophy, Department of Chemical Engineering, Imperial College London, London, UK, 2016.

[15]   K. Z. Gumargalieva, I. G. Kalinina, S. A. Semenov, and G. E. Zaikov, "Bio-Damages of Materials. Adhesion of Microorganisms on Materials Surface," *Molecular Crystals and Liquid Crystals,* vol. 486, no. 1, pp. 213/[1255]-229/[1271], 2008, doi: 10.1080/15421400801921538.

[16]   I. G. Kalinina and K. Z. Gumargalieva, "Adhesion of conidia of Trichoderma viride to metal surfaces," *Protection of Metals and Physical Chemistry of Surfaces,* vol. 50, no. 7, pp. 910-912, 2014, doi: 10.1134/s2070205114070089.

[17]   M. B. Linder, G. R. Szilvay, T. Nakari-Setala, and M. E. Penttila, "Hydrophobins: the protein-amphiphiles of filamentous fungi," *FEMS Microbiol Rev,* vol. 29, no. 5, pp. 877-96, Nov 2005, doi: 10.1016/j.femsre.2005.01.004.

[18]   W. Sun, M. Tajvidi, C. Howell, and C. G. Hunt, "Functionality of Surface Mycelium Interfaces in Wood Bonding," *ACS Appl Mater Interfaces,* vol. 12, no. 51, pp. 57431-57440, Dec 23 2020, doi: 10.1021/acsami.0c18165.

[19]   F. Poohphajai, J. Sandak, M. Sailer, L. Rautkari, T. Belt, and A. Sandak, "Bioinspired Living Coating System in Service: Evaluation of the Wood Protected with Biofinish during One-Year Natural Weathering," *Coatings,* vol. 11, no. 6, 2021, doi: 10.3390/coatings11060701.

[20]   M. F. Sailer, E. J. van Nieuwenhuijzen, and W. Knol, "Forming of a functional biofilm on wood surfaces," *Ecological Engineering,* vol. 36, no. 2, pp. 163-167, 2010, doi: 10.1016/j.ecoleng.2009.02.004.

[21]   E. J. van Nieuwenhuijzen, M. F. Sailer, L. R. Gobakken, O. C. G. Adan, P. J. Punt, and R. A. Samson, "Detection of outdoor mould staining as biofinish on oil treated wood," *International Biodeterioration & Biodegradation,* vol. 105, pp. 215-227, 2015, doi: 10.1016/j.ibiod.2015.09.001.

[22]   D. Moore, G. D. Robson, and A. P. J. Trinci, *21st century guidebook to fungi.* Cambridge, UK: Cambridge University Press, 2011.

[23]   S. Bengtson *et al.*, "Fungus-like mycelial fossils in 2.4-billion-year-old vesicular basalt," *Nat Ecol Evol,* vol. 1, no. 6, p. 141, Apr 24 2017, doi: 10.1038/s41559-017-0141.

References

[24]   Y. Eshet, M. R. Rampino, and H. Visscher, "Fungal event and palynological record of ecological crisis and recovery across the Permian-Triassic boundary," *Geology,* vol. 23, no. 11, 1995, doi: 10.1130/0091-7613(1995)023<0967:Feapro>2.3.Co;2.

[25]   J. W. Deacon, *Fungal Biology*, 4th ed. Malden, MA, USA: Blackwell Publishing Ltd, 2006.

[26]   K. W. T. Chethana *et al.*, "What are fungal species and how to delineate them?," *Fungal Diversity,* vol. 109, no. 1, pp. 1-25, 2021, doi: 10.1007/s13225-021-00483-9.

[27]   H. A. B. Wosten, "Filamentous fungi for the production of enzymes, chemicals and materials," *Curr Opin Biotechnol,* vol. 59, pp. 65-70, Oct 2019, doi: 10.1016/j.copbio.2019.02.010.

[28]   M. L. Smith, J. N. Bruhn, and J. B. Anderson, "The fungus Armillaria bulbosa is among the largest and oldest living organisms," *Nature,* vol. 356, no. 6368, pp. 428-431, 1992, doi: 10.1038/356428a0.

[29]   P. Ruijten, H. P. Huinink, and O. C. G. Adan, "Hyphal growth of Penicillium rubens in changing relative humidity," *Appl Microbiol Biotechnol,* vol. 105, no. 12, pp. 5159-5171, Jun 2021, doi: 10.1007/s00253-021-11343-6.

[30]   H. Rözycki, "Effect of heavy metals (Pb, Zn, Cu and Cd) on mycelial growth of Cylindrocarpon destructans (zinssm.) scholten," *Zentralblatt für Mikrobiologie,* vol. 148, no. 4, pp. 265-275, 1993, doi: 10.1016/s0232-4393(11)80102-2.

[31]   M. Haneef, L. Ceseracciu, C. Canale, I. S. Bayer, J. A. Heredia-Guerrero, and A. Athanassiou, "Advanced Materials From Fungal Mycelium: Fabrication and Tuning of Physical Properties," *Sci Rep,* vol. 7, p. 41292, Jan 24 2017, doi: 10.1038/srep41292.

[32]   M. E. Antinori, L. Ceseracciu, G. Mancini, J. A. Heredia-Guerrero, and A. Athanassiou, "Fine-Tuning of Physicochemical Properties and Growth Dynamics of Mycelium-Based Materials," *ACS Applied Bio Materials,* vol. 3, no. 2, pp. 1044-1051, 2020, doi: 10.1021/acsabm.9b01031.

[33]   A. Brand and N. A. R. Gow, "Tropic Orientation Responses of Pathogenic Fungi," in *Morphogenesis and Pathogenicity in Fungi*, (Topics in Current Genetics, 2012, ch. Chapter 2, pp. 21-41.

[34]   J. P. Latge, "The cell wall: a carbohydrate armour for the fungal cell," *Mol Microbiol,* vol. 66, no. 2, pp. 279-90, Oct 2007, doi: 10.1111/j.1365-2958.2007.05872.x.

[35]   J. H. Sietsma and J. G. H. Wessels, "Chemical analysis of the hyphal walls of Schizophyllum commune," *Biochimica et Biophysica Acta (BBA) - General Subjects,* vol. 496, no. 1, pp. 225-239, 1977, doi: 10.1016/0304-4165(77)90131-3.

[36]   H. L. Ehren, F. V. W. Appels, K. Houben, M. A. M. Renault, H. A. B. Wosten, and M. Baldus, "Characterization of the cell wall of a mushroom forming fungus at atomic resolution using solid-state NMR spectroscopy," *Cell Surf,* vol. 6, p. 100046, Dec 2020, doi: 10.1016/j.tcsw.2020.100046.

[37]   N. A. R. Gow, J. P. Latge, and C. A. Munro, "The Fungal Cell Wall: Structure, Biosynthesis, and Function," *Microbiol Spectr,* vol. 5, no. 3, May 2017, doi: 10.1128/microbiolspec.FUNK-0035-2016.

[38]   I. Geoghegan, G. Steinberg, and S. Gurr, "The Role of the Fungal Cell Wall in the Infection of Plants," *Trends Microbiol,* vol. 25, no. 12, pp. 957-967, Dec 2017, doi: 10.1016/j.tim.2017.05.015.

[39]   K. Dzięgielewski, D. Nalepka, A. Chlebicki, and A. Walanus, "Too young for tinder? The palaeoecological context and possible function of subfossil fungi (basidiomes) found in the settlement from the Early Iron Age in Podłęże, S Poland," *Journal of Archaeological Science: Reports,* vol. 36, 2021, doi: 10.1016/j.jasrep.2021.102837.

[40]   U. Pientner and R. Poder, "Ethnomycological remarks on the Iceman's fungi," 2000.

[41]   D. N. Pegler, "Useful fungi of the world: Amadou and Chaga," *Mycologist,* vol. 15, no. 4, pp. 153-154, 2001, doi: 10.1016/s0269-915x(01)80004-5.

[42]   W. M. V. Horn, B. F. Shema, W. H. Shockley, and J. H. Conkey, "Sheets comprising filaments of fungi," USA Patent 2811422, 1957.

[43]   M. A. Johnson and J. A. Carlson, "Mycelial Paper: A Potential Resource Recovery Process?," in "IPC Technical Paper Series," The Institute of Paper Chemistry, Appleton, Wisconsin, December 1977 1977.

[44]   W. J. A. Dschida, "Fungal cell wall production and utilization as a raw resource for textiles," United States Patent 5854056, 1998.

[45]   S. Yamanaka and R. Kikuchi, "Complex of fibers and fungi and a process for preparation therof," United States Patent 5074959, 1991.

[46]   B. Sagar, P. Hamlyn, and D. Wales, "Nonwoven fabric," UK Patent GB 2165865A Patent Appl. 8525265, 1986.

[47]   G. A. Holt, G. McIntyre, D. Flagg, E. Bayer, J. D. Wanjura, and M. G. Pelletier, "Fungal Mycelium and Cotton Plant Materials in the Manufacture of Biodegradable Molded Packaging Material: Evaluation Study of Select Blends of Cotton Byproducts," *Journal of Biobased Materials and Bioenergy,* vol. 6, no. 4, pp. 431-439, 2012, doi: 10.1166/jbmb.2012.1241.

[48]   M. Jones, T. Huynh, C. Dekiwadia, F. Daver, and S. John, "Mycelium Composites: A Review of Engineering Characteristics and Growth Kinetics," *Journal of Bionanoscience,* vol. 11, no. 4, pp. 241-257, 2017, doi: 10.1166/jbns.2017.1440.

References

[49]   S. C. Khoo *et al.*, "Development of formaldehyde-free bio-board produced from mushroom mycelium and substrate waste," *J Hazard Mater,* vol. 400, p. 123296, Dec 5 2020, doi: 10.1016/j.jhazmat.2020.123296.

[50]   Z. Tacer-Caba, J. J. Varis, P. Lankinen, and K. S. Mikkonen, "Comparison of novel fungal mycelia strains and sustainable growth substrates to produce humidity-resistant biocomposites," *Materials & Design,* vol. 192, 2020, doi: 10.1016/j.matdes.2020.108728.

[51]   E. Elsacker, S. Vandelook, J. Brancart, E. Peeters, and L. De Laet, "Mechanical, physical and chemical characterisation of mycelium-based composites with different types of lignocellulosic substrates," *PLoS One,* vol. 14, no. 7, p. e0213954, 2019, doi: 10.1371/journal.pone.0213954.

[52]   R. Liu *et al.*, "Preparation of a kind of novel sustainable mycelium/cotton stalk composites and effects of pressing temperature on the properties," *Industrial Crops and Products,* vol. 141, 2019, doi: 10.1016/j.indcrop.2019.111732.

[53]   F. V. W. Appels *et al.*, "Fabrication factors influencing mechanical, moisture- and water-related properties of mycelium-based composites," *Materials & Design,* vol. 161, pp. 64-71, 2019, doi: 10.1016/j.matdes.2018.11.027.

[54]   R. Abhijith, A. Ashok, and C. R. Rejeesh, "Sustainable packaging applications from mycelium to substitute polystyrene: a review," *Materials Today: Proceedings,* vol. 5, no. 1, pp. 2139-2145, 2018, doi: 10.1016/j.matpr.2017.09.211.

[55]   M. Jones, A. Mautner, S. Luenco, A. Bismarck, and S. John, "Engineered mycelium composite construction materials from fungal biorefineries: A critical review," *Materials & Design,* vol. 187, 2020, doi: 10.1016/j.matdes.2019.108397.

[56]   C. Girometta *et al.*, "Physico-Mechanical and Thermodynamic Properties of Mycelium-Based Biocomposites: A Review," *Sustainability,* vol. 11, no. 1, 2019, doi: 10.3390/su11010281.

[57]   E. Elsacker, S. Vandelook, A. Van Wylick, J. Ruytinx, L. De Laet, and E. Peeters, "A comprehensive framework for the production of mycelium-based lignocellulosic composites," *Sci Total Environ,* vol. 725, p. 138431, Jul 10 2020, doi: 10.1016/j.scitotenv.2020.138431.

[58]   W. M. F. W. Nawawi, K. Y. Lee, E. Kontturi, A. Bismarck, and A. Mautner, "Surface properties of chitin-glucan nanopapers from Agaricus bisporus," *Int J Biol Macromol,* vol. 148, pp. 677-687, Apr 1 2020, doi: 10.1016/j.ijbiomac.2020.01.141.

[59]   M. Jones, M. Kujundzic, S. John, and A. Bismarck, "Crab vs. Mushroom: A Review of Crustacean and Fungal Chitin in Wound Treatment," *Mar Drugs,* vol. 18, no. 1, Jan 18 2020, doi: 10.3390/md18010064.

References

[60]   W. M. F. W. Nawawi, M. P. Jones, E. Kontturi, A. Mautner, and A. Bismarck, "Plastic to elastic: Fungi-derived composite nanopapers with tunable tensile properties," *Composites Science and Technology,* vol. 198, 2020, doi: 10.1016/j.compscitech.2020.108327.

[61]   W. M. F. W. Nawawi, M. Jones, R. J. Murphy, K. Y. Lee, E. Kontturi, and A. Bismarck, "Nanomaterials Derived from Fungal Sources-Is It the New Hype?," *Biomacromolecules,* vol. 21, no. 1, pp. 30-55, Jan 13 2020, doi: 10.1021/acs.biomac.9b01141.

[62]   M. R. Islam, G. Tudryn, R. Bucinell, L. Schadler, and R. C. Picu, "Morphology and mechanics of fungal mycelium," *Sci Rep,* vol. 7, no. 1, p. 13070, Oct 12 2017, doi: 10.1038/s41598-017-13295-2.

[63]   J. Bustillos *et al.*, "Uncovering the Mechanical, Thermal, and Chemical Characteristics of Biodegradable Mushroom Leather with Intrinsic Antifungal and Antibacterial Properties," *ACS Applied Bio Materials,* vol. 3, no. 5, pp. 3145-3156, 2020, doi: 10.1021/acsabm.0c00164.

[64]   F. V. W. Appels, J. Dijksterhuis, C. E. Lukasiewicz, K. M. B. Jansen, H. A. B. Wosten, and P. Krijgsheld, "Hydrophobin gene deletion and environmental growth conditions impact mechanical properties of mycelium by affecting the density of the material," *Sci Rep,* vol. 8, no. 1, p. 4703, Mar 16 2018, doi: 10.1038/s41598-018-23171-2.

[65]   F. V. W. Appels, J. G. van den Brandhof, J. Dijksterhuis, G. W. de Kort, and H. A. B. Wosten, "Fungal mycelium classified in different material families based on glycerol treatment," *Commun Biol,* vol. 3, no. 1, p. 334, Jun 26 2020, doi: 10.1038/s42003-020-1064-4.

[66]   N. Attias *et al.*, "Biofabrication of Nanocellulose–Mycelium Hybrid Materials," *Advanced Sustainable Systems,* vol. 5, no. 2, 2020, doi: 10.1002/adsu.202000196.

[67]   X. Zhou, Y. Liu, G. E. Thompson, G. M. Scamans, P. Skeldon, and J. A. Hunter, "Near-Surface Deformed Layers on Rolled Aluminum Alloys," *Metallurgical and Materials Transactions A,* vol. 42, no. 5, pp. 1373-1385, 2010, doi: 10.1007/s11661-010-0538-2.

[68]   Y. Liu *et al.*, "Evolution of near-surface deformed layers during hot rolling of AA3104 aluminium alloy," *Surface and Interface Analysis,* vol. 42, no. 4, pp. 180-184, 2010, doi: 10.1002/sia.3135.

[69]   "IR Spectrum Table & Chart." https://www.sigmaaldrich.com/ES/es/technical-documents/technical-article/analytical-chemistry/photometry-and-reflectometry/ir-spectrum-table (accessed 2021).

[70]   "Typical IR Absorption Frequencies For Common Functional Groups." Northern Illinois University, Department of Chemistry and Biochemistry. https://www.niu.edu/clas/chembio/research/analytical-lab/ftir/ir-frequencies-table.shtml (accessed 2021).

[71]   P. Beauchamp, "IR Spectroscopy Power Point slides," Cal Poly Pomona, Power point presentation.

References

---

[72]   "Infrared   Spectroscopy   Absorption   Table."
        https://chem.libretexts.org/Ancillary_Materials/Reference/Reference_Tables/Spectroscopic_Parameters
        /Infrared_Spectroscopy_Absorption_Table (accessed 2021).

[73]   U. Donatus, J. V. de Sousa Araujo, C. de Souza Carvalho Machado, N. V. Vardhan Mogili, R. A. Antunes, and I.
        Costa, "The effect of manufacturing process induced near-surface deformed layer on the corrosion
        behaviour of AA2198-T851 Al–Cu–Li alloy," *Corrosion Engineering, Science and Technology,* vol. 54, no. 3,
        pp. 205-215, 2018, doi: 10.1080/1478422x.2018.1558932.

[74]   J. Kirtzel *et al.*, "Organic acids, siderophores, enzymes and mechanical pressure for black slate
        bioweathering with the basidiomycete Schizophyllum commune," *Environ Microbiol,* vol. 22, no. 4, pp.
        1535-1546, Apr 2020, doi: 10.1111/1462-2920.14749.

[75]   Á. Machuca, D. Navias, A. Milagres, M. F. C. Daniel, and Y. Guillén, "Efects of metal ions (Cd2+, Cu2+, Zn2+)
        on the growth and chelating-compound production of three ectomycorrhizal fungi," *Interciencia,* vol. 39, 4,
        pp. 221-227, April 2014 2014.

[76]   Z. Chen *et al.*, "Characterization of physicochemical and biological properties of Schizophyllum commune
        polysaccharide extracted with different methods," *Int J Biol Macromol,* vol. 156, pp. 1425-1434, Aug 1 2020,
        doi: 10.1016/j.ijbiomac.2019.11.183.

[77]   T. D. Leathers, M. S. Nunnally, and N. P. Price, "Co-production of schizophyllan and arabinoxylan from corn
        fiber," *Biotechnol Lett,* vol. 28, no. 9, pp. 623-6, May 2006, doi: 10.1007/s10529-006-0028-1.

[78]   P. J. Denissen, "In-situ Visual Quantification of Corrosion and Corrosion Protection," Aerospace
        Engineering, Novel Aerospace Materials, Delft University of Technology, 2020.

[79]   G. Molero and H.-J. Sue, "Scratch behavior of model epoxy resins with different crosslinking densities,"
        Materials & Design, vol. 182, 2019, doi: 10.1016/j.matdes.2019.107965.

[80]   M. Osinska-Jaroszuk *et al.*, "Extracellular polysaccharides from Ascomycota and Basidiomycota: production
        conditions, biochemical characteristics, and biological properties," *World J Microbiol Biotechnol,* vol. 31, no.
        12, pp. 1823-44, Dec 2015, doi: 10.1007/s11274-015-1937-8.

[81]   H. A. B. Wösten, F. H. J. Schuren, and J. G. H. Wessels, "Interfacial self-assembly of a hydrophobin into an
        amphipathic protein membrane mediates fungal attachment to hydrophobic surfaces," *EMBO,* vol. 13, no.
        24, pp. 5848-5854, 1994.

[82]   G. L. Guerriero, "Thermotropic Liquid Crystalline Thermosetting Polymers as Protective Coatings for
        Aerospace," PhD, Technische Universiteit Delft, 2012.

[83]   H. Jiang, R. Browning, and H.-J. Sue, "Understanding of scratch-induced damage mechanisms in polymers,"
   *Polymer,* vol. 50, no. 16, pp. 4056-4065, 2009, doi: 10.1016/j.polymer.2009.06.061.

[84]   R. L. Browning, G. T. Lim, A. Moyse, H. J. Sue, H. Chen, and J. D. Earls, "Quantitative evaluation of scratch resistance of polymeric coatings based on a standardized progressive load scratch test," *Surface and Coatings Technology,* vol. 201, no. 6, pp. 2970-2976, 2006, doi: 10.1016/j.surfcoat.2006.06.007.

[85]   E. A. Vlasov, V. A. Lipin, R. A. Seytenov, N. V. Maltseva, and N. A. Odincova, "Features of Pseudoboehmite from Alumina Production," in *Light Metals 2018*, (The Minerals, Metals & Materials Series, 2018, ch. Chapter 11, pp. 71-77.

[86]   N. Saleema, D. K. Sarkar, R. W. Paynter, D. Gallant, and M. Eskandarian, "A simple surface treatment and characterization of AA 6061 aluminum alloy surface for adhesive bonding applications," *Applied Surface Science,* vol. 261, pp. 742-748, 2012, doi: 10.1016/j.apsusc.2012.08.091.

[87]   B. Yin *et al.*, "Bioinspired construction on aluminum alloy surfaces with stable super-hydrophobicity and their resulting wettability," *Surface and Interface Analysis,* vol. 44, no. 5, pp. 584-589, 2012, doi: 10.1002/sia.3875.

[88]   *C1624 - 05 (Reapproved 2015) Standard Test Method for Adhesion Strength and Mechanical Failure Modes of Ceramic Coatings by Quantitative Single Point Scratch Testing*, A. International, West Conshohocken, PA, 2015.

[89]   Y. M. Kim and H. G. Song, "Effect of fungal pellet morphology on enzyme activities involved in phthalate degradation," *J Microbiol,* vol. 47, no. 4, pp. 420-4, Aug 2009, doi: 10.1007/s12275-009-0051-8.

[90]   A. Mohammadi, S. A. Shojaosadati, H. J. Tehrani, S. M. Mousavi, T. Saleh, and A. C. Khorasani, "Schizophyllan production by newly isolated fungus Schizophyllum commune IBRC-M 30213: optimization of culture medium using response surface methodology," *Annals of Microbiology,* vol. 68, no. 1, pp. 47-62, 2017, doi: 10.1007/s13213-017-1316-9.

[91]   N. Singh, U. Batra, K. Kumar, and A. Mahapatro, "Investigating TiO2–HA–PCL hybrid coating as an efficient corrosion resistant barrier of ZM21 Mg alloy," *Journal of Magnesium and Alloys,* vol. 9, no. 2, pp. 627-646, 2021, doi: 10.1016/j.jma.2020.08.003.

Appendix A

Growing mycelium on Al – inoculum on top: methodology & supplemental data for surface coverage analysis

Processing & thresholding the images
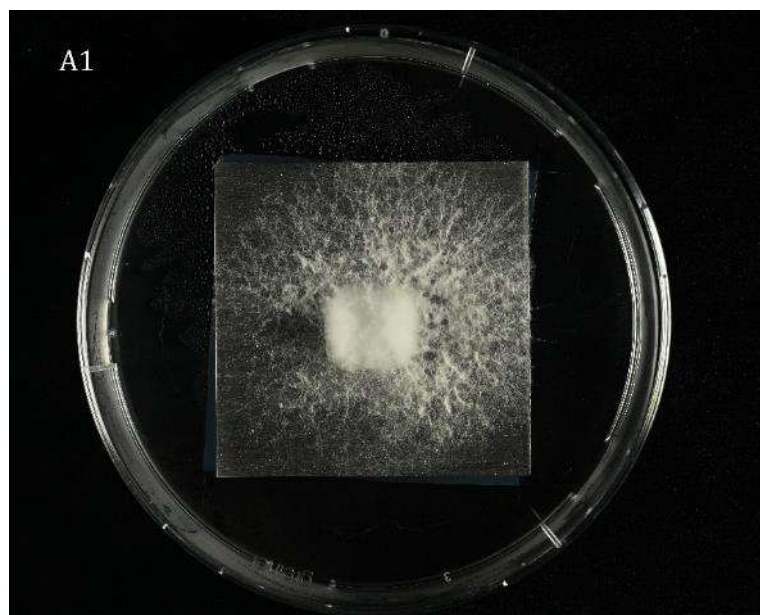
Figure A.1 Example of a raw image before processing. Example of a raw image before processing. This image shows the top view of mycelial growth coverage on aluminum as it is still wet and in the petri dish. The sample used for this example is "no food underneath/small feeding block" sample #1, at day 6 of mycelial growth.

1. Set a global scale by measuring the width of a plate as 50mm

2. Cropped the raw images (mycelium still wet in petri dish, Figure) to 49 x 49mm, leaving out the edges as they were very noisy

3. Covered the feeding block area with white so it could be excluded from the result. We are interested in growth on the metal, not on the feeding block.

a. An area of 15 x 15mm was used for the "small feeding blocks"

b. An area of 25 x 25mm was used for the "large feeding blocks"

c. These areas were sufficient to ensure all feeding blocks on all samples were fully covered. Due to size differences between feeding blocks, in some

Example of a raw image before processing. This

d. samples some of the metal surface was also whited out. This is a source of error in the results.

4. De-noised the images using the process → noise → remove outliers function in imageJ Fiji (Figure A.)

a. Removed first the bright outliers with radius 10 and threshold of 50, then the dark outliers with the same setting
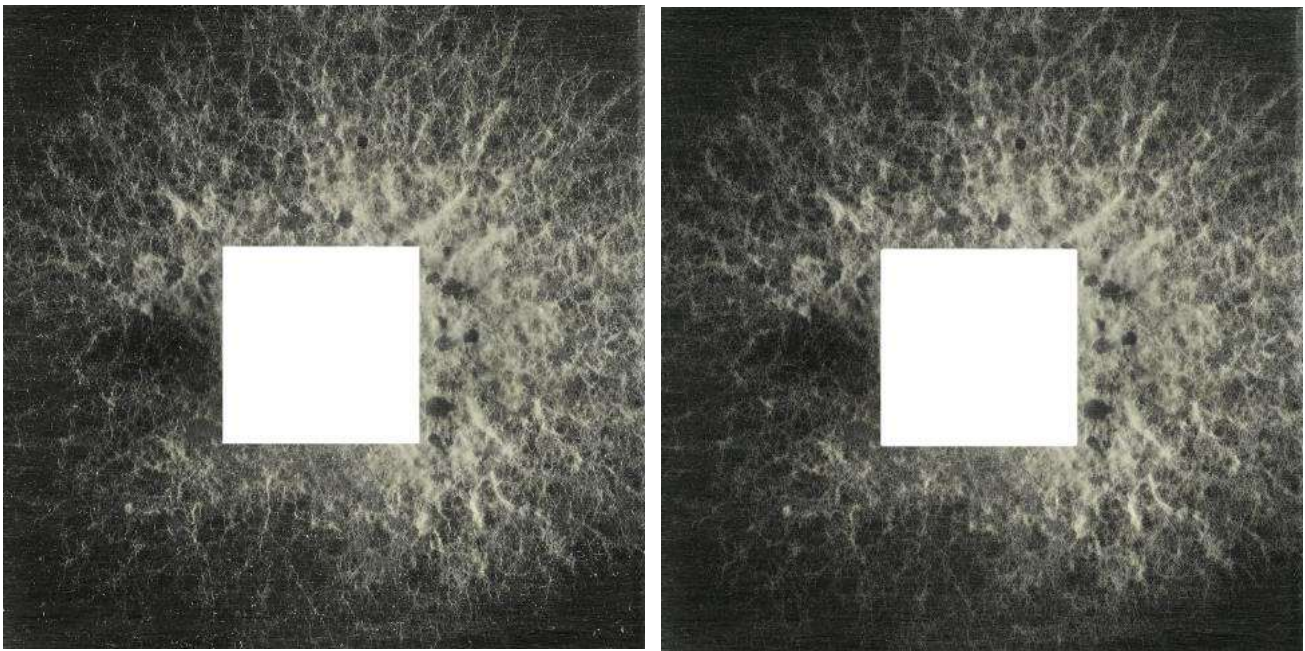
Figure A.2 Imaging processing de-noising example. Side-by-side comparison of mycelium-covered aluminum surface cropped to 49 x 49mm (left) and that same image de-noised using the method described above (right). Notice that speckles and bright spots have do not appear so intensely on the image to the right. The sample used for this example is "no food underneath/small feeding block" sample #1, at day 6 of mycelial growth.

b. This removed the noise-adding effect of speckles, scratches, dents, dirt/dust, and other artefacts that are not intended to be included in the threshold

5. Converted the images to 8-bit (Figure A.3), using the built-in function.
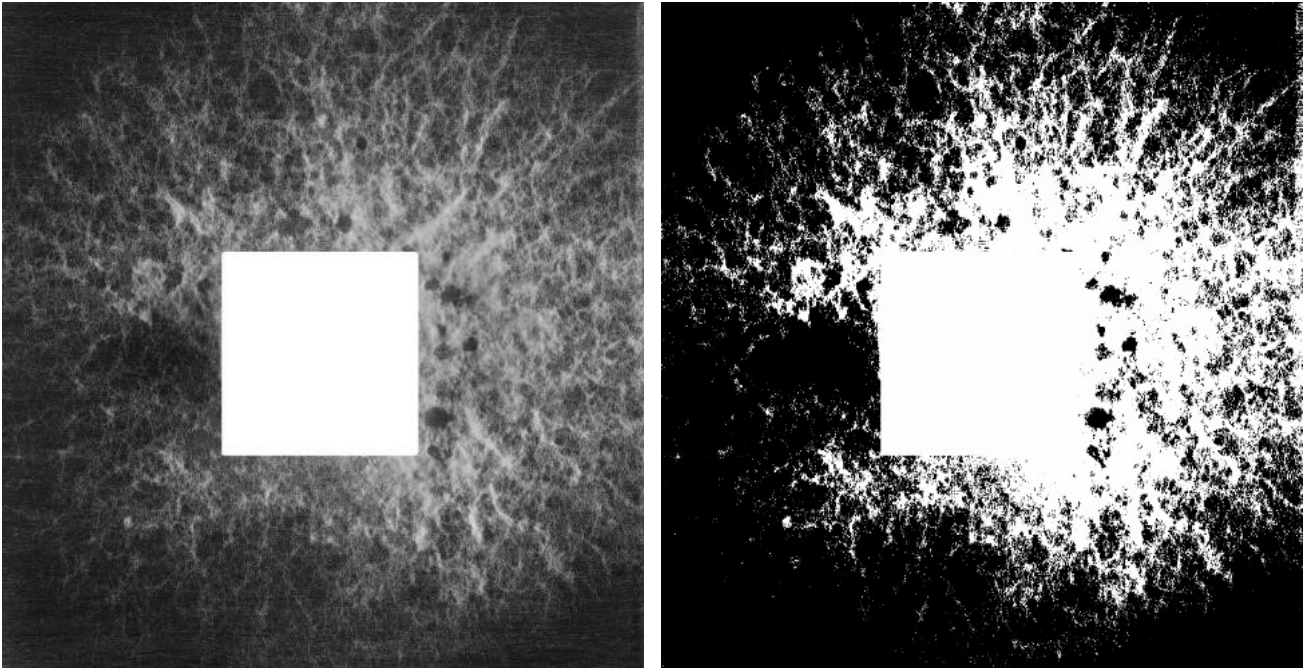
Figure A.3 Image processing thresholding example. Side-by-side comparison of mycelium-covered aluminum surface processed into 8-bit (left) and that same image converted to binary using the selected threshold of 97 (right). The sample used for this example is "no food underneath/small feeding block" sample #1, at day 6 of mycelial growth.

6. Choosing a threshold

a. Find the average of the auto threshold values for the three samples of the "no food underneath/small feeding block" condition

b. Use this average as the threshold value for all samples for a given day of imaging. This average threshold changed from day 6 to day 9 because the shutter speed was increased, which increased the average image brightness for all samples day 9 and later.

c. The threshold values per day were as follows

     i. 97 for all samples of day 6

    ii. 77 for all samples of day 9, 12, and 14

7. Apply the threshold to all images to obtain a binary image in which white represents mycelium covering the aluminum surface.

8. Measure the white area as percent of the total area, then subtract the white area of the feeding block to obtain the final values of mycelium on surface in mm2.

Figures A.4 thru A.10 show the raw and thresholded surface coverage images for day 6 to day 14 of mycelial growth. Table A.1 and Table A.2 list the values of surface coverage at each day by raw area and percent of available surface.
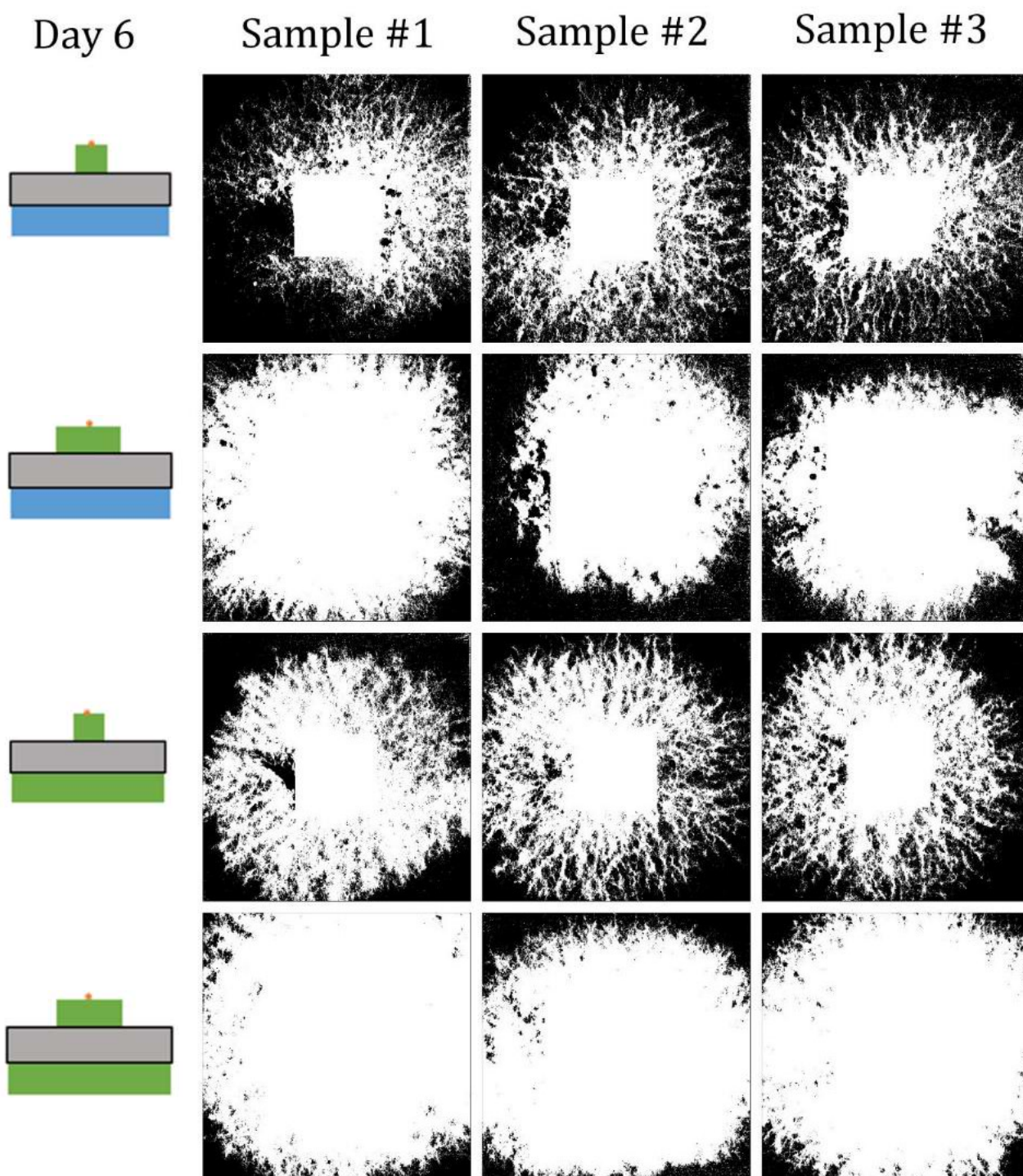
Figure A.4 Thresholded images of aluminum surfaces after six days of mycelial growth.
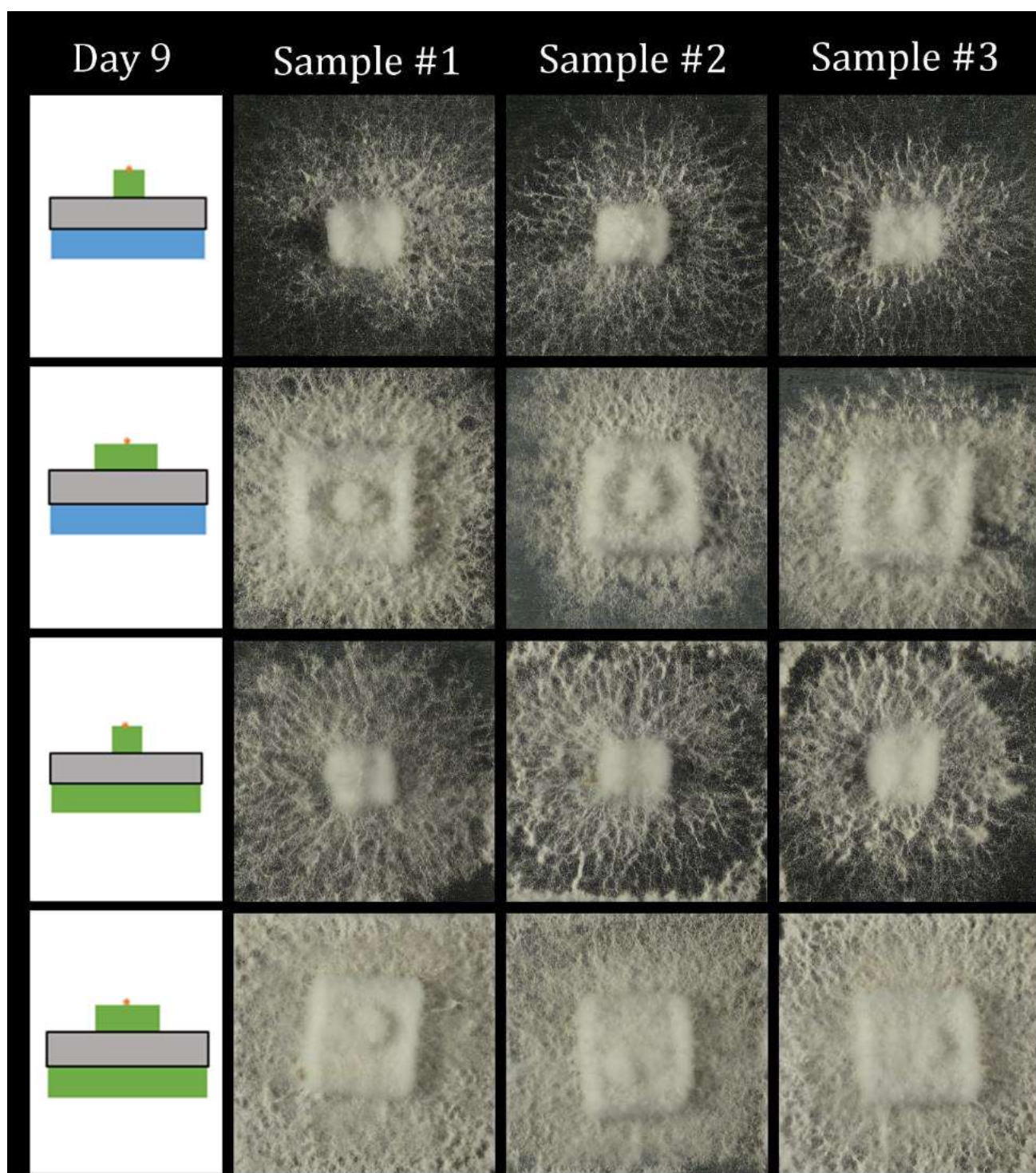
Figure A.5 Cropped optical images of aluminum surfaces after nine days of mycelial growth.
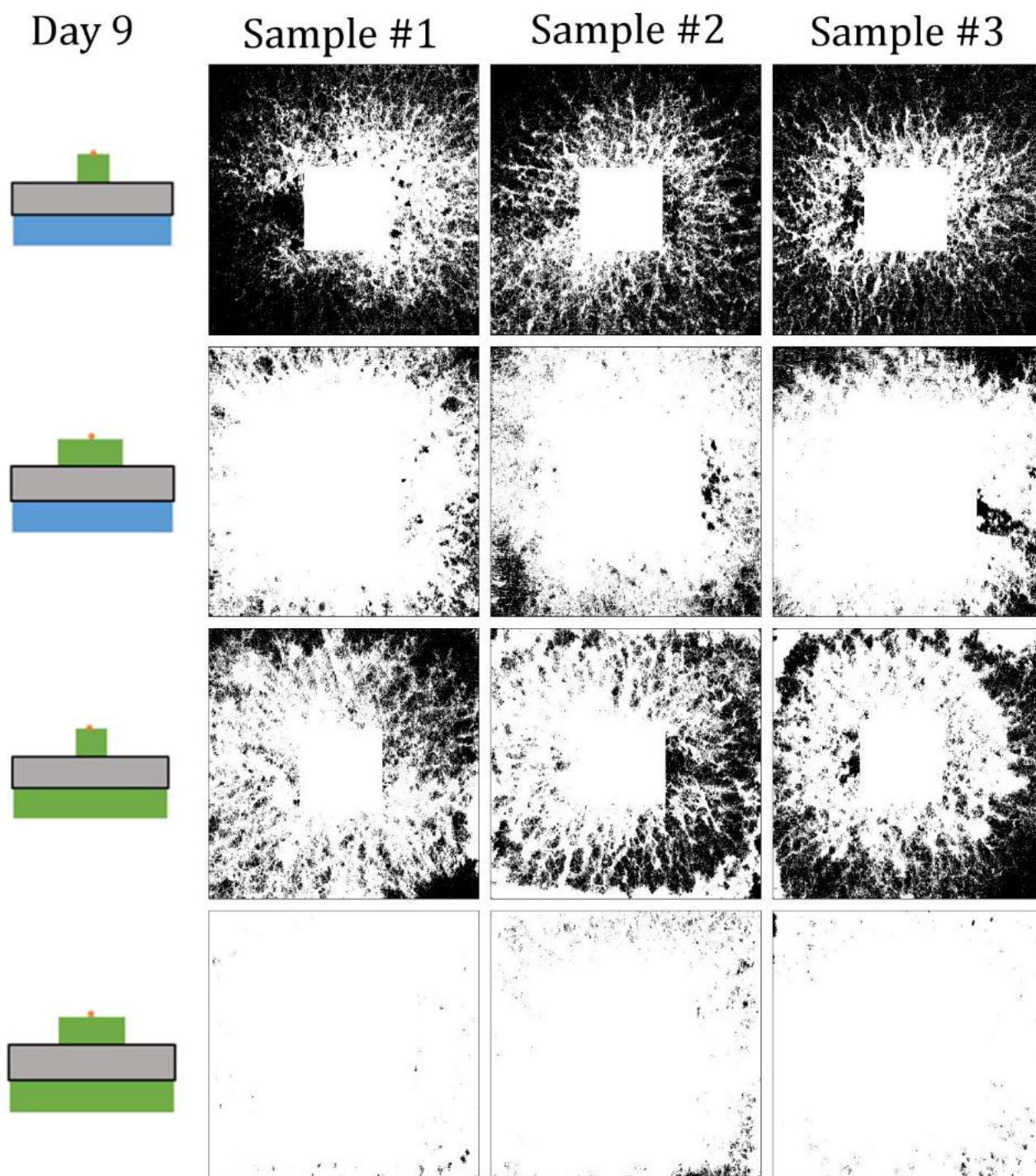
Figure A.6 Thresholded images of aluminum surfaces after nine days of mycelial growth.
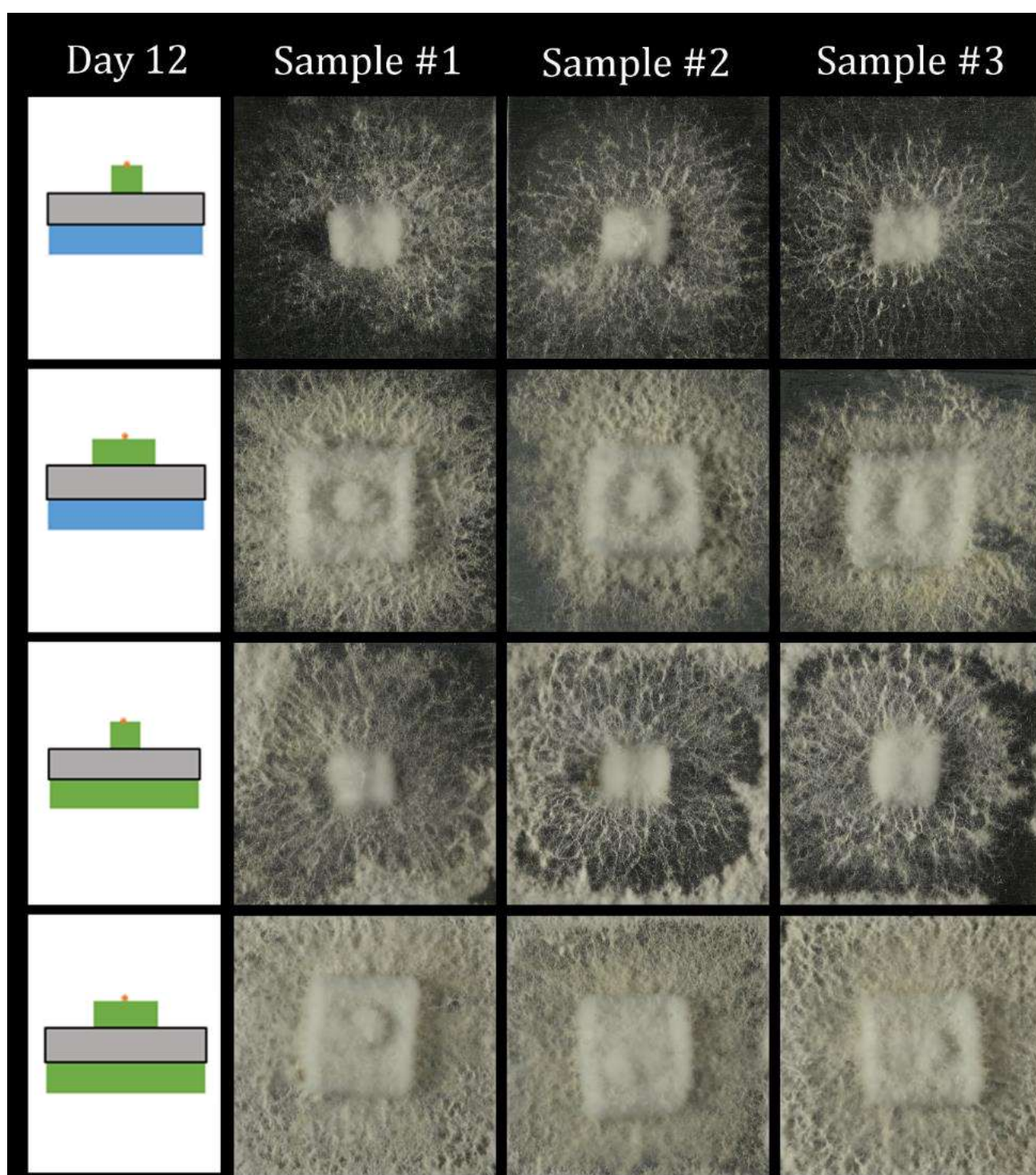
Figure A.7 Cropped optical images of aluminum surfaces after 12 days of mycelial growth.
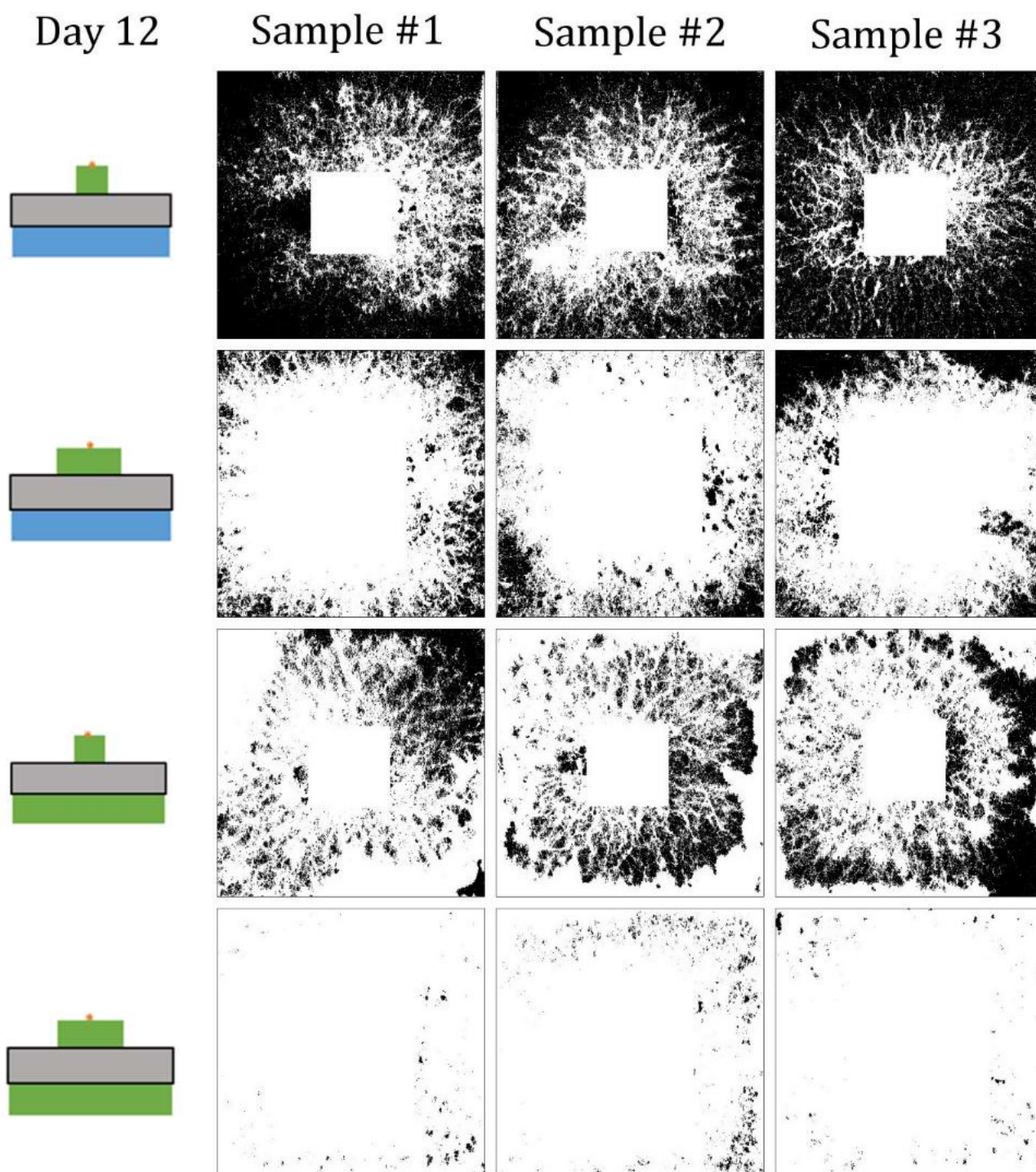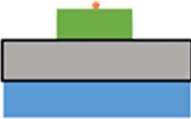
Figure A.8 Thresholded images of aluminum surfaces after 12 days of mycelial growth.
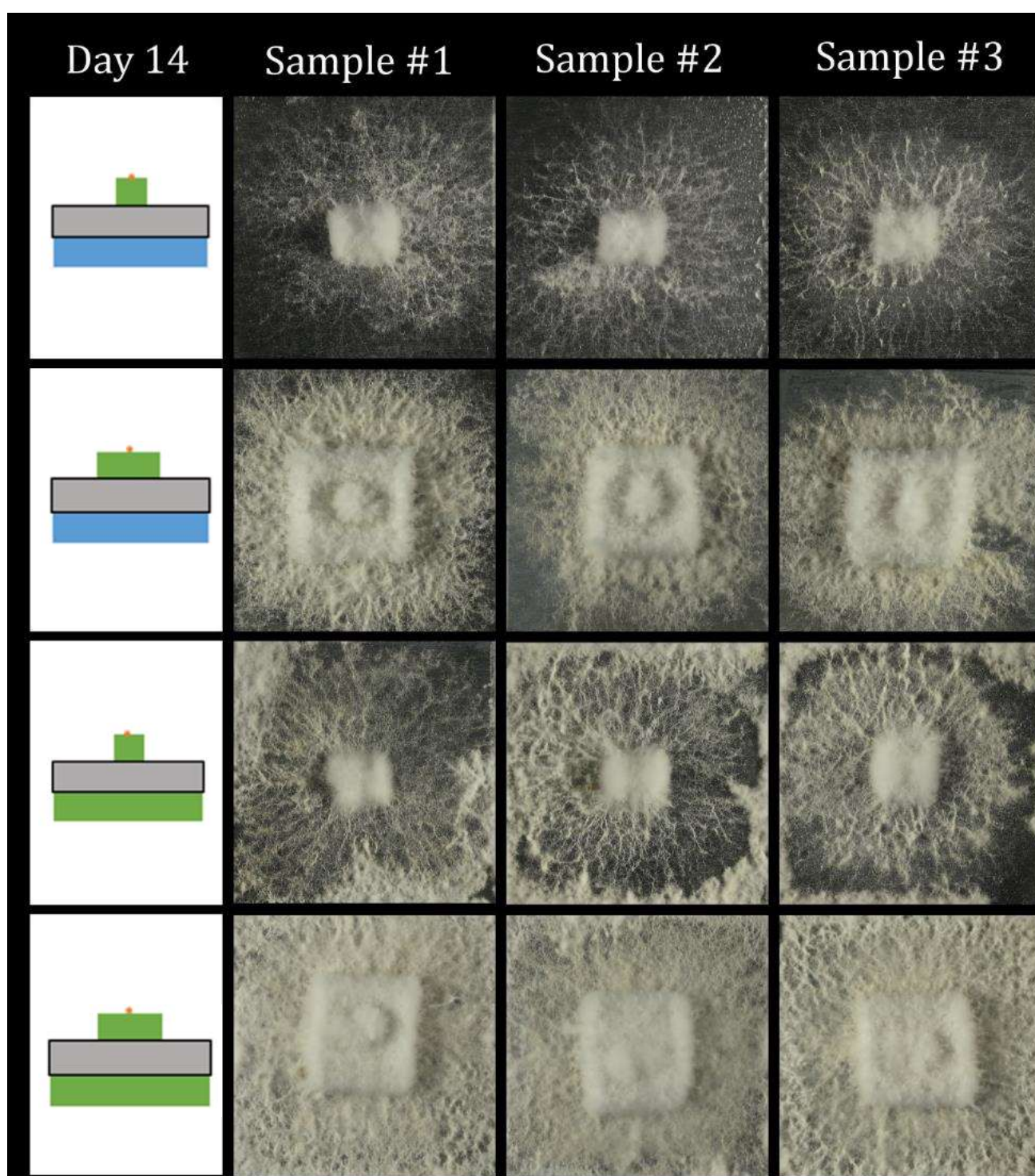
Figure A.9 Cropped optical images of aluminum surfaces after 14 days of mycelial growth.
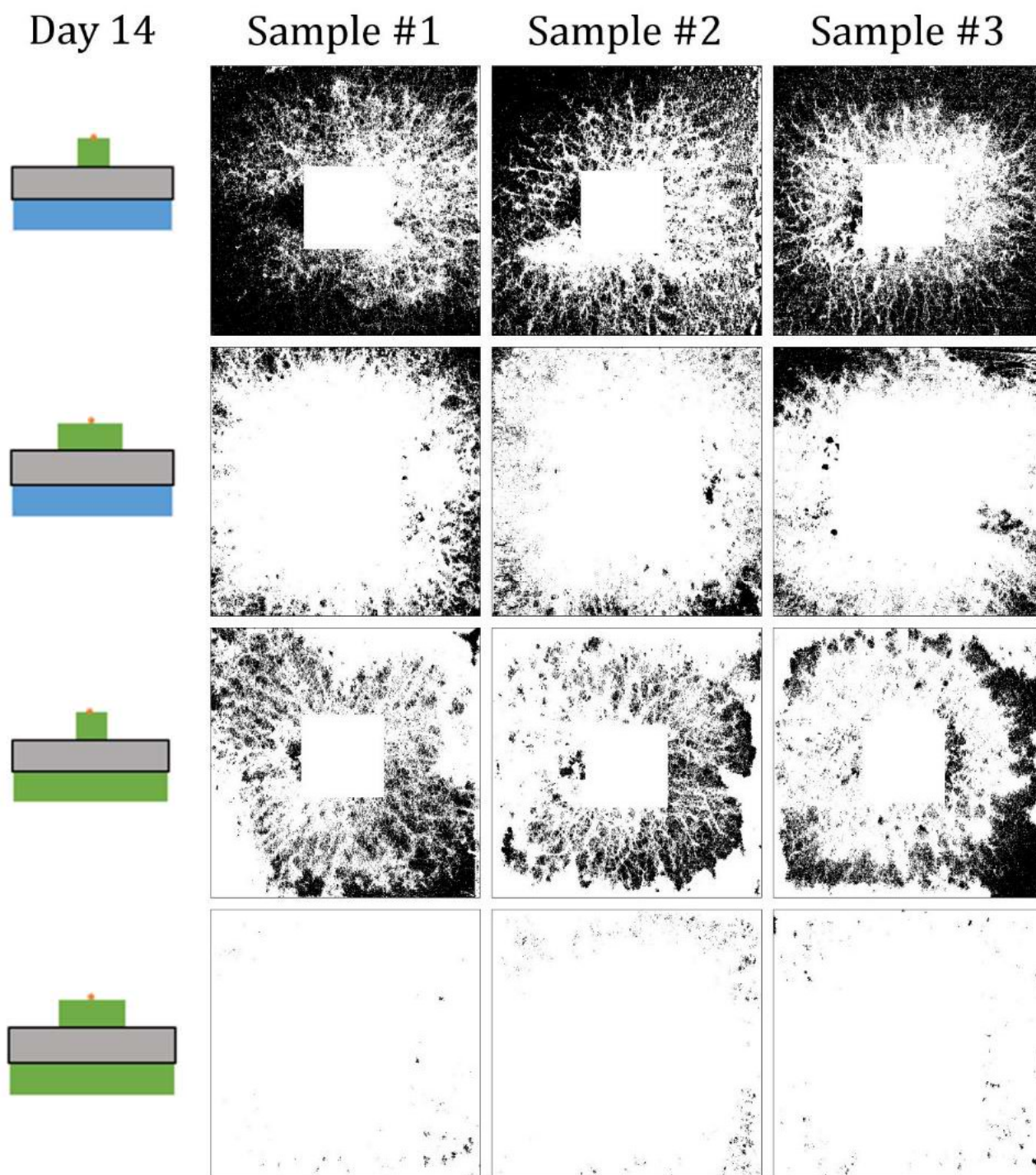
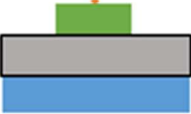Figure A.10 Thresholded images of aluminum surfaces after 14 days of mycelial growth.

Table A.1 Raw values of mycelium coverage of aluminum plates derived by thresholding.

	Area [mm²]	Area [mm²]	Area [mm²]	Area [mm²]
Day 6				
Sample 1	684.0	1401.2	1209.3	1539.6
Sample 2	808.1	867.2	1047.7	1323.7
Sample 3	749.4	1052.0	1058.2	1503.2
Average	745.8	1106.8	1105.1	1455.5
STD	50.7	221.4	73.8	94.4
Day 9				
Sample 1	747.9	1563.58	1446.8	1770.7
Sample 2	705.4	1511.1	1471.9	1725.9
Sample 3	662.5	1447.8	1359.5	1761.7
Average	705.3	1507.5	1426.0	1752.8
STD	34.9	47.4	48.2	19.4
Day 12				
Sample 1	645.8	1393.1	1642.3	1762.4
Sample 2	862.3	1464.0	1628.5	1724.9
Sample 3	522.1	1305.2	1439.8	1760.7
Average	676.7	1387.4	1570.2	1749.3
STD	140.6	65.0	92.4	17.3
Day 14				
Sample 1	766.0	1476.3	1596.7	1770.6
Sample 2	1020.8	1586.8	1719.5	1760.2
Sample 3	919.6	1439.0	1628.8	1765.6
Average	902.1	1500.7	1648.3	1765.5
STD	104.7	62.7	52.0	4.2

Table A.2 Mycelium coverage of aluminum plates corrected for the area of free surface available, reported as a percent.

	Area [%]	Area [%]	Area [%]	Area [%]
Day 6				
Sample 1	31.4	79.9	55.6	86.7
Sample 2	37.1	48.8	48.2	74.5
Sample 3	34.3	59.2	48.6	84.6
Average	34.3	62.3	50.8	82
STD	2.3	12.5	3.4	5.3
Day 9				
Sample 1	34.4	88.0	66.5	99.7
Sample 2	32.4	85.1	67.6	97.2
Sample 3	30.5	81.5	62.5	99.2
Average	32.4	84.9	65.5	98.7
STD	1.6	2.7	2.2	1.1
Day 12				
Sample 1	29.7	78.4	75.5	99.2
Sample 2	39.6	82.4	74.8	97.1
Sample 3	24.0	73.5	66.2	99.1
Average	31.1	78.1	72.2	98.5
STD	6.5	3.7	4.2	1.0
Day 14				
Sample 1	35.2	83.1	73.4	99.7
Sample 2	46.9	89.4	79.0	99.1
Sample 3	42.3	81.0	74.9	99.4
Average	41.5	84.5	75.8	99.4
STD	4.8	3.5	2.4	0.2

Appendix B

Growing mycelium on Al – inoculum on top: methodology & supplemental data for grayscale histogram analysis

Grayscale value histograms (Figure B.1) were obtained from the surface coverage images which had been converted to 8-bit (Figure A.3, left) using the built-in function in ImageJ Fiji.
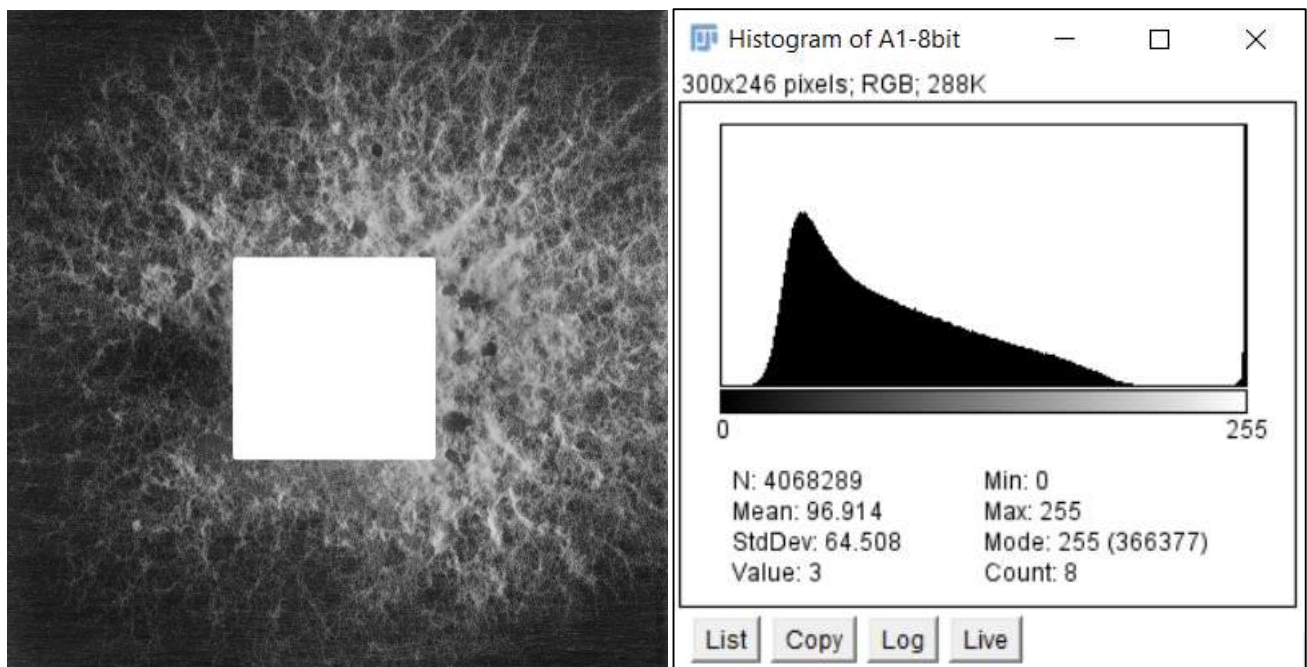

Figure B.1 8-bit image of mycelial surface coverage, and its corresponding grayscale value histogram obtained using ImageJ.

Data treatment:

White values (255) were excluded (count set to zero) as they were only present in large quantity due to the square covering the feeding block. Data sets were smoothed using a Savitzky-Golay filter with 10 points of window, and polynomial order 2.

Appendix C

Growing mycelium on Al – inoculum to the side: methodology & supplemental data for surface coverage analysis

Image processing:

Cropped and de-noised using the same procedure described in Appendix A. The main difference was in threshold selection for converting to binary.

When the distribution was bimodal, the threshold was taken as the minimum point between the peaks (Figure C.1).
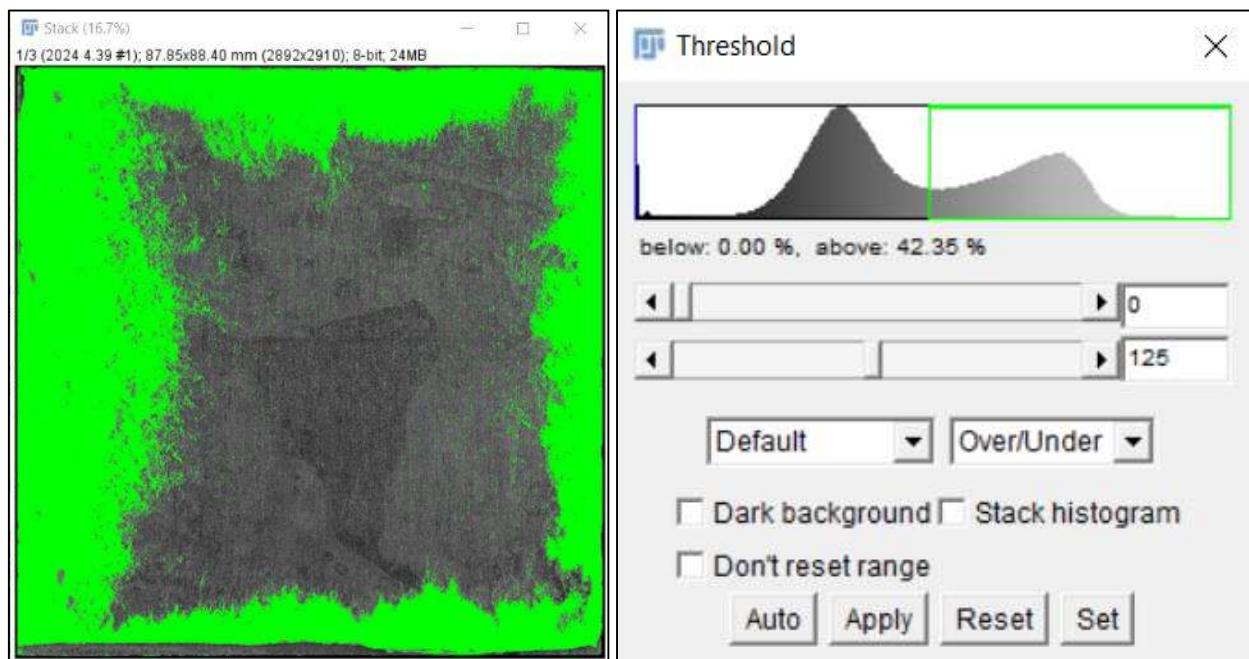

Figure C.1 Thresholding process from "inoculum on side" setup.

The thresholded surface coverages of mycelium grown with inoculum to the side are shown in Figure C.2 thru Figure C.5, and the final values of surface coverage and threshold values used are shown in Table C.1 and Table C.2
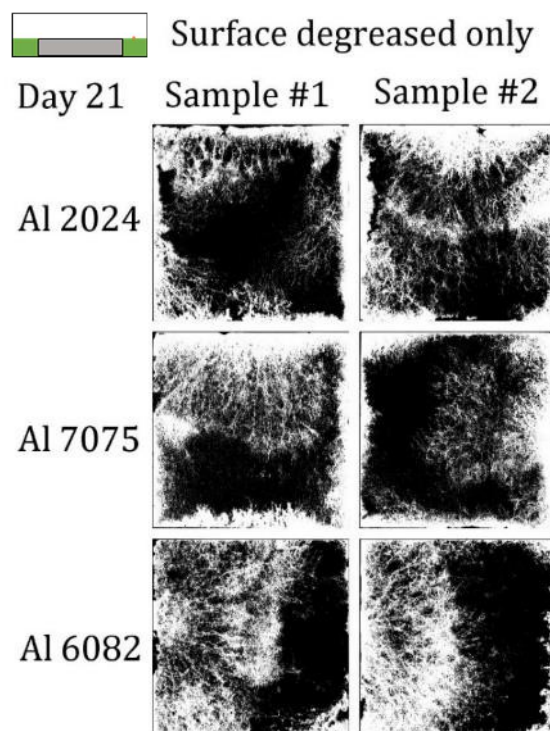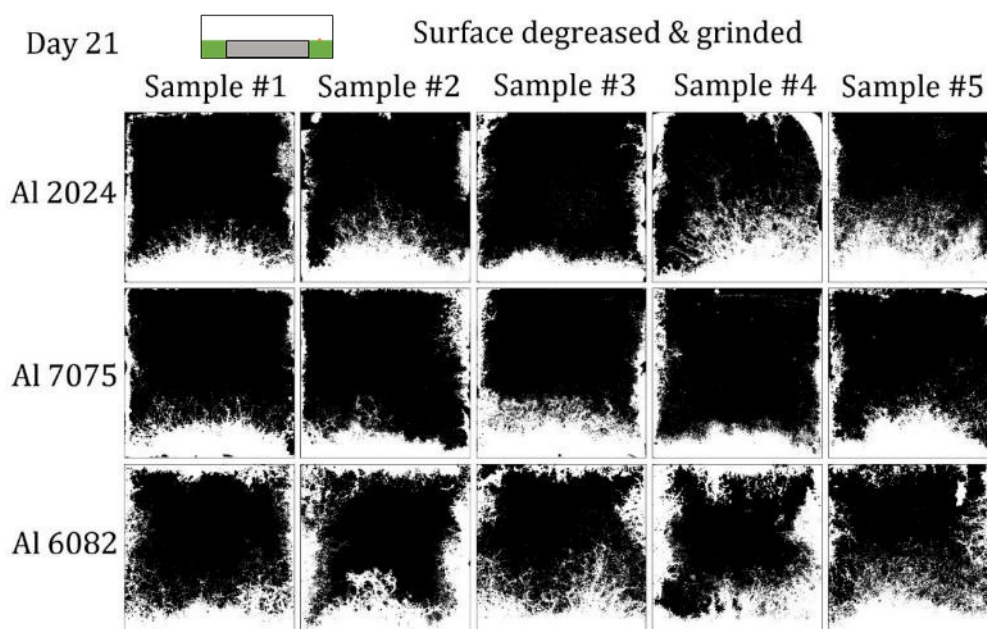
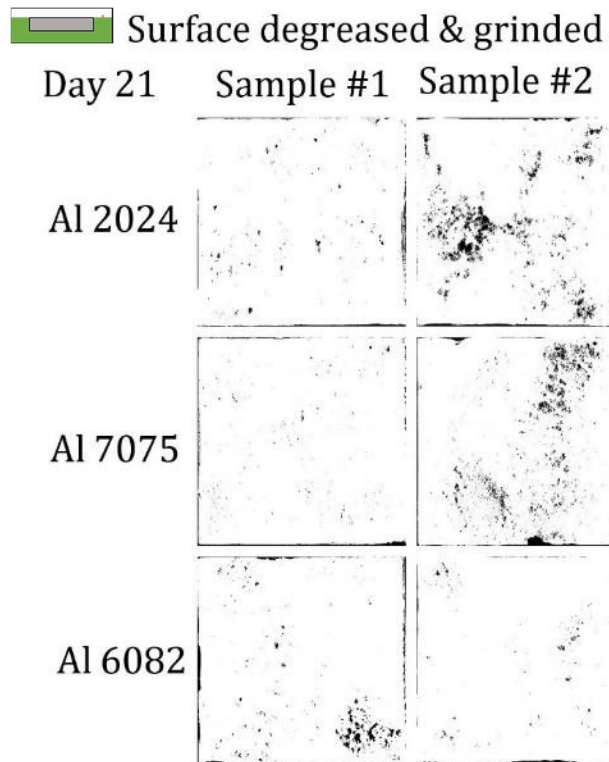Figure C.2 Thresholded images p1.
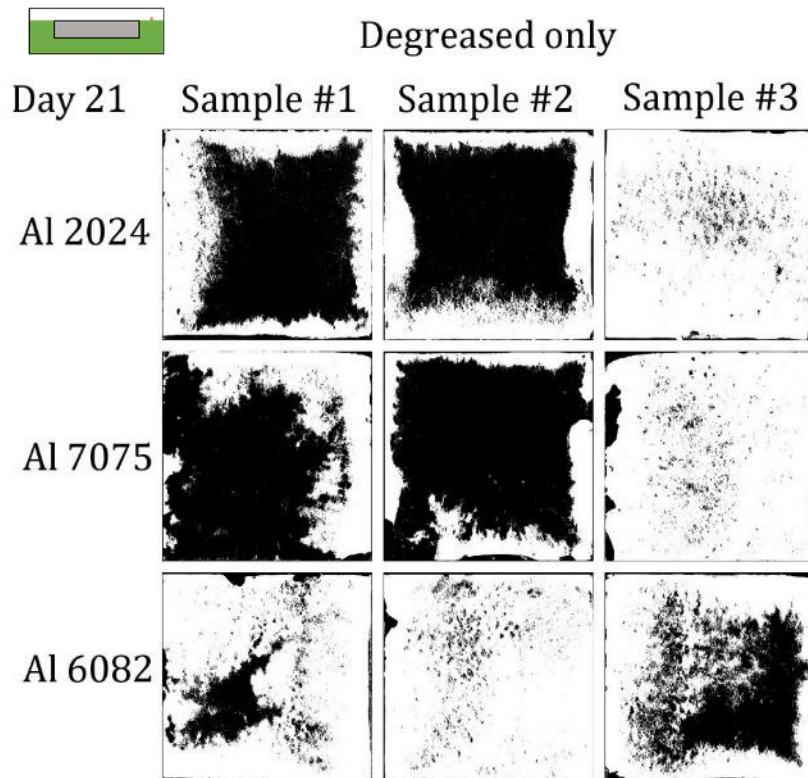

Figure C.3 Thresholded images p2.

Figure C.4 Thresholded images p3.

Figure C.5 Thresholded images p4.

Table C.1 Final mycelium coverage of aluminum plates.

	Degreased only	Degreased + grinded	Degreased only	Degreased + grinded
	Area [%]	Area [%]	Area [%]	Area [%]
Al 2024				
Sample 1	31.0	26.5	40.9	96.9
Sample 2	43.2	28.4	39.2	91.3
Sample 3	-	22.1	93.9	-
Sample 4	-	37.2	-	-
Sample 5	-	36.8	-	-
Average	37.1	30.2	58.0	94.1
STD	6.1	5.9	25.4	2.8
Al 7075				
Sample 1	42.4	24.1	36.2	97.1
Sample 2	33.9	22.9	25.7	94.9
Sample 3	-	33.7	92.9	-
Sample 4	-	24.0	-	-
Sample 5	-	29.2	-	-
Average	38.1	26.8	51.6	96.0
STD	4.3	4.1	29.5	1.1
Al 6082				
Sample 1	47.2	33.3	87.5	94.1
Sample 2	48.0	41.4	92.7	96.3
Sample 3	-	36.6	60.0	-
Sample 4	-	45.1	-	-

Table C.2 Thresholding values used.

	Degreased only	Degreased + grinded	Degreased only	Degreased + grinded
	Threshold	Threshold	Threshold	Threshold
Al 2024				
Sample 1	101	116	129	*86
Sample 2	101	108	126	*85
Sample 3	-	115	*109	-
Sample 4	-	111	-	-
Sample 5	-	109	-	-
Al 7075				
Sample 1	105	113	110	*85
Sample 2	98	149	123	*75
Sample 3	-	111	*120	-
Sample 4	-	140	-	-
Sample 5	-	134	-	-
Al 6082				
Sample 1	87	77	*121	*86

*Threshold value calculated automatically by triangle method in ImageJ. All other thresholds were calculated automatically by the default method.

Appendix D

Solids content in water from sequential mycelium washed

Solids content in water from sequential mycelium washes
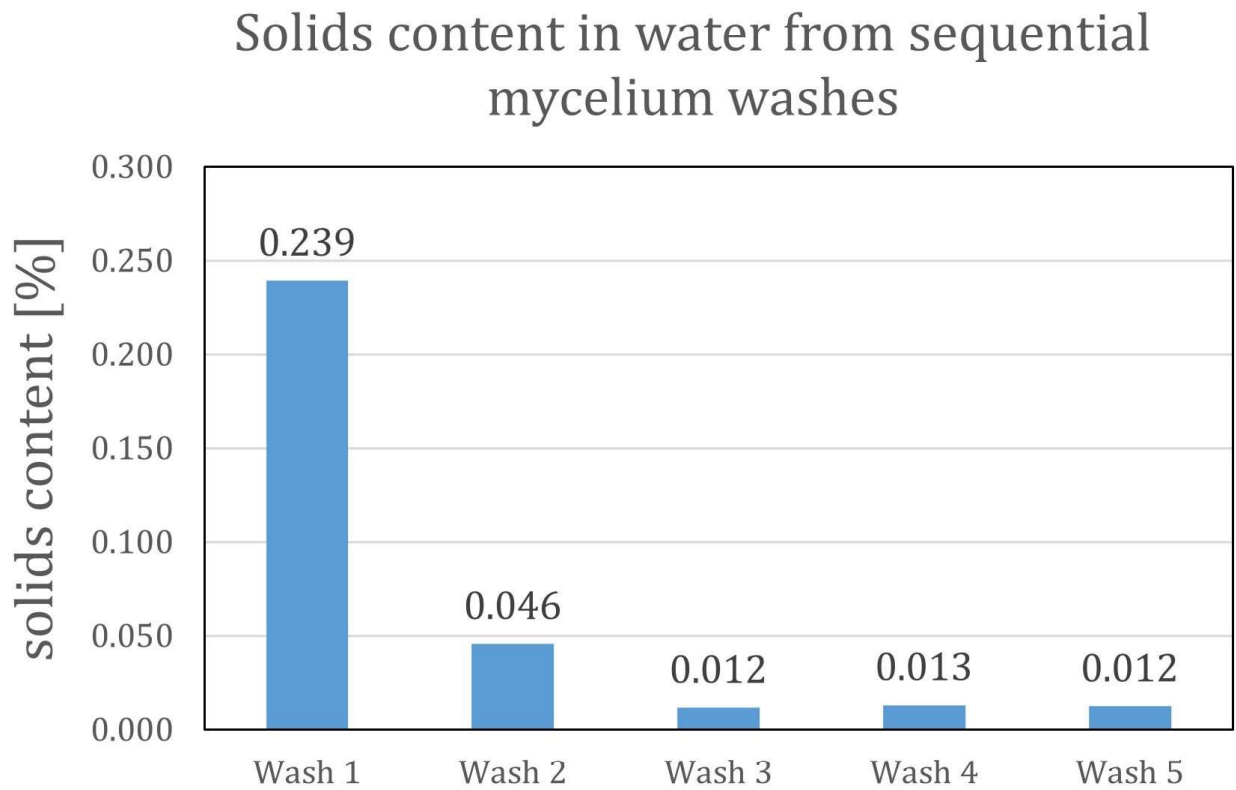
Appendix E

Constant load scratch image processing and analysis

Experimental method for determing percent area delaminated from constant load scratches by image analysis in ImageJ Fiji:

- Use wand tool to select the red scale bar and click analyze → measure to find the width in pixels
- Set the scale of the width in pixels found above to the known width in microns. Set it global
- Draw a line parallel to the scratch through the middle of the scratch, find the angle, then rotate the image to that line
- Crop the image just a bit to get rid of the rotated corners
- Duplicate/save the image now as the 'edited scratch profile'
- Edit → selection → specify. Create a rectangle of 3200 x 200 micron (the scratch lane plus 200micron for the ends)
- Save the relection to ROI. Analyze → tools → ROI manager → more → save/load
- Process → find edges, process → binary → make binary, process → binary → close
- Use the wand tool to select the delaminated area, then fill it with white paint. While still selected the delam area, press edit → clear outside
- Edit → invert the whole image (not the selection)
- Then from the ROI manager, select the box for the scratch track and place it lined up with the scratch
- Analyze → measure. The %area listed is our approximation of the delaminated area.